The Thesis Committee for Ricardo Federico Salas Porras
Certifies that this is the approved version of the following thesis:

Compressibility of Nanoparticle Stabilized Foams for Foamed Cement Applications

APPROVED BY
SUPERVISING COMMITTEE:

Supervisor: _____
Steven L. Bryant

Co-Supervisor: _____
Paul M. Bommer

Compressibility of Nanoparticle Stabilized Foams for Foamed Cement Applications

by

Ricardo Federico Salas Porras, B.S.C.E.

Thesis

Presented to the Faculty of the Graduate School of

The University of Texas at Austin

in Partial Fulfillment

of the Requirements

for the Degree of

Master of Science in Engineering

The University of Texas at Austin

December 2014

Dedication

To my family and friends.

Acknowledgements

Most of all, I would like to thank my advisor Dr. Steven L. Bryant for his insights, guidance and constant support during this research. I am also extremely grateful to my co-advisor Dr. Paul M. Bommer for his teachings that gave me the background knowledge to start this project and continuous support throughout. Dr. Bryant's and Dr. Bommer's mentorship was priceless and beyond this project helped me grow as a person. I would also like to express my enormous gratitude to Mexico's Consejo Nacional de Ciencia y Tecnología (CONACYT) for providing financial funding during my studies and research project.

I too want to show my appreciation to Andrew Worthen and Dr. Chun Huh for their teachings in the nanoparticle subject matter. Glen Baum, lab supervisor, for all his help in setting/building my experimental set-up. Daryl Nygaard and Mark Smith for machining various components made specifically for this study. Gary Miscoe, for his help in calibrating laboratory instruments. My fellow students, lab mates and friends Scott Gabel, James Patterson, Roy Wung and Archawin Aroonsri for their camaraderie and insights.

Finally, I want to thank all the entities that provided sponsorship and materials for this research. AkzoNobel for the nanoparticles and surfactants, Nissan Chemical for the nanoparticles, 3M for the nanoparticles, Lehigh cement for the cement and the Nanoparticle for Subsurface Engineering (NSE) consortium for funding. NSE members include Apache Corporation, Baker Hughes, Maersk Oil, Occidental Petroleum Corporation, Petrobras and Wintershall.

Abstract

Compressibility of Nanoparticle Stabilized Foams for Foamed Cement Applications

by

Ricardo Federico Salas Porras, M.S.E.

The University of Texas at Austin, 2014

Supervisors: Steven L. Bryant, Paul M. Bommer

Foamed cement is widely used in the oil and gas industry to provide zonal isolation. Foamed cement provides various advantages vs. pure cement. The primary purpose of foamed cement is to reduce the density of the cement mixture. Consequently, foamed cement can be used in weak formations were reduced exerted hydrostatic pressure is needed to prevent/control cement circulation loss into the formation. However, Due to gas compressibility, foamed cement's gas injection rate has to be constantly adjusted in order to create a constant density slurry through the height of the cement column. Furthermore, foamed cement's properties include higher ductility, constant pressure exertion to the formation during cement transition time (gelling) and lower thermal conductivity.

The ability of solid silica nanoparticles to generate stable gas/water foams was researched for foamed cement applications. Solid nanoparticles have been shown to permanently stabilize foams by assembling into layers at the gas/water interface. A potential decrease in compressibility of the gas phase by the presence of these armoring

bubble layers was investigated. Enhancement of cement's splitting tensile strength and compressive strength by silica nanoparticles was also investigated.

The addition of uncoated silica nanoparticles at various concentrations did not appear to enhance neither cement's splitting tensile or compressive strength. In most tests with varying silica nanoparticles concentrations, the samples with nanoparticles exhibited a slightly reduced splitting tensile and compressive strength. The exception being the compressive strength of the samples mixed with the highest nanoparticle concentration tested. However, the strength improvement was small vs. its pure cement counterpart.

An apparatus to test the compressibility of nanoparticle stabilized foams was built for this research. The functionality of the apparatus was validated using various test fluids. The validation process allowed for the establishment of a compressibility benchmark to compare the compressibility of nanoparticle stabilized foams. A vital conclusion of this process was that generating the particle stabilized foams under pressure would allow for greater discernment between the existence of the armored bubble effect and gas dissolution into the water phase.

A type of nanoparticle was identified as having the capacity to generate long term stable foams without the need of surfactant. Partially hydrophobic surface treated silica nanoparticles were utilized to generate gas/water foams under pressure and subsequently their compressibility was measured. The compressibility of these foams did not appear to show the armored bubble effect behaving as an equivalent ideal gas + water mixture. An additional surfactant and particle stabilized foam recipe was tested and displayed the same results. It was concluded that either the particle layers were not fully forming in the foam or in the case they were forming; either foam geometry was not conductive to the distribution of forces or they likely had limited rigidity and buckled when compressed. If the latter was true, the apparatus was not sensible enough to measure the limited rigidity.

Table of Contents

List of Tables

List of Figures

Chapter 1

Introduction

1.1 MOTIVATION AND BACKGROUND

Cementing is a widespread practice used in wellbore completion operations. Cement is pumped in the annular space between the casing string and the geologic formation and allowed to set in place. Once set, the hardened cement physically bonds the exterior of the pipe and the geologic formation. The hardened cement sheath provides physical support to the casing and prevents the migration of fluid between the geologic formation and the wellbore due to its low permeability. It also achieves "zonal isolation" by preventing vertical migration of fluids from one geologic layer to another.

Prior to setting, the fluid cement slurry exerts hydrostatic pressure corresponding to the height and density of the slurry. If this pressure is greater than the fracture strength of the geologic formation, damage can occur and cement flow will be diverted into the fractured region. Low density foamed cement or "light weight" cement is commonly used in weak formations in order to reduce the amount of hydrostatic pressure exerted and prevent/control cement circulation loss into the formation. In addition to having a lower density, the gas bubbles entrained in foamed cement slurry constantly exert pressure in all directions and decrease the possibility of undesired fluid channeling (i.e. ingress of fluids, especially gas, from geologic formations into the cement-filled annulus) as the slurry transitions from a fluid into a hardened solid (Chatteriji et al, 2003). Furthermore, foamed cement has ductility that is an order of magnitude greater than pure cement. This increased ductility allows the cement sheath to yield if the casing expands/deforms when being subjected to pressure and temperature induced stresses (Kopp et al, 2000). As a

consequence of the increased ductility, foamed cement is less likely to develop cracks and provide better long term wellbore zonal isolation.

Foamed cement is generally produced by adding surfactants and other stabilizers to cement slurry and then entraining gas, usually nitrogen, in the slurry. Cement stability and quality (gas v/v %) is of critical importance to maintain even distribution of the desired cement properties. Typically foamed cement is generated at pressure between 200 to 700 psi and experiments have shown that optimal class H foamed cement "in place" quality is between 20% and 35% (Moore et al, 2000). The fact that gases are compressible fluids has to be taken into account when designing/mixing the foamed cement slurry since its quality will change as the slurry travels through the depth of the wellbore. When finally stopping at its targeted location, the slurry's "in place" quality is reached and ideally, if the slurry is stable, remains constant as the gas bubbles stay in place without migrating upwards.

The motivation of this study was to explore the possibility of generating new and improved foamed cement formulations with the addition of nanoparticles. The main objective was to determine if nanoparticles could be used to control the compressibility of foamed cement by creating nanoparticle "armored" bubbles. Previous research such as Shih et al (2006) and Potapov et al (2011) also showed the possibility to enhance cement's strength properties with the use of nanoparticles .The potential improvement on long term, 28 or more days (Tsivilis & Parissakis, 1995), cement strength was also of interest, focusing primarily on tensile and compressive strength.

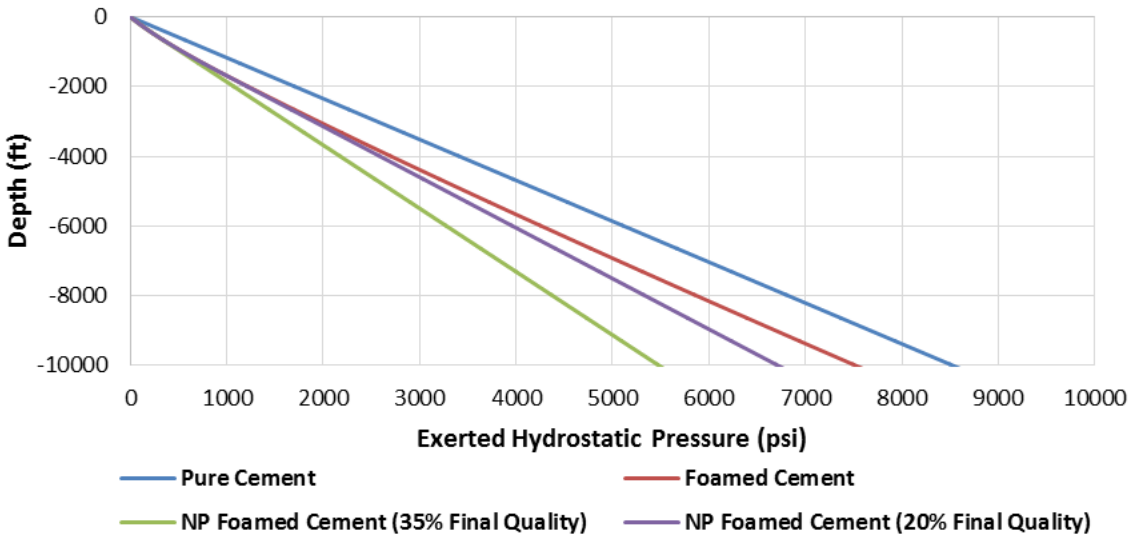

Figure 1.1 Illustration of simulated hydrostatic pressure behavior of nanoparticle stabilized foamed cement vs. pure cement and foamed cement. Initial foam quality is taken as 50%. The gas in the foamed cement is compressible and thus the cement density approaches that of regular cement at a depth of 6000 ft. In contrast the nanoparticle-stabilized foam cements are assumed to become incompressible when the bubbles become armored.

Figure 1.1 is used to illustrate the target wellbore hydrostatic pressure behavior sought if in fact foamed cement slurry compressibility could be controlled. In this illustration, the density of pure cement slurry was assumed to be 16.4 lb/gal; this is equivalent to a hydrostatic pressure gradient of $\rho g = 0.853$ psi/ft. The pressure at which the foamed slurries were generated is taken to be 300 psi and their surface initial quality is 50%. The pure cement slurry, which is considered incompressible, exerts an increasing hydrostatic pressure with a linear dependence on depth D, i.e. $P_{pure} = 0.853*D$ psi. Foamed cement exerts less hydrostatic pressure because it is less dense; at 50% quality its density is 8.2 lb_m/gal. However as the foamed cement travels down the wellbore the gas is compressed, the slurry's density increases and ultimately approaches the density of pure cement, resulting in a linear hydrostatic pressure vs. depth trend (red line in Figure 1.1)

having the same slope as pure cement (blue line). The foamed cement thus reduces the hydrostatic pressure of a full column of cement by a maximum of 1000 psi regardless of depth in this example.

The nanoparticle stabilized foamed cement displays a similar behavior to regular foamed cement at shallow depths, but as the armored bubble effect sets in, the density of the slurry stops increasing and the rate of increase of hydrostatic pressure with depth remains smaller than for pure cement. For example, if a foamed slurry of initial quality 50% has been designed to reach a target final quality of 35% (green line) at a total pressure of 560 psi (hydrostatic head + foam generation pressure), then the pressure is significantly smaller than the traditional foamed cement at depths greater than 5000 ft. As another example, consider a slurry that reaches a final quality of 20% at a total pressure of 1200 psi (purple line). In this case the difference between nanoparticle-stabilized and traditional surfactant stabilized formulations is smaller. Hence attaining larger values of final quality at smaller pressures produces the greatest benefit. In practice the solubility of gas in the slurry will cause small increases in density with depth for all foamed cement, an effect not taken into consideration in this illustration.

Another potential advantage of a nanoparticle stabilized foam, is the possibility of a more uniform in-place quality over a large depth range. Figure 1.2 shows how the quality of the same foamed cement recipes from Figure 1.1 behave at different pressures. The simulated conventional foamed cement is generated at 300 psi and 50% quality, but once it reaches a pressure of 8000 psi its quality is around ~3.7%. If this foamed cement were to remain in the 20 to 35% quality range it would have to stay at a total pressure roughly between 560 and 1200 psi (hydrostatic head + foam generation pressure). From Figure 1.1 this pressure would be between 520 and 1970 ft. and there would be a 15% quality variation between the top and bottom depth. Currently, industry solves this by varying the

generation quality and/or pressure targeted for separate depth segments or "stages" (Nelson & Guillot, 2006). In contrast to this behavior, the nanoparticle stabilized foamed cements reach a final quality when the armored bubble effect takes place, and the quality remains constant over a large depth range. This would reduce number of stages and simplify the design of the cement job. As with the previous illustration, the relatively minor effect of gas dissolution, which applies to any foamed cement, was not considered here.

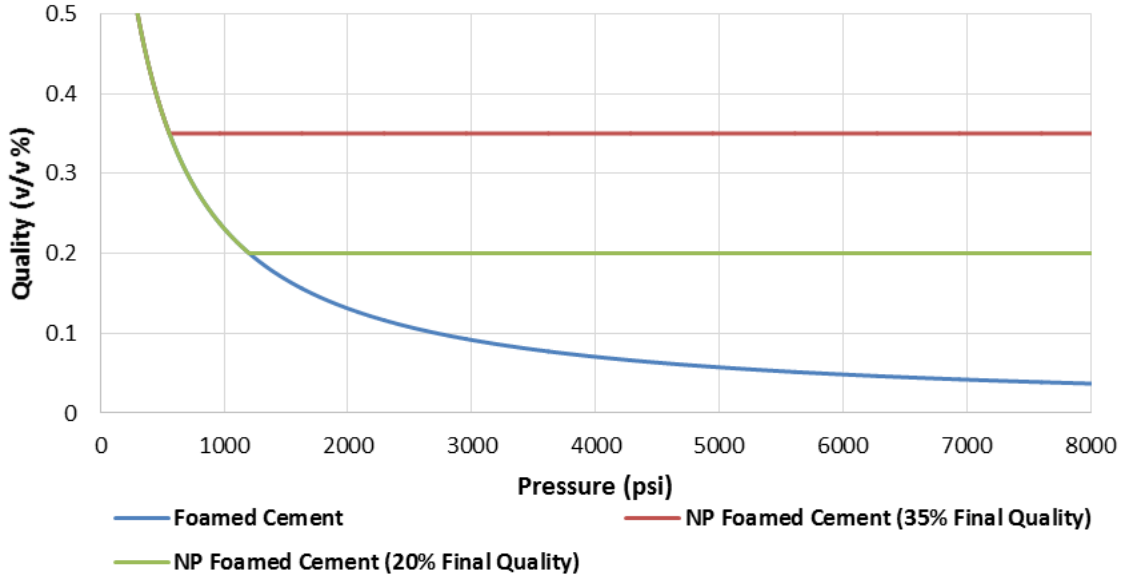

Figure 1.2 Illustration of quality vs. pressure of nanoparticle stabilized foamed cements and conventional foamed cement.

1.2 HYPOTHESIS AND RESEARCH APPROACH

The premise behind this research is based on the solid phase nature of the nanoparticles stabilizing the foam. The proposed hypothesis is the following:

If the bubbles in a nanoparticle stabilized foam are coated with a close-packed layer of particles, the solid particles will physically interact with each other and create an "armor" around the bubbles, enabling the bubbles to become rigid against compression.

It is assumed that if such rigid structure could be formed, a series of prior conditions would have to be fulfilled

- Nanoparticles must go to gas/water interface and stabilize the bubbles.
- Enough nanoparticles must be present to cover bubble surface area after pressure is applied or, in the ideal case, at the pressure at which foam is made.
- Particles must remain at the interface and not "pop off" with time or as pressure is applied.
- Sufficient gas must be initially present to allow for mass transfer of the gas into the liquid phase without complete dissolution of the bubbles.

The mechanism underlying the proposed hypothesis is depicted in Figure 1.3. In this case the generated bubble at pressure P_0 is initially not sufficiently covered by nanoparticles. As pressure increases to $P = 2*P_0$, simulating the foamed cement slurry traveling down the well bore, the gas bubble is compressed to the point where the solid nanoparticles create a close-packed layer. At this point the bubble is now rigid or almost incompressible. If pressure furthers increases $P= 3*P_0$, the bubble will not compress any further and at this stage the foamed cement density will become practically constant with depth.

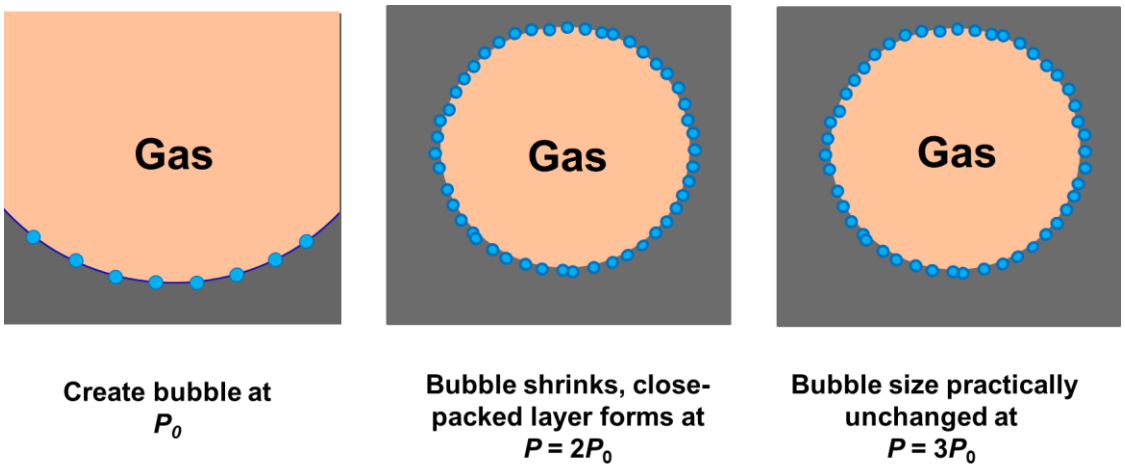

Figure 1.3 Hypothetical mechanism proposed to control foamed cement compressibility by using nanoparticles to create an armored bubble effect. The incomplete coverage of the bubble surface at P_0 (left) becomes complete (middle) as the bubble shrinks because the nanoparticles remain adhered to the interface. Further increase in pressure does not change bubble size (right) because the armor of nanoparticles is rigid.

This research study was performed using an experimental approach. The compressibility of various fluids including water, gas, foams and foamed cement stabilized with surfactants and/or nanoparticles were measured. The data gathering process involved placing a known initial volume of these fluids inside a vessel and increasing the pressure by incrementally reducing the volume occupied by the fluid with a piston. Because the mechanical strength of cement is a critical property, the influence of nanoparticles on compressive and tensile strength was also measured.

1.3 THESIS OUTLINE

There are six chapters in this thesis. The first chapter is an introduction into this research project. It includes a description of the motivation, background material and research approach used in the project. The second chapter is a literature review of relevant work related to the research presented in this thesis. The review encompasses foamed

cement, nanoparticles and their interaction with pure cement and finally nanoparticle stabilized foams. The third, fourth, and fifth chapters describe the materials, procedures, results and discussions of the experiments performed to attempt to support/prove the presented hypothesis. Chapter three will investigate the possibility of enhancing cement's splitting tensile strength and compressive strength by the addition of nanoparticles. The fourth chapter is focused on validating the apparatus used to test the compressibility of fluids. The apparatus was tested with various fluids and a comparison benchmark was established for future experiments. Chapter five encompasses the experiments done to generate nanoparticle stabilized foams under various pressures. Once a consistent method was developed, the compressibility of these foams was measured in order to search for the potential nanoparticle armored bubble effect. Finally, the sixth chapter discusses the conclusions drawn from this research as well as recommendations for future research work.

Chapter 2

Literature Review

2.1 Foamed Cement

Foamed cement consists of base cement slurry, surfactant and a gas phase dispersed throughout the slurry. The gas phase is usually nitrogen and the foamed cement often has additional components to improve stability. From a practical point of view, the density of the gas phase is much smaller than that of the base slurry. Depending on pressure, the density of nitrogen is close to 0 lbm/gal at atmospheric conditions and ~4 lbm/gal at 10,000 psia. The base cement slurry conventionally has a density between 15 and 16.5 lbm/gal, mostly depending on water fraction. As such, dispersing gas in cement slurry can be effectively used to reduce cement slurry density. It is possible for other components to affect density, but in the presented base case they are not considered part of the base slurry.

Two main types of foamed cement jobs exist, constant nitrogen ratio and constant density. In a constant nitrogen ratio foamed cement job, nitrogen is added at a constant volumetric flow rate. Due to nitrogen compression, this technique results in a variable density. Foamed cement is densest at the bottom and lightest at the top. In a constant density foamed cement job, nitrogen flow is constantly adjusted with the aid of computers, so to that a similar density exists throughout the height of the cement column. Constant density jobs are commonly designed and implemented in stages, or segments of the cement column, each with a different target nitrogen flow rate. Performing the cement job in stages increases the chances of obtaining a constant average density (Nelson & Guillot, 2006).

In addition to its lower density and thus hydrostatic head to prevent weak formation damage, foamed cement has other valuable properties. During hydration pure cement goes through a transition state in which it does not behave as a solid or fluid. While in this transition state the cement decreases in volume, does not transmit full hydrostatic pressure and hydrocarbon influx might occur. The compressed gas in foamed cement makes it "expandable" during the transition phase and allows it to uphold pore pressure (Tinsley et al, 1980). Foamed cement is thixotropic which makes it ideal for isolation of vuggy lost circulation zones and depleted zones (Davies et al, 1981). Furthermore, the low hydrostatic head of foamed cement enables the of long cement columns without the need of sliding sleeves, this further guarantees casing integrity and can reduce costs. Also, foamed cement's lower thermal conductivity than pure cement, a property that can be useful in heavy oil production (Benge et al, 1982). Last, foamed cement does not have the limitations of hollow fly ash or glass spheres which crush above certain pressures (McElfresh & Boncan, 1982).

Foamed cement made with class H cement shows optimal properties in a gas phase quality range between 20% and 35%. Below 20% the cement becomes more brittle closer to pure cement and above 35% the cement is usually too porous to provide good isolation (Moore et al, 2000). Furthermore, in the 20% to 35% quality range, foamed cement typically has ductility that is an order of magnitude greater than pure cement. (Kopp et al, 2000). The lower compressive strength of foamed cement vs. pure cement does not increase the risk of fracture initiation and propagation during hydraulic fracturing treatment. The stresses exerted in the cement sheath during such treatment are tensile and foamed cement has ideal properties for such well treatment (Harlan et al, 2001).

2.2 Effects in Cement Properties by Addition of Nanoparticles

Hydrophilic silica nanoparticles have been shown to accelerate the hydration of tricalcium silicate (C_3S), the major and characteristic component of Portland cement. The presence of silica nanoparticles accelerate C_3S dissolution, the formation of calcium silicate hydrate (C-S-H) gel and remove non-hydrogen bonded hydroxyl (OH) groups (Björnström et al, 2004). Silica nanoparticles have also shown to increase the hydration rate of dicalcium silicate (C_2S), an important constituent of Portland cement whose slower hydration vs. C_3S contributes to cement strength typically beyond seven days. A C_2S mixture with silica nanoparticles developed compressive strength in one day which was equal to that developed over 14 days of a comparable mix with silica fume. (Qing et al, 2006). These accelerated processes as well as the simultaneous formation of portlandite, has been shown to increase the hydration heat in cement with nanoparticles vs. its counterpart without silica nanoparticles. The larger relative hydration heat is directly related to the specific surface of the silica nanoparticles, the greater the specific surface (smaller nanoparticles) the larger the increase in hydration heat. Essentially the large surface area serves as larger nucleation site. As a result of the higher hydration heat, there is an earlier development in cement strength (Land & Stephan, 2012).

Previous studies have reported the possibility of enhancing cement's long term compressive strength with the use of silica nanoparticles. Mixing ASTM Type I Portland cement with 0.6 % by weight of cement (bwoc) unnamed 20 nm silica particles and a 0.55 water to cement ratio, Shih et al (2006) reported a 43.8% increase in compressive strength vs. its pure cement equivalent in a 56 day curing time period. Potapov et al (2011), showed a non-monotonic increase in compressive strength by addition of silica nanoparticles to mixtures of sand and cement. The base mix had a 28 day compressive strength of 42.7 MPa. Addition of 0.0075% bwoc, 0.4% bwoc and 0.18% bwoc nanoparticles increased the

strength to 59.1 MPa, 50.4 MPa and 59 MPa respectively. The nanoparticles had a diameter range between 10 to 100 nm and were prepared by the authors from natural hydrothermal solutions. The samples were mixed with 500DO Portland cement, a 1: 3 cement to sand weight ratio and a 0.4 water to cement ratio. In cement mixtures with fine and coarse aggregates added to cement, Jalal et al (2012) showed enhanced compressive and splitting tensile strength with the addition of nanoparticles. A 90 day curing period and 0.38 water to cement ratio was used.

In a study related to Portland cement, Nazari and Riahi, (2011) showed an improvement in splitting tensile strength when nanoparticles were added to ground granulated blast furnace (GGBFS) used as a cementitious binder. After a 90 day during period, the pure GGBFS exhibited a ~2.1 MPa splitting tensile strength, whereas the same mix with 3% bwoc silica nanoparticles had a 4.5 MPa splitting tensile strength. The water to cement ratio used was 0.4 and 1 wt% of the water content was replaced by superplasticizer to improve workability.

The augmented long term strength properties of cement mixtures with silica nanoparticles have generally been attributed to a combination of factors. As previously stated, nanoparticles act as nucleation sites to form C-S-H. This not only accelerates the development of early strength, but it also improves the microstructure of cement. In turn this modified microstructure as well as the nanoparticles working as a “filler” for void spaces likely results in denser less porous cement. In the case of uncoated amorphous silica, it is also thought that the silica nanoparticles aid the pozzolanic reaction slowly reacting with calcium hydroxide and forming additional C-S-H crystals (Santra et al, 2012). Specific to oil and gas industry applications and class G oil-well cement, there are additional resulting benefits. The smaller capillary pores reduce permeability and the modified microstructure has superior chemical resistance (De la Roij et al, 2012).

An important consideration is that depending on the concentration, the addition of nanoparticles greatly reduces the workability of cement due to the instantaneous reaction between the silica nanoparticles and the liquid phase of cementitious mixes, (Berra et al, 2012). This phenomenon can lead to large variation in cement strength properties within a cement batch. Using silica nanoparticles of various specific surfaces, Khaloo et al (2011) reported that agglomeration and non-uniform dispersion of silica nanoparticles in cement slurry results in heterogeneous strength zoning within prepared samples. Thus, a larger strength variation is likely in cement mixtures prepared with silica nanoparticles. Additionally, the authors reported a potential increase of up 78% in compressive strength at optimum silica nanoparticles replacement of cement when dispersed evenly. Optimum nanoparticle % bwoc concentration was determined to be a function of the specific surface of the particles and is to be determined on a case by case basis.

2.3 NANOPARTICLE STABILIZED FOAMS

It has been previously demonstrated that solid colloidal particles can have similar behavior to surfactants, especially when adsorbed onto a fluid/fluid interface. In oil/water emulsions, once adsorbed to the interface, these particles form monolayers which can have solid-like rigidity (Binks, 2002). Indefinitely stable oil and water emulsions have been generated solely by the use of small colloidal particles (Binks & Lumsdon, 2000). Stability and how strongly the solid particles attach to the fluid/fluid interface depend on the fluid/fluid contact angle and the properties of the particles (Binks & Clint, 2002). The particle properties include shape, size, hydrophobicity and concentration (Horozov, 2008).

In a similar manner, Binks & Horozov (2005) demonstrated that foams (gas/water dispersions) could be generated and stabilized by silica nanoparticles without the need of surfactant. The authors used originally hydrophilic silanol (SiOH) surface covered fumed

silica nanoparticles that underwent silanization, with dichlorodimethylsilane, to create intermediate hydrophobicity. In air/water systems, the foams displayed the largest stability when SiOH residual surface coverage was between 20% and 42%. Above 70% and below 14% no foam was generated. The addition of sodium chloride (NaCl) salt was also shown to increase formability and stability in particles with residual SiOH coverage of 42% and 51%. Moreover, the authors marked a key difference between foams and emulsions stabilized with nanoparticles vs. surfactant. The energy needed to remove particles of size $r \approx 10^{\wedge -7}$ m from a fluid/fluid interface with a contact angle of 90° is several orders of magnitude greater than the thermal energy. From a practical point of view, this means the particles are permanently adsorbed into the fluid/fluid interface. Surfactants on the other hand can much easier adsorb and desorb from the fluid/fluid interface into the bulk phase.

Typically, foams are thermodynamically unstable systems. When a foam is generated thermodynamic equilibrium is gradually obtained by spontaneous reduction of the total surface area as the average size of the bubbles grow. The process is known as foam coarsening. Coarsening occurs through two main processes, gas diffusion between bubbles due to pressure gradients and bubble coalescence due to liquid film rupturing between bubbles during liquid gravity drainage (Hilgenfeldt et al, 2001). When particles are selected appropriately, particle layers in foams can significantly hinder or even completely arrest the coarsening process. If a bubble's surface is completely covered by particles, the layer's surface elasticity completely inhibits coarsening (Martinez et al, 2008).

Using Langmuir trough measurements, the work by Martinez et al (2008) also described the possibility of these particle monolayers to have solid-like properties when compressed. Building on this work and too the Langmuir trough technique, Zang et al (2010) presented the indication that deposited particle layers as analogous to adsorbed

layers appear to be softer than compressed layers. Using the similar techniques, the work by Stocco et al (2011) described the particle layers as having 2-D glassy solid behavior. Based on this work that the armored bubble hypothesis was developed. It was thought that the solid particle layers of particle stabilized foams might have similar solid-like properties when compressed.

Chapter 3

Influence of Nanoparticles on Cement Strength

Cement is used as the oil and gas industry standard for wellbore zonal isolation so that hydrocarbons can be produced safely while other fluids remain in their original layers of rock. During the operational life of a well, variations in temperature and pressure can induce stresses in the wellbore that can exceed the material properties of cement. The cement used should meet the requirements to maintain its integrity when submitted to the short and long term operational stresses in the well.

While cement's gel time and compressive strength at various time periods is commonly known, the oil and gas industry has focused on the short term properties when cement is still in slurry form. Short term properties are important for uniform slurry properties and placement. Nevertheless, the long term resilience of cement is of utmost importance and depends on its material/mechanical properties such as tensile strength, compressive strength and Young's modulus. When a well is subjected to large changes in stress, appropriate long term cement properties become even more important (Ravi et al, 2002)

Chapter 3 describes a series of experiments in order to observe if silica nanoparticles could be used to increase the long term properties of cement with a focus in tensile and compressive strength. The experiments were carried out by preparing conventional class H oil well cement samples and testing their strengths. Subsequently, cement with nanoparticles samples were prepared, their strengths tested and compared to the benchmark samples.

The materials and techniques used in order to create the samples and subsequently test their strength followed as closely as possible those proposed by the American Society for Testing and Materials (ASTM) and the American Petroleum Institute (API).

3.1 MATERIALS AND EXPERIMENTAL METHODS

3.1.1 Materials

Cement

Conventional class H oil well cement was used in all recipes. The cement was obtained as a donation from the Lehigh Cement Company located in Buda Texas. The cement was stored in a moisture free environment at 68 °F. The chemical composition from the cement batch used can be found in Table 3.1. The information was received from Lehigh cement. All samples were prepared from the same batch.

Analyte	Concentration (wt%)
Na_2O	0.16
MgO	0.97
Al_2O_3	3.27
SiO_2	20.96
P_2O_5	0.11
SO_3	2.83
Cl	0.0
K_2O	0.46
CaO	63.2
Fe_2O_3	6.47

Table 3.1 Chemical composition of class H cement

Nanoparticle Dispersion

The nanoparticle dispersion used was the Cembinder W50 silica and was obtained as a donation by AkzoNobel. According to AkzoNobel, the Cembinder series nanoparticles were designed to enhance early compressive strength, reduce Wait on Cement (WOC)

time, and stabilize the cement slurry thus eliminating free water. The average particle diameter is 5 nm, the dispersion has a 15 wt% of silica in water, is alkaline with a pH of 10, has a negative surface charge, has a density of 1.1 g/cm^3 and a viscosity of 3 cP.

Cube Molds

Cubic molds were used to create the samples tested for compressive strength. The cube shaped molds have a length of 5 cm and have an open top side. The molds are made of slightly opaque plastic and are disposable. One mold was used per sample created. Hard, clear plastic square covers were machined in order to seal the molds. The covers are 1.5 cm thick and the square sides are 8 cm in length. The covers have a 2 mm diameter hole in the middle.

Cylindrical molds

Cylindrical molds were used to create the samples tested for splitting tensile strength. The molds have a diameter of 4.16 cm and a length/height of 15 cm. The molds are made of clear plastic and are disposable. One mold was used per sample created. The molds have elastomeric material caps that seal the sides of the cylinder.

Water

De-ionized (DI) water was used to mix the various cement slurries. The DI water had a resistivity of 18.2 MΩ-cm and was prepared using a Thermo Scientific Barnstead E-Pure system.

Blender

An OFI Testing Equipment (OFITE) Constant Speed Blender model 120-60 was used. The blender has a 1 L stainless steel mixing cup with hardened stainless steel mixing

blades. The blender has all the necessary settings to create cement slurries under API Specification 10 (Specification for Cements and Materials for Well Cementing).

Strength Testing Apparatus

The apparatus used in order to test cement's compressive and splitting tensile strength was a Chandler Engineering API Compressive Strength Tester Model 4207. It can increase the load pressures at rates between 500 and 4000 psi/min in 500 psi/min increments. It has two analog gauges one with a LOW range between 0 and 18 kN (0 and 4,000 lbf) with 0.2 kN markings and the second with a HIGH range between 0 and 180 kN (0 and 40,000 lbf) with 2kN markings. The machine was calibrated December 10th, 2012.

3.1.2 Cement Preparation Considerations

All cement slurry recipes were derived from the standard class H cement formula described in the Halliburton RedBook Engineering Tables handbook (Halliburton, 1994). The properties of the standard recipe described can be seen in Table 3.2.

Water Content (gal/Sk)	4.3
Slurry Weight (lb/gal)	16.4
Slurry Volume (ft^3/Sk)	1.06

Table 3.2 Properties of standard class H cement slurry recipe used in the Halliburton RedBook Engineering Tables handbook. Sk = sack.

As seen in the Table 3.2, the recipe calls for a 4.3 gallons of water per sack of cement. One sack of cement has a mass of 94 lb. Considering the density of water is approximately 8.33 lb/gal, then in a mass ratio relationship the water to cement ratio would be 0.381. In this study the water to cement ratio was kept constant at 0.38.

Adjusting to the capacity of the blender, the standard recipe utilized was 431.2 grams of DI water and 1134.7 grams of class H cement. This recipe would generate approximately 800 mL of slurry which was typically enough to fill 6 molds of either cubes, cylinders or a combination of both. Whenever nanoparticles were added to the recipe, the solid particles were accounted as being part of the cementitious material. This method is abbreviated bwoc (by weight of cement). The fact that the particles came in an aqueous dispersion was taken into account. Since the nanoparticles used come in a 15 wt % aqueous dispersion, each recipe later described takes into account the separate nanoparticles and water mass contribution coming from the dispersion.

Amongst various requirements, ASTM standard C-470/C470M (Standard Specification for Molds for Forming Concrete Test Cylinders Vertically), specifies that the molds used should have inside diameters between 5 and 90 cm and that the nominal inside height should equal twice the nominal diameter. As described in section 3.1.1 the cylindrical mold diameter was 4.16 cm and the height 15 cm. Initially cylinders were made with a target height of 8.32 cm, in order to adhere as close as possible to ASTM C470/C470M. The molds were marked at such height and filled accordingly. After testing a few practice samples, it was noticed that the sample strength would sometimes lie in a force reading just barely passing the maximum of the LOW range in the strength tester. The HIGH gauge range has much larger markings. At this point it was decided to obtain increased accuracy and precision by making the samples with a target height of 6.24 cm (about 1.5 times the diameter). The molds were not cut to that height in order to make it easier to handle the cement slurry when placing the top cap of the mold.

All cement samples were cured in a DI water bath at the room temperature of 68 °F. The cement molds were sealed so that no water flow or turbulence could disturb them inside the water bath, but so that they could draw moisture from the saturated environment

if needed. Due to scheduling restrictions, a 96 hour curing period was used for all samples. ASTM standards state that a 24 hour curing period is the minimum to be used as an early indication of long term strength, which is considered to be achieved at 28 days (73.5 ± 3.5 °F). As such, it was considered the chosen 96 hour curing time was satisfactory.

3.1.3 Cement Preparation and Curing Procedure

1. Prepare and label the molds
    a. If cube molds are to be used nothing is needed at this point
    b. If cylindrical molds, place a cap in one side of the mold and mark the mold to a height of 6.24 cm.
2. Measure the mass of recipe components
3. Place the water in the mixing cup
4. (Optional) If nanoparticle dispersion is to be used, add it into the water in the blender
5. Record the date, time and which labeled samples were created at that time
6. Place the top in the blending cup and turn blender on at the 4,000 rpm setting
7. Remove the top and carefully and steadily add the cement to the water
8. Place the top back on and change the mixer setting up to 12,000 rpm. Let mix stir for one minute.
9. Turn off the mixer
10. (Optional) Take density measurement
11. If filling a cube mold
    a. Fill all the way to the top and slightly flatten the top part with a spatula. If the cube is overfilled, use a spatula to scrape extra cement so that its leveled to the mold's height

b. Wipe the cement off the top edges of the mold
c. Apply a watertight sealant such as Dow Corning vacuum grease or similar to top edges of the mold
d. Place hard plastic cover on top, slightly pressing until it seals all the sides
e. Place additional grease on hole in cover. If it is desired that the samples constantly be exposed to water, leave the cover hole uncovered. In these experiments just enough grease was applied so that an air bubble was trapped to conduct water moisture, but the bulk water phase did not contact the cement.

12. If filling a cylindrical mold
    a. Place cylinder vertically and fill up to the height mark
    b. Since capping requires a certain degree of manual strength, place cap as carefully as possible in order to not disturb the cement or the mold's circularity.
    c. Make a small incision in the cap so that moisture can flow through the air phase, but the bulk water phase cannot flow through
13. Place the filled molds inside the DI water bath.

3.1.4 Crushing Procedure

1. Turn on strength testing machine. Its manual suggests to turn on for a few minutes prior to operating
2. Remove the sample from the water bath
3. Carefully remove the sample from the mold
    a. If mold is a cube
        i. Remove top part and wipe off grease

ii. Use a box cutter to cut the sides of the mold being very careful not to damage or scratch the cement sample

iii. Break or fold the mold sides and pull the sample out

b. If mold is a cylinder

i. Remove both end caps

ii. Use box cutter to trace a cutting line through the mold starting with the side where the cement sample is.

iii. Retrace the cutting line gently

iv. Cut the mold through the traced line but only in the side where no cement is present

v. Pull apart the mold from the cement-free side, the mold should tear apart along the traced cutting line without damaging or scratching the cement sample.

4. Obtain the sample measurements up to the closest hundredth of a cm

a. If sample is a cube

i. Starting with bottom face, use calipers to measure the first side length of the cube. Measure across the middle of the sample and record

ii. Take a second measurement orthogonal to the first measurement and record

iii. Take a final measurement orthogonal to the first and second measurements and record (Height)

iv. Repeat i-iii starting for top face

b. If sample is a cylinder

i. Use calipers to measure height of cylinder

ii. Take a second height measurement perpendicular to the first
iii. Sometimes one height is slightly larger than the other. If the heights are different by more than 2% (around 0.12 cm) from each other, use a file to slightly reduce the side with the greater height until condition is met
iv. Measure the diameter at either end of the sample
v. While holding the calipers and sample steady, rotate the sample while holding pressure in the calipers and record the maximum and minimum diameters.

5. Press the "Release" button in the strength tester to lower the bottom plate until sample can fit in between the plates.
6. Place sample inside strength tester
    a. If sample is a cube, place it in the middle of the plate. For consistency reasons always place the cube in the same direction relative to the mold. That is, choose a cube face either bottom or top of the mold. Do not place it on a side face due to sample height (length number 3) being the measurement with the most variability
    b. If sample is a cylinder, place sample horizontally in the corrugated plastic bottom and top holders. The holders were made only to set the sample in place so it doesn't roll around, but do not affect the strength measurement. Place the sample in the center of the plate and so that one of the circular sides is facing forward and easily seen relative to the strength tester from panel
7. Choose the desired force range. The LOW setting was used for the cylinders. The HIGH setting was used for the cubes

8. Choose the loading rate. A loading rate of 4000 psi/min was used for the cubes. A loading rate of 1500 psi/min was used for the cylinders.
9. Make sure the red test needle in the gauge is reset to 0. This red needle will remain in place recording the max applied force upon sample failure
10. Press and hold the "Depress for set/run" button on the left of the control console
11. While holding the "Depress for set/run" press the "set" button on the right for about 3 seconds, until the top plate slides upward into place and becomes locked into place.
12. While holding the "Depress for set/run" press the "run" button
    a. If sample is a cube, failure will occur with a sudden loss of force. Do not release the "run" button until this occurs.
    b. If sample is a cylinder, carefully monitor and look at the sample. At the moment when the first fracture appears, quickly release the "run" button. A single facture will appear along the diameter of the sample. Ample care has to be taken when doing this, if force is applied beyond this point, the force recorded will no longer be usable for the splitting tensile strength calculation.
13. Press the "release" button until samples can easily be removed
14. Record the failure force and reset the red needle
15. Remove crushed sample
16. Clean any leftover cement fragments making sure none are left to potentially disturb flat plate surface.

3.1.5 Cement Recipes and Sample Size

Recipe	Water (g)	Nanoparticles (g)	Cement (g)	Cubes tested	Cylinders tested
Pure Class H Cement	431.2	0	1134.7	15	10
H + 0.15% bwoc Cembinder W50	431.2	1.71	1132.99	8	8
H + 0.5% bwoc Cembinder W50	431.2	5.67	1129.03	8	8
H + 1% bwoc Cembinder W50	431.2	11.34	1123.36	9	11

Table 3.3 Cement recipes for sample strength testing

The variation in the number of samples tested between recipes arises from the fact that some of the samples did not meet the testing criteria such as dimensions or that the samples were damaged (chipped) as they were being removed from the mold. The number of pure H cube samples is considerably greater because and additional batch was mixed toward the end of the experimental time period to prove that the cement had been properly stored and that it had not degraded over time.

3.2 DATA ANALYSIS

3.2.1 Qualitative Analysis for Broken Cylindrical Samples

After breaking each of the cylindrical samples, their geometry was analyzed to observe if they had fractured appropriately. In order to obtain an appropriate splitting tensile strength calculation, cylinders should split through the diameter of the sample or close to it as shown in Figure 3.1. A single fracture along the length/height of the sample was the acceptable geometry. In some cases a few small shards would split from much

smaller parallel fractures; this was considered acceptable. Any data collected from samples that did not fail in this geometry were not used.

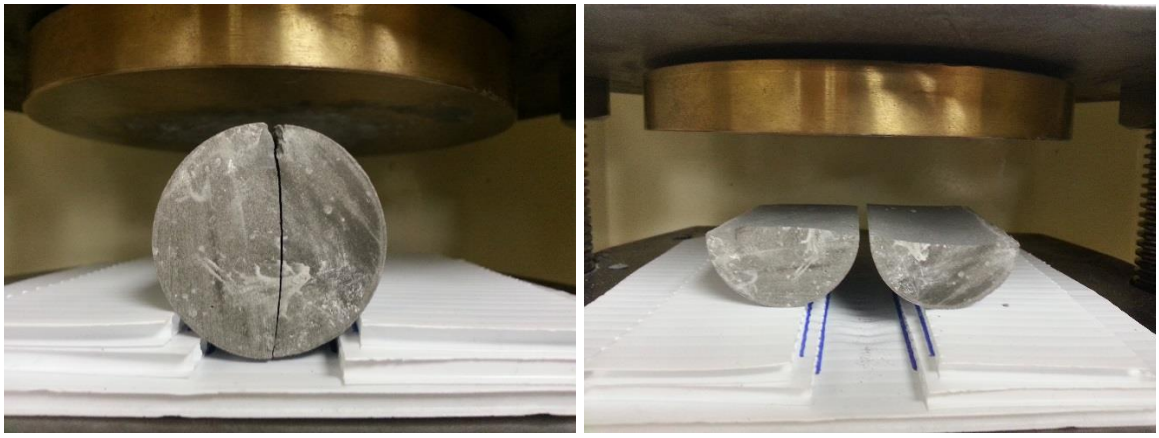

Figure 3.1 Example of appropriate cylinder fracture geometry

A similar analysis was not necessary for the cubes.

3.2.2 Slurry Density

The density of three pure H cement benchmark slurries was measured in order to compare their density to that found in the Halliburton RedBook. Density was not calculated for any batches besides these. It was only calculated in the first three batches in order to observe if the slurry had comparable properties from the Halliburton RedBook. The following equation was used to calculate density.

$$\rho = \frac{m}{V}$$

where: m=mass of the samples, V= volume of the sample

3.2.3 Compressive Strength

Compressive strength σ_c of the cube samples was calculated from the following equation found in ASTM standard C109/C109M-11b.

$$\sigma_C = \frac{F}{A}$$

The area *A* utilized for all samples was the average of the calculated top and bottom face areas. A 2% max difference between the two areas was chosen as acceptable (0.5 cm^2). The force *F* was taken as the maximum compressive force applied to the sample upon failure. Compressive strength was calculated in MPa, but was converted and charted in psi. A conversion factor of 145.037738007 psi/MPa was used.

3.2.4 Tensile Strength

Splitting tensile strength σ_T of the cylindrical samples was calculated from the following equation found in ASTM standard C496/C496M-11.

$$\sigma_T = \frac{2F}{\pi HD}$$

The diameter value used *D*, was the average value between the maximum and minimum diameters. A 1% max difference between the two was chosen as acceptable (0.041 cm). The height *H* value used was the average value between the two height measurements. A 2% difference between the two was chosen as acceptable. The force *F* was the value at which a single fracture first appeared across the diameter and height of the sample. Splitting tensile strength was calculated in MPa, but was converted and charted in psi. A conversion factor of 145.037738007 psi/MPa was used.

3.3 RESULTS AND DISCUSSIONS

3.3.1 Slurry Density

The slurry density of three class cement H batches was measured. As mentioned earlier, the water to cement ratio was kept constant at 0.38.

Batch	Specific gravity	Density lb/gal
1	1.97	16.41
2	1.98	16.49
3	1.97	14.61

Table 3.4 Density of pure class H cement slurry

The results for the three measurements are in line with the 16.4 lb/gal value found in the Halliburton RedBook for 0.381 water/cement ratio. No additional measurements were taken. It was decided that the collected data were satisfactory to demonstrate no abnormalities with the density properties of the class H cement used to prepare the samples.

3.3.2 Cube Compressive Strength and Dimensions

Sample cube	Bottom length (cm)	Top length (cm)	Bottom width (cm)	Top width (cm)	Height 1 (cm)	Height 2 (cm)	Bottom area (cm^2)	Top area (cm^2)	Average area (cm^2)	Failure force (N)	Compressive strength (MPa)	Compressive strength (psi)
1	5	5.05	4.98	5.06	4.8	4.78	24.90	25.55	25.23	40000	15.86	2300
2	4.99	5.07	4.98	5.04	4.79	4.8	25.20	25.55	25.38	39000	15.37	2229
3	5	5.05	4.99	5.05	4.77	4.75	25.23	25.50	25.36	38000	14.98	2173
4	5	5.04	5.01	5.05	4.8	4.77	25.25	25.45	25.35	41500	16.37	2374
5	4.98	5.08	4.99	5.03	4.82	4.81	25.20	25.55	25.38	36600	14.42	2092
6	5	5.08	4.99	5.08	4.75	4.72	25.38	25.81	25.59	43500	17.00	2465
7	4.96	5.05	4.97	5.06	4.75	4.74	25.10	25.55	25.33	43000	16.98	2462
8	5	5.06	5	5.05	4.63	4.6	25.28	25.55	25.41	38000	14.95	2169
9	5.01	5.05	5.02	5.06	4.82	4.81	25.35	25.55	25.45	37000	14.54	2108
10	5.01	5.05	5	5.07	4.72	4.73	25.33	25.60	25.46	38000	14.92	2164
11	5.01	5.08	5.02	5.1	4.89	4.87	25.53	25.91	25.72	44000	17.11	2481
12	5.02	5.09	5	5.09	5.01	5	25.50	25.91	25.71	45750	17.80	2581
13	5.01	5.07	5.01	5.08	4.89	4.9	25.43	25.76	25.59	47000	18.37	2664
14	5	5.06	5	5.07	4.85	4.82	25.33	25.65	25.49	52000	20.40	2959
15	5.01	5.07	5	5.08	4.9	4.87	25.40	25.76	25.58	58500	20.52	2977
											Average	2413
											Standard Deviation	285

Table 3.5 Compressive strength and dimensions of pure class H cement cube samples

Sample cube	Bottom length (cm)	Top length (cm)	Bottom width (cm)	Top width (cm)	Height 1 (cm)	Height 2 (cm)	Bottom area (cm^2)	Top area (cm^2)	Average area (cm^2)	Failure force (N)	Compressive strength (MPa)	Compressive strength (psi)
1	5	5.06	5	5.05	4.61	4.58	25	25.55	25.28	38200	15.11	2192
2	5.01	5.05	5.02	5.06	4.65	4.68	25.15	25.55	25.35	39000	15.38	2231
3	5.01	5.05	5	5.07	4.7	4.68	25.05	25.60	25.33	37500	14.81	2147
4	5.01	5.1	5.01	5.08	4.89	4.96	25.1	25.91	25.50	38000	14.90	2161
5	5.01	5.1	5.01	5.09	4.93	4.9	25.1	25.96	25.53	32000	12.53	1818
6	5	5.09	5.02	5.1	4.89	4.89	25.1	25.96	25.53	50000	19.59	2841
7	5.01	5.06	5.01	5.08	4.91	4.89	25.1	25.70	25.40	36500	14.37	2084
8	5	5.05	5.01	5.05	4.86	4.88	25.05	25.50	25.28	37000	14.64	2123
											Average	2200
											Standard Deviation	288

Table 3.6 Compressive strength and dimensions of class H cement +0.15% bwoc cembinder W50 cube samples

Sample cube	Bottom length (cm)	Top length (cm)	Bottom width (cm)	Top width (cm)	Height 1 (cm)	Height 2 (cm)	Bottom area (cm^2)	Top area (cm^2)	Average area (cm^2)	Failure force (N)	Compressive strength (MPa)	Compressive strength (psi)
1	5	5.09	5.01	5.07	4.89	4.92	25.05	25.81	25.43	34000	13.37	1939
2	5.01	5.09	5	5.07	4.88	4.93	25.05	25.81	25.43	31000	12.19	1768
3	5	5.07	5.01	5.07	4.91	4.96	25.05	25.70	25.38	30000	11.82	1715
4	5	5.06	5	5.07	4.99	4.95	25	25.65	25.33	36000	14.21	2062
5	5	5.09	5.01	5.09	5.04	5.02	25.05	25.91	25.48	45000	17.66	2562
6	5	5.07	5	5.07	5.05	5.04	25	25.70	25.35	33500	13.21	1916
7	5	5.06	5.01	5.07	4.95	4.97	25.05	25.65	25.35	36000	14.20	2060
8	5.01	5.06	5.01	5.05	4.93	4.92	25.1	25.55	25.33	37000	14.61	2119
											Average	2018
											Standard Deviation	262

Table 3.7 Compressive strength and dimensions of class H cement +0.5% bwoc cembinder W50 cube samples

Sample cube	Bottom length (cm)	Top length (cm)	Bottom width (cm)	Top width (cm)	Height 1 (cm)	Height 2 (cm)	Bottom area (cm^2)	Top area (cm^2)	Average area (cm^2)	Failure force (N)	Compressive strength (MPa)	Compressive strength (psi)
1	5	5.07	5	5.09	4.95	4.93	25	25.81	25.40	42000	16.53	2398
2	5.02	5.06	5.01	5.08	5	5.03	25.15	25.70	25.43	33500	13.17	1911
3	4.99	5.06	5	5.07	4.89	4.93	24.95	25.65	25.30	45000	17.79	2580
4	5	5.08	4.99	5.09	4.9	4.91	24.95	25.86	25.40	47000	18.50	2683
5	5	5.07	5	5.09	4.87	4.86	25	25.81	25.40	46000	18.11	2626
6	5	5.08	5	5.09	4.88	4.9	25	25.86	25.43	48000	18.88	2738
7	5	5.07	5	5.09	4.89	4.9	25	25.81	25.40	54000	21.26	3083
8	5.01	5.07	5	5.09	4.87	4.86	25.05	25.81	25.43	48000	18.88	2738
9	5.02	5.09	5	5.09	4.9	4.92	25.1	25.91	25.50	44750	17.55	2545
											Average	2589
											Standard Deviation	316

Table 3.8 Compressive strength and dimensions of class H cement +1.0% bwoc cembinder W50 cube samples

3.3.3 Cylinder Splitting Tensile Strength and Dimensions

Sample cylinder	Diameter 1 (cm)	Diameter 2 (cm)	Average diameter (cm)	Height 1 (cm)	Height 2 (cm)	Average height (cm)	Failure force N	Tensile strength (MPa)	Tensile strength (psi)
1	4.19	4.17	4.18	6.23	6.22	6.225	8800	2.15	312
2	4.19	4.15	4.17	6.23	6.22	6.225	16600	4.07	590
3	4.19	4.16	4.18	6.25	6.27	6.26	7900	1.92	279
4	4.2	4.16	4.18	6.17	6.16	6.165	12200	3.01	437
5	4.16	4.19	4.18	6.55	6.6	6.575	15400	3.57	518
6	4.16	4.18	4.17	6.15	6.17	6.16	10000	2.48	359
7	4.18	4.18	4.18	6.29	6.35	6.32	15000	3.61	524
8	4.15	4.18	4.17	6.33	6.31	6.32	13700	3.31	481
9	4.14	4.18	4.16	6.48	6.49	6.485	9000	2.12	308
10	4.16	4.17	4.17	6.4	6.43	6.415	11600	2.76	401
								Average	421
								Standard Deviation	106

Table 3.9 Splitting tensile strength and dimensions of pure class H cement cylinder samples

Sample cylinder	Diameter 1 (cm)	Diameter 2 (cm)	Average diameter (cm)	Height 1 (cm)	Height 2 (cm)	Average height (cm)	Failure force N	Tensile strength (MPa)	Tensile strength (psi)
1	4.2	4.16	4.18	6.2	6.22	6.21	7600	1.86	270
2	4.19	4.16	4.18	6.3	6.3	6.3	6300	1.52	221
3	4.2	4.16	4.18	6.41	6.43	6.42	7100	1.68	244
4	4.2	4.16	4.18	6.3	6.28	6.29	8600	2.08	302
5	4.2	4.16	4.18	6.27	6.32	6.295	10400	2.52	365
6	4.21	4.14	4.18	6.12	6.08	6.1	11600	2.90	421
7	4.19	4.17	4.18	6.16	6.22	6.19	9400	2.31	335
8	4.19	4.17	4.18	6.16	6.15	6.155	12300	3.04	441
								Average	325
								Standard Deviation	80

Table 3.10 Splitting tensile strength and dimensions of class H cement +0.15% bwoc cembinder W50 cylinder samples

Sample cylinder	Diameter 1 (cm)	Diameter 2 (cm)	Average diameter (cm)	Height 1 (cm)	Height 2 (cm)	Average height (cm)	Failure force N	Tensile strength (MPa)	Tensile strength (psi)
1	4.19	4.17	4.18	6.43	6.47	6.45	11900	2.81	408
2	4.15	4.2	4.18	6.14	6.2	6.17	10800	2.67	387
3	4.21	4.16	4.19	6.22	6.31	6.265	9200	2.23	324
4	4.16	4.2	4.18	6.47	6.51	6.49	9400	2.21	320
5	4.14	4.19	4.17	6.21	6.23	6.22	11200	2.75	399
6	4.2	4.13	4.17	6.25	6.21	6.23	10800	2.65	384
7	4.14	4.2	4.17	6.24	6.17	6.20	7200	1.77	257
8	4.15	4.19	4.17	6.23	6.17	6.2	8800	2.17	314
								Average	349
								Standard Deviation	53

Table 3.11 Splitting tensile strength and dimensions of class H cement +0.5% bwoc cembinder W50 cylinder samples

Sample cylinder	Diameter 1 (cm)	Diameter 2 (cm)	Average diameter (cm)	Height 1 (cm)	Height 2 (cm)	Average height (cm)	Failure force N	Tensile strength (MPa)	Tensile strength (psi)
1	4.16	4.19	4.18	6.2	6.23	6.215	11000	2.70	391
2	4.16	4.19	4.18	6.14	6.18	6.16	11500	2.85	413
3	4.18	4.19	4.19	6.49	6.53	6.51	14400	3.36	488
4	4.15	4.16	4.16	6.25	6.18	6.215	9700	2.39	347
5	4.19	4.15	4.17	6.17	6.13	6.15	12600	3.13	454
6	4.15	4.2	4.18	6.18	6.22	6.2	11230	2.76	401
7	4.15	4.18	4.17	6.23	6.2	6.215	10200	2.51	364
8	4.15	4.18	4.17	6.3	6.28	6.29	12800	3.11	451
8	4.15	4.17	4.16	6.26	6.2	6.23	13150	3.23	468
10	4.15	4.17	4.16	6.5	6.43	6.465	9700	2.30	333
11	4.14	4.18	4.16	6.25	6.16	6.205	9700	2.39	347
								Average	405
								Standard Deviation	54

Table 3.12 Splitting tensile strength and dimensions of class H cement +1% bwoc cembinder W50 cylinder samples

3.3.4 Effects of Nanoparticles on Cement Strength

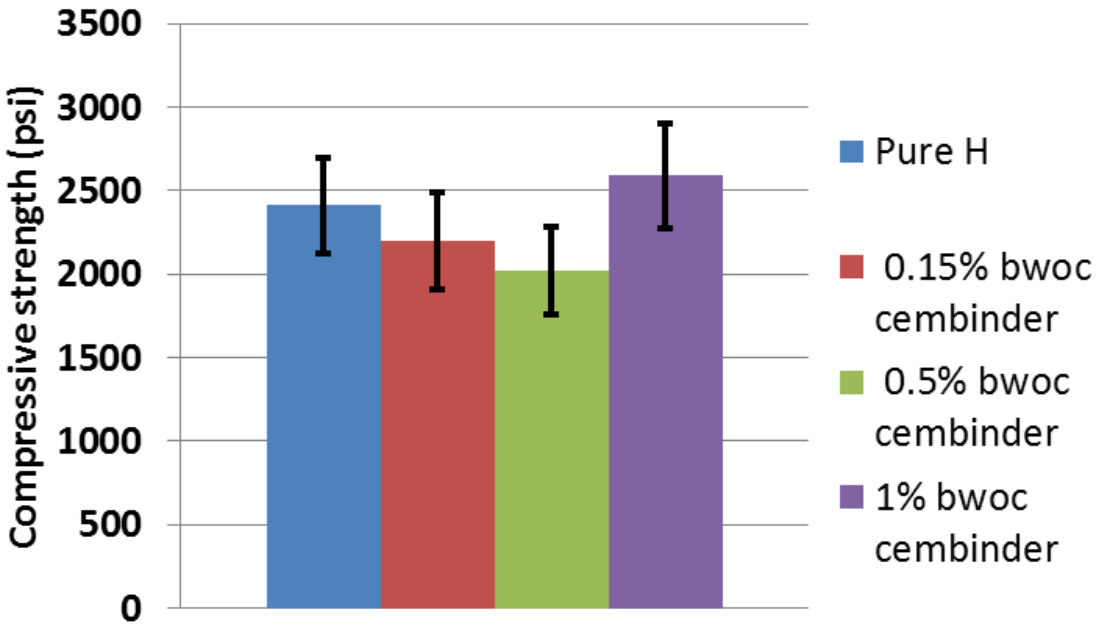

Figure 3.2 Compressive strength comparison of recipes used

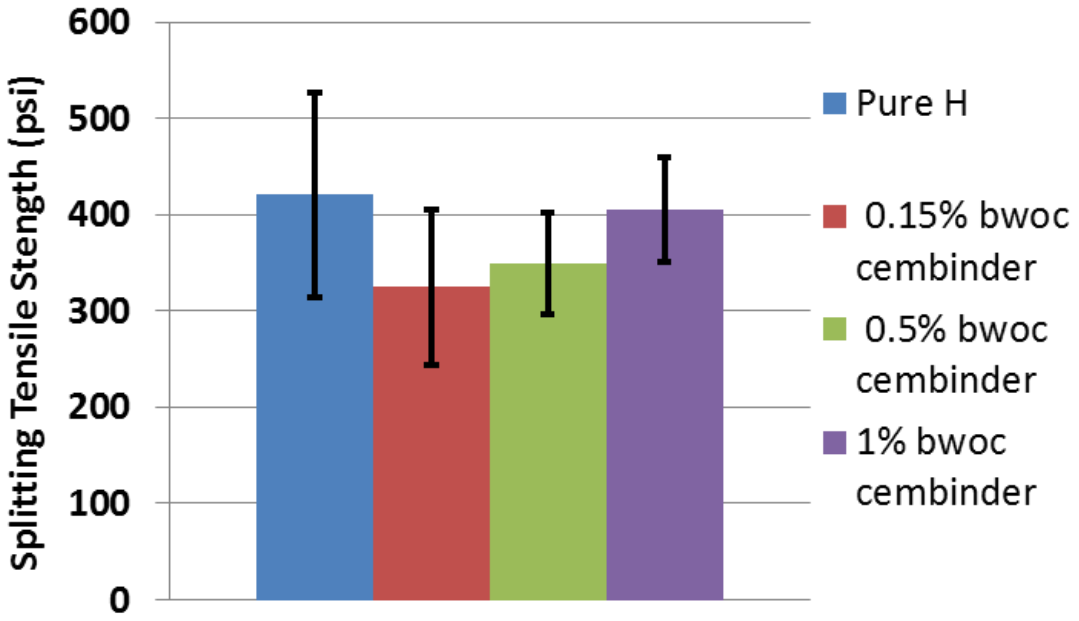

Figure 3.3 Splitting Tensile strength comparison of recipes used

Recipe	Compressive/Tensile strength ratio
Pure H	5.73
H + 0.15% bwoc Cembinder W50	6.77
H + 0.5% bwoc Cembinder W50	5.78
H+ 1.0% bwoc Cembinder W50	6.39

Table 3.13 Compressive to splitting tensile strength ratios

3.4 Overall Chapter Discussions

The Cembinder W50 silica nanoparticles were chosen for compression and splitting tensile strength testing experiments because they are a commercially available product and are marketed for cement use. The thought was to potentially research these nanoparticles to potentially enhance splitting tensile strength and also be used to stabilize foamed cement. Although not researched, qualitatively the claim by the manufacturer that these nanoparticles reduce wait on cement time appears be true. Strength testing of cement

recipes with concentrations greater than 1% bwoc nanoparticles were not tested as it proved to be extremely difficult to mix evenly due to slurry rapid thickening. At any of the concentrations tested, especially the 1% bwoc nanoparticles, the slurry thickened much faster after the cement solids were mixed into the water with nanoparticles than in pure water.

Nanoparticle concentration appeared to show a non-monotonic relationship to both compressive and splitting tensile strength. The particles appeared to slightly weaken the cement at the concentrations of 0.15% and 0.5% bwoc vs. pure cement. At the concentration of 1% bwoc, the nanoparticles appeared to have a slight enhancement in compressive strength, and a marginally smaller splitting tensile strength vs. pure cement. Based on the observations in these experiments, presumably if nanoparticles were to be used in foamed cement recipes, the nanoparticles will not substantially impair or enhance cement strength, whether they stabilize the foam or not.

The cement samples were prepared and cured at room the room temperature 68 °F, although ATSM standards dictate a curing temperature between 73.5 ± 3.5 °F. It is not believed this affected the experiment's integrity, as all the samples were prepared and cured in the same conditions.

3.5 CHAPTER CONCLUSIONS

Using the a 96 hour curing period and at 68 °F, Cembinder W50 uncoated silica nanoparticles did not show significant improvements on class H cement average compressive strength. The tested concentrations were 0.15%, 0.5% and 1% bwoc nanoparticles. At the lowest (0.15% bwoc) and middle (0.5% bwoc) concentrations used, it appeared to have an adverse effect. The 0.15% bwoc and 0.5% bwoc concentrations average compressive strength was correspondingly 8.85% and 16.4% lower than its pure

H cement counterpart. The 1% bwoc cement concentration recipe exhibited a slight improvement in compressive strength. Average compressive strength was 7.28% greater than its pure H counterpart. The compressive strength calculated standard deviation was considered to be very similar for all recipes and was between ± 11.8% and 13.1 % from their respective mean.

The effects of the nanoparticle concentration in splitting tensile strength appeared to have a similar pattern to compressive strength. Although splitting tensile strength was lower in all recipes with nanoparticles vs. its pure H counterpart, the recipe with highest nanoparticle concentration tested also displayed the highest average splitting tensile strength. Conversely, of the recipes with nanoparticles, the lowest nanoparticle concentration recipe tested exhibited the lowest average splitting tensile The average splitting tensile strengths of the 0.15%, 0.5% bwoc and 1% bwoc recipes were lower than their pure class H counterpart by 22.8% 17.1% and 3.75% respectively. It is important to remark that the pure class H cement and 0.15 % bwoc recipes showed the largest splitting tensile strength standard deviation being 25% from their mean. The 0.5% bwoc and 1% bwoc recipes had corresponding standard deviations of 15% and 13% from the their mean.

It is possible that higher Cembinder W50 nanoparticle concentrations than 1% bwoc display strength enhancement properties. However, concentrations above 1% bwoc were not tested due to blending limitations. At concentrations higher than 1% bwoc, the rapid slurry thickening upon addition of the cement solids made it difficult to ensure even cement mixing.

Chapter 4

Compressibility of Foam and Foamed Cement

In order to measure the compressibility of nanoparticle stabilized foams and foamed cements, a vessel was designed and built for this purpose. After assembling the vessel, the next steps were to validate the vessel's proper operation. The compression vessel was tested using various fluids whose compressibility has been documented by previous research.

The testing fluids included water, air and CO_2. Once tested, the compressibility of foam/foamed cement generated at atmospheric pressure and stabilized with surfactants and/or nanoparticles was measured. The results from these experiments were used to establish a comparison standard for the experiments in Chapter 5. All experiments were carried out at room temperature which ranged between 67 and 69 °F. The chapter also includes the results of experiments performed to choose a surfactant for the foam/foamed cement recipes.

4.1 Materials and Experimental Methods

4.1.1 Materials

Materials and equipment utilized previously described in Chapter 3:

- Blender
- Cembinder W50 nanoparticle dispersion
- DI water

Nanoparticle Dispersion

Nyacol DP 9711 nanoparticle dispersion. This dispersion was purchased from Nyacol Nano Technologies. The nanoparticles are coated colloidal silica with an average diameter of approximately 20 nm. The coating is a trade secret of Nyacol Nano Technologies. The dispersion has a 30 wt% of silica in water, a specific gravity of 1.3, a viscosity of 60 cP.

Compression Vessel

The compression vessel used is a stainless steel vessel with cylindrical shape and was designed to operate at a pressure up to 5000 psi. Including the screw-in top and bottom caps, it has a length of 18 cm and an outer diameter of 12.5 cm. The wall thickness is 2.5 cm and the inner diameter is 7.5 cm. The length of the space that can be filled once the covers have been screwed in is 10.8 cm. The vessel has a piston that fits inside with a thickness of 2.5 cm. The piston has two O-rings that prevent fluid flow between the spaces the piston separates. The top and bottom and bottom caps have two 1/8 inch outlets each. Each of the four outlets has a Swagelok needle valve connected for isolation purposes.

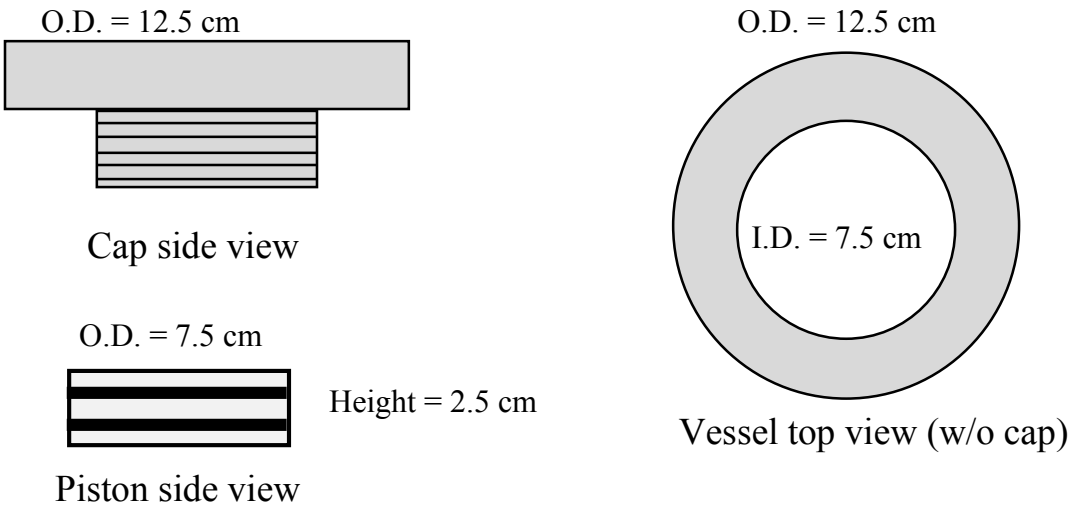

Figure 4.1 Sketch of compression vessel top view, cap, and piston

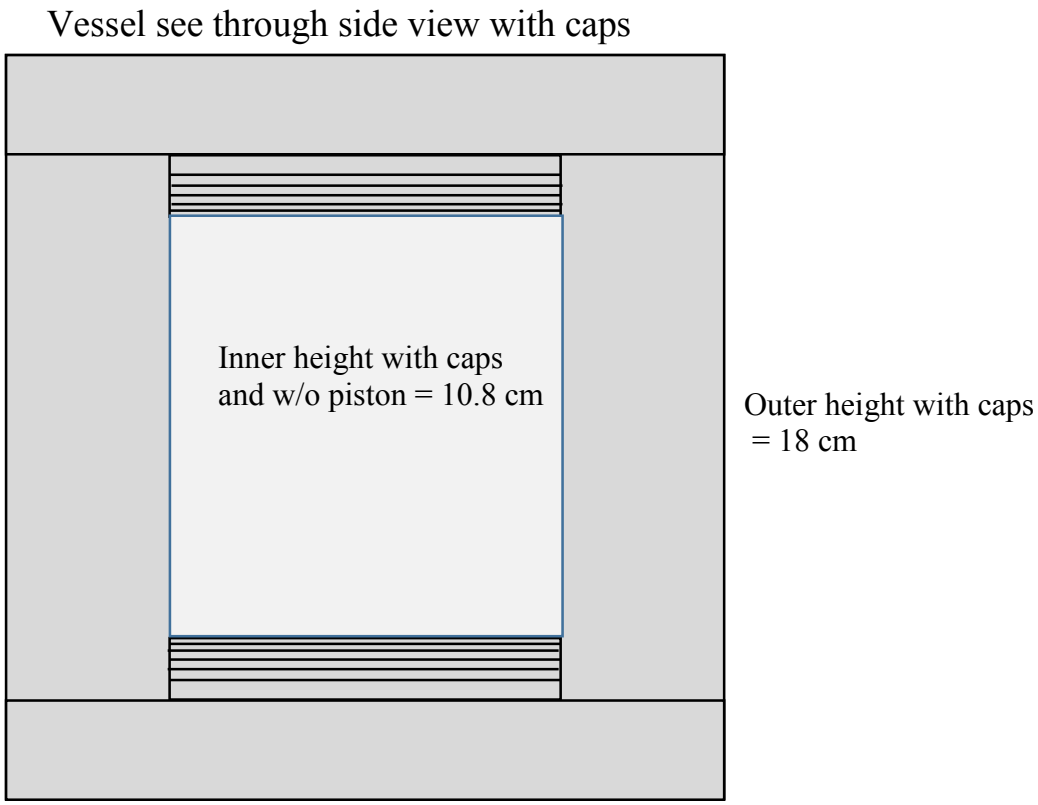

Figure 4.2 See through sketch of compression vessel side view with caps on

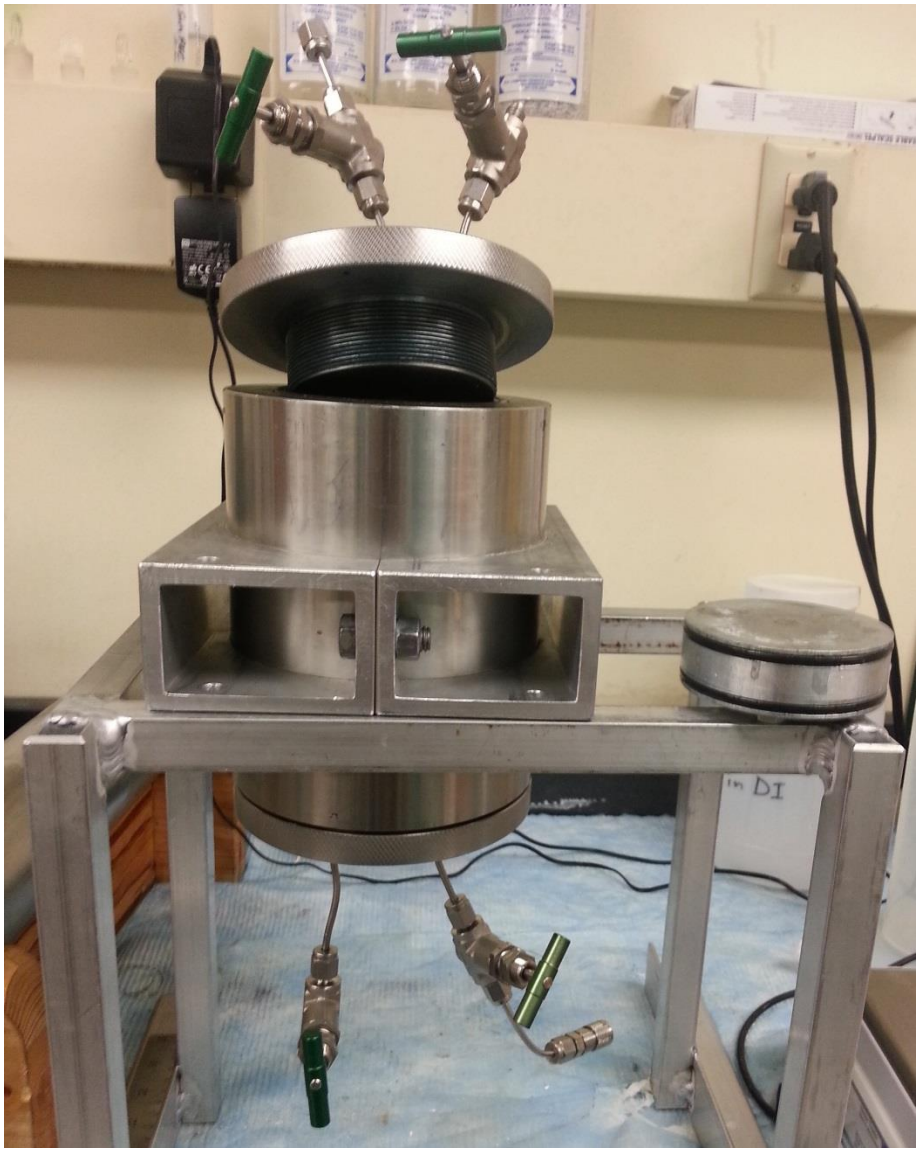

Figure 4.3 Photograph of compression vessel. Top cap has been unscrewed to have perception of thread depth. Piston has been removed and lies to the right of the vessel. The two black O-rings can be seen in the piston. The four green knobs are the isolation needle valves.

Using the equation for the volume of a cylinder, it was initially estimated that the volume of the space inside the vessel was 477 cm^3 without the piston, and 367 cm^3 with it.

These numbers were later adjusted to account for any additional space by measuring how much water could be displaced inside the vessel, measuring such volume with the ISCO syringe pump. The results can be seen in section 4.2.1

Surfactants

AkzoNobel Aromox APA TW anionic surfactant. A tallowalkylamidopropyl-dimethylamine oxide, this material has an unspecified alkaline pH, density of 0.99 g/cm^3 and a viscosity of 450 cP. Its composition is 40-60 wt% amine oxide, 40-60 wt% propylene glycol, and 5-10 wt% water.

AkzoNobel Witcolate 1247 H anionic surfactant. An alpha-olephinic sulfonate (AOS) ammonium salt, it has a pH between 7 and 8.5, density of 1.05 g/cm^3 and a viscosity of 2.3 cP. Its composition is 63% AOS, 23 wt% water, 12wt% isopropanol and 2wt% C6-C10 ethoxylated alcohols.

Stephan Petrostep CG 50 amphoteric/zwitterionic surfactant. A cocamidopropyl betaine (CAPB), it has a pH between 5 and 7, density of 1.07 g/cm^3 and a viscosity of 76 cP. Its composition is 44 wt% solids (37 wt% active), 50-60 wt% water and 2-4 wt% sodium chloride.

Pump

One positive displacement syringe pump was used to pump water as the driving fluid in the compression vessel. The pump is a Model 500D Teledyne ISCO syringe pump. It has a reservoir capacity of 507 mL, is capable of pumping at a constant between 0.001 and 204 mL/min and has a maximum operating pressure of 3750 psi.

The pump was fitted with a three way valve on the top, so that the pump could draw water from a reservoir, or pump it into the compression vessel. Downstream of the three way valve in the direction of the compression vessel, the pump had a permanently connected tubing line with a ball valve and a pressure transducer right after it.

Pressure Transducers and LabView Software

Two Validyne differential pressure transducers model DP15 were used to measure the pressure inside each of the chambers separated by the piston. The transducers were calibrated with a range between 0 and 2000 psi. One of the sides of each transducer was open to atmosphere so they would measure gauge pressure. The transducers were connected to a computer with LabView software which displayed the pressure measurement of each transducer. If desired, the pressure readings could also be recorded.

4.1.2 Compressibility Testing Apparatus Schematic

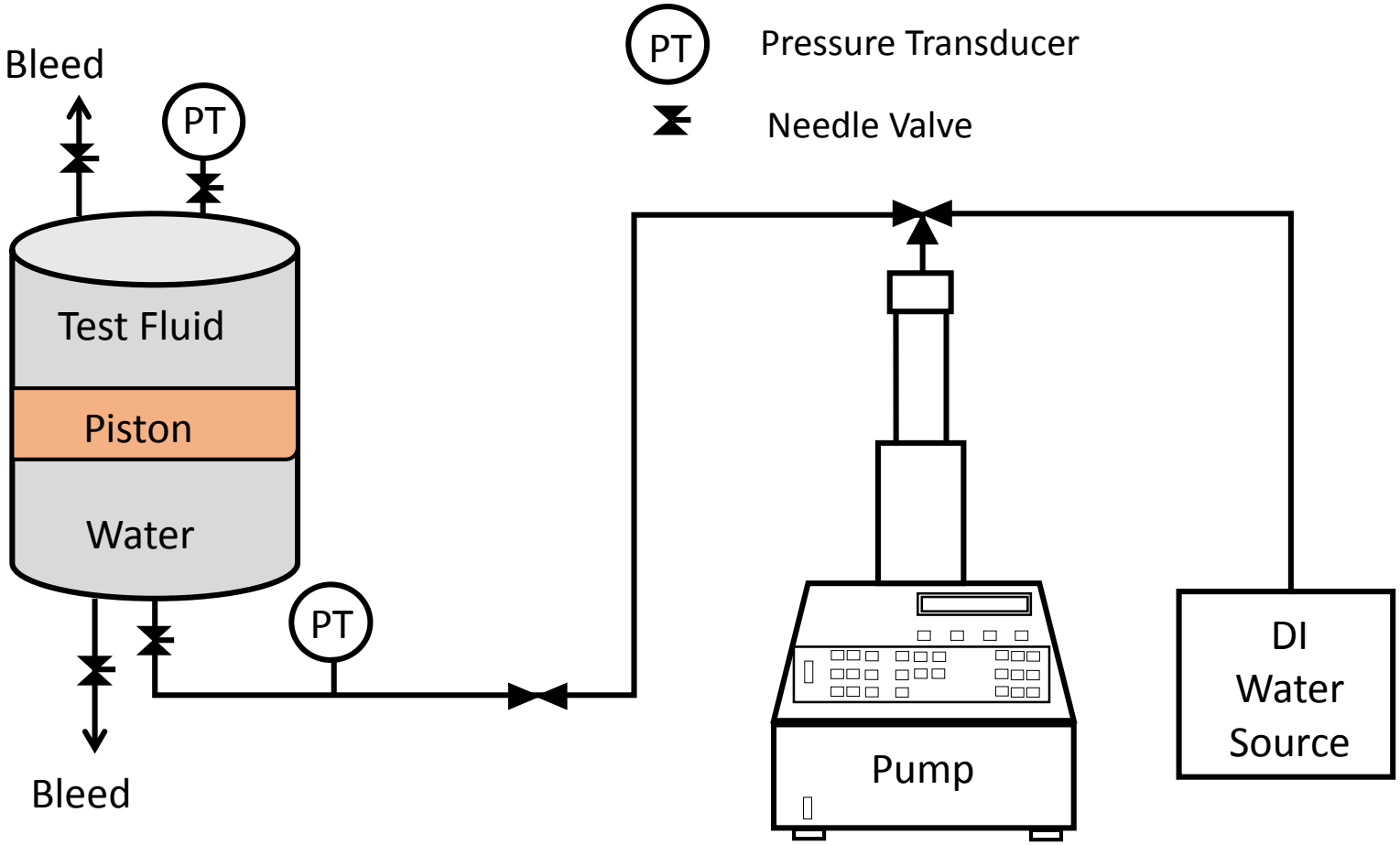

Figure 4.4 Schematic of compressibility testing apparatus

4.1.3 Vessel Loading and Preparation Procedure

The vessel interior is symmetrical and the lines up to isolation needle valves in top and bottom are also very close to symmetrical in length. Due to this reason, any of the two sides could be chosen to be either the top or the bottom of the vessel. For consistency reasons, one side was labeled as top and for this set of experiments was consistently loaded with the fluid whose compressibility was tested.

4.1.3.1 Loading of a Fluid at Atmospheric Pressure

1. (Optional) If fluid being tested is cement/foamed cement. Use a syringe to fill the top pressure transducer with mineral oil as well as the tubing line with which it connects to the second needle valve. The mineral oil will work as a barrier to prevent cement going into the pressure transducer. Ideally this process should be done prior to mixing the cement/foamed cement in order to save time as the slurry only has a limited time behaving as a fluid.
2. Open the needle valves in the top cap
3. Assuming both caps are currently screwed in, unscrew/remove the top cap of the vessel
4. Open the needle valves in the bottom cap of the vessel
5. Use a plastic rod to push the piston all the way down. Use a rubber hammer to lightly strike the plastic rod to make sure the piston is all the way to the bottom
6. Load the top of the vessel with fluid whose compressibility is to be measured. Add enough fluid so that it fills the vessel right under the threads into which the top cap screws into.
7. Remove any bubbles stuck to the vessel walls with a 1 mL syringe

8. Slowly screw back in the top cap, towards the end a small amount of fluid will spill out of both of the top needle valves.
9. Lock one of the needle valves
10. If the fluid is not cement/foamed cement
    a. Connect the top pressure transducer in the other needle valve
    b. Remover bleed screw in pressure transducer
    c. Continue screwing top cap until tight. Fluid will bleed out of pressure transducer, this will make sure not air is trapped in the lines/pressure transducer.
    d. Screw in pressure transducer bleed screw
11. If fluid is cement or foamed cement
    a. Continue screwing the cap until tight. Cement/foamed cement will bleed out of the second needle valve.
    b. Connect the pressure transducer filled with mineral oil to either of the top needle valves, making sure no air bubbles are trapped when making the connection.

4.1.3.2 Loading of a Pressurized Fluid

1. Check that the piston is all the way to the top. This will prevent air in the chamber from contaminating the fluid (If the fluid is compressed air, then the piston can be at the bottom).
2. Confirm both the top and bottom caps are tight and in place
3. Open at least one of the needle valves in the bottom cap
4. Both needle valves in the top cap should be open

5. Connect line with pressurized fluid to one of the needle valves on top
6. Slowly open line with pressurized fluid source. Fluid should flow through the top part and bleed of second needle valve.
7. Close the second needle valve. The pressurized fluid should push the piston to the bottom if it was originally at the top position. Air should be pushed out of the bottom needle valve/valves as the piston moves
8. Let the fluid reach an equilibrium pressure with its source
9. Close the second needle valve in the top cap and also close the valve from the pressurized fluid source
10. Disconnect the pressurized fluid source
11. Connect the top pressure transducer to either one of the top needle valves
12. Open the needle valve to which the pressure transducer is connected. At this point a pressure reading should be available for the pressure in the top chamber of the vessel
13. If pressure is higher than target pressure, use second needle valve to slowly bleed fluid until desired pressure is reached

4.1.3.3 Connecting the ISCO Syringe Pump to the Compression Vessel

1. Line up the three way valve on top of the ISCO pump toward the water reservoir
2. Fill the pump's reservoir with DI water
3. Line up the pump towards the line that connects to the compression vessel
4. Make sure the ball valve in the line is open
5. Run the pump at a slow rate (2-5 mL/min) and confirm the line is filled with water, water will spill out

6. Connect the line to one of the needle valves in the bottom cap
7. Run the pump at a rate of 1 mL/min, and wait until any trapped air comes out and only water flows out of the second needle valve in the bottom cap
8. Stop the pump and close the second needle valve
9. Unscrew the bleed screw in the bottom side pressure transducer which is part of the pump's connecting line
10. Turn the pump on at 1 mL/min
11. Bleed any air in the transducer
12. Stop pump and replace the transducer's bleed screw
13. If fluid inside vessel is at atmospheric pressure, the vessel if ready
14. If fluid inside vessel is pressurized
    a. Inject water at a slow rate (1-5 mL/min, the rate will depend on the initial pressure of the fluid), the water reservoir pressure will increase until it is at equilibrium with the pressurized fluid in the chamber opposite to the piston
    b. When the pressure is equal or there is a slight increase in the top chamber, stop the pump. A slight increase should indicate the piston has moved
    c. If the pressure increased in the top chamber, bleed out a small amount of water from the bottom needle valve until the pressures are at equilibrium. If needed run the pump again until the equilibrium pressure is reached

Do not run the pump in reverse to reach the equilibrium pressure. During the course of these experiments, it was discovered that running the pump in reverse and then immediately forward and starting compression from that point would produce a distorted/larger compressibility calculation in the first data point. In the case of a low compressibility fluid such as water it occurred in the first couple of data points.

4.1.4 Compression Data Collection Procedure

1. Record the temperature in the room.
2. Record the starting pressure if pressurized fluid is being tested, otherwise pressure readings should be 0 psi. For this set of experiments the pressure reading from the pump was used. The pressure reading of the transducers was recorded as redundant data, but was not utilized for to calculate compressibility of the fluid.
3. Record the reservoir volume in the pump to the nearest one hundredth of a mL
4. Run the pump to inject water in the bottom chamber, the rate will depend on the fluid being tested and/or its initial pressure. For low compressibility fluids such as water and cement slurry, a rate of 1-2 mL per minute was used. For fluids such as gases at atmospheric conditions, the initial rate was up to 80 mL/min and slowly decreased as the pressure inside the vessel increased, usually down to 1-2 mL/min. When the vessel was loaded with a pressurized gas or foam, the initial rate used was between 10 to 50 mL/min depending on the fluid's initial pressure.
5. Stop the pump at least every ~100 psi pressure increase intervals. The intervals will depend on the fluid being tested and/or its initial pressure, or if an increased data resolution was targeted at certain pressure intervals

6. Wait 1 min and let the system equilibrate. The pressure reading will immediately drop as kinetic drag forces are not in place anymore. The pressure might further drop, 1 to 2 psi usually and then become constant
7. Record the pressure and the new reservoir volume.
8. Repeat steps 3 to 6 until a targeted pressure of 2000 to 2200 psi is reached.
9. Run the pump in reverse until initial pressure in the top chamber is reached
10. Carefully bleed any pressurized fluid if needed
11. Disconnect the vessel from pump
12. Disassemble the vessel and clean all of its components, being especially meticulous if cement or foamed cement had been compressed

4.1.5 Foam/Foamed Cement Mixing Procedure

The mixing procedure in order to generate foams and foamed cement is very similar to steps 2 to 9 in section 3.1.3.

1. Measure the mass of recipe components
2. Place the water in the mixing cup
3. Add surfactant into the water in blender
4. (Optional) If nanoparticle dispersion is to be used, stir water surfactant/mix gently with glass stirring rod prior to adding nanoparticle dispersion. When surfactant is evenly mixed, add nanoparticle dispersion it into the blender
5. Place the top in the blending cup and turn blender on at the 4,000 rpm setting
6. (Optional) If foamed cement is to be mixed, carefully and steadily add cement

7. Change the mixer setting up to 12,000 rpm. Carefully remove the top and observe the mixture. Let mix stir until foam does not seem to increase in volume and has achieved its maximum air entrainment/quality
8. Turn off the mixer
9. Take density measurement if foam quality is to be calculated

4.1.6 Foam Stability Testing Procedure

In order to choose a surfactant or surfactant combination to make foams and foamed cement, foam stability tests were performed. The tests involved generating foams, measuring a known volume, and observing the rate at which the foam's quality diminished over time as the foam broke.

1. Generate a foam using procedure in section 4.1.5
2. Take density measurement (can be done at same time as step 3 as long as mass of graduated cylinder is taken into account)
3. Pour foam into graduated cylinder. The sample volume chosen was 250 mL. A 250 mL graduated cylinder was used. The cylinder had markings every 2 mL
4. Record time
5. Observe foam as it breaks over time. Different time intervals were used depending on the foam as some were more stable than the others. At each interval record time, the total remaining volume and the liquid volume that has settled the bottom

4.2 DATA ANALYSIS

4.2.1 Vessel Volume Measurements

In order to calculate an accurate volume of the compression vessel, a series of experiments were performed in which water was pumped using the ISCO syringe pump and observing when the vessel became full of water. The pump has a digital reading that displays the volume of its fluid reservoir. The compression vessel was set with the piston at the bottom and both caps were fully tightened. The ISCO pump reservoir was filled with DI water, any air in the reservoir and connecting line was bled. The reservoir volume was recorded at this time. The line was connected to the compression vessel through one of the top needle valves and the pump was ran until water came out of the second needle valve at the top. At this point the pump was stopped and the final reservoir volume was recorded. The following equation was used to calculate the volume of the vessel:

$$V_{vessel} = Vreservoir_{initial} - Vreservoir_{final}$$

This calculation was performed prior to running each of the experiments where the fluid tested was initially at atmospheric conditions. The reason for this was to account the for any volume variability, however small, from the initial position of the piston and the final position after tightening the end caps. Analogous measurements were performed in a few compressibility experiments where the piston was not inside the vessel. For experiments where the vessel was filled with a pressurized fluid that displaced the piston as the vessel was filled, five vessel volume measurement were performed and the average of these five was used.

4.2.2 Foam Stability Tests

As an indication of foam stability in order to choose a surfactant, the foam volume fraction change over time was used. Foam fraction *f* was the volume fraction of the total sample volume occupied by foam.

$$f = \frac{V_{foam}}{V_{Total}}$$

It is important to mention that for each of the foams tested, the initial quality was slightly different, and the total volume (foam + liquid) level decreased at different rate.

4.2.3 Compressibility Calculations

The compressibility *c* of each fluid was calculated using the following equation:

$$c = -\frac{1}{V_0}\frac{\Delta V}{\Delta P}$$

where V_0 is the initial volume occupied by the fluid, ΔV is the change in volume and ΔP is the change in pressure. The compressibility was calculated at various ΔV-ΔP intervals and relative to a V_0 of the previous interval and not the absolute V_0. A sample calculation has been performed with data shown in Figure 4.5.

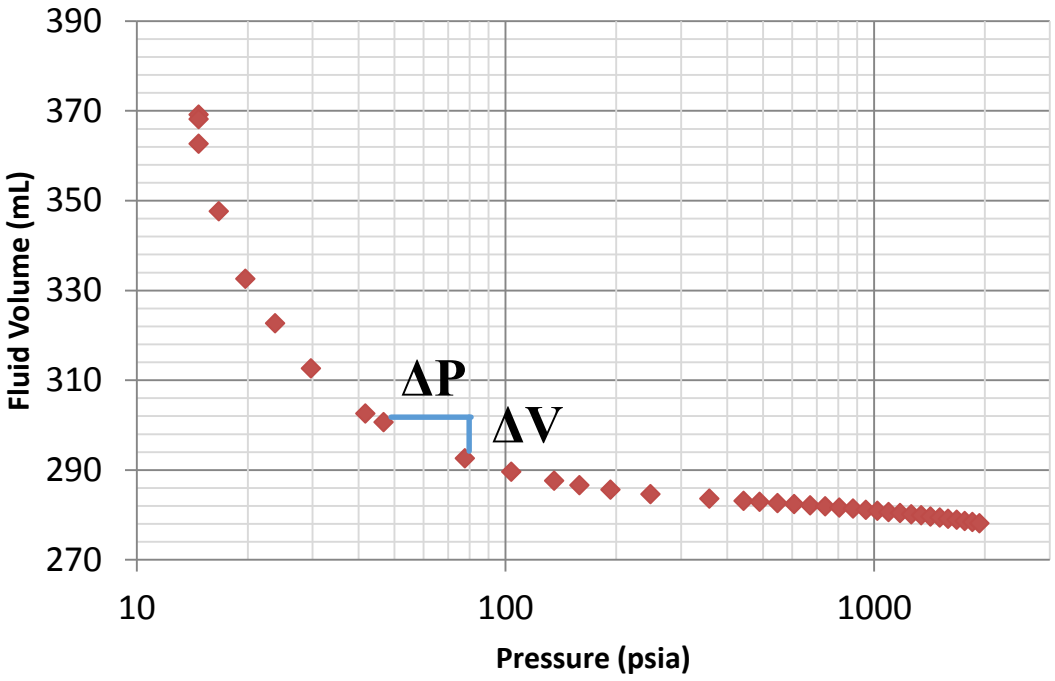

Figure 4.5 Semi log plot of sample experimental data showing a fluid's change in volume ΔV with an increase in pressure ΔP. These measurements were used to calculate compressibility.

The compressibility for the selected data points can be calculated as following

$$c = -\frac{1}{302.64\ mL}\ \frac{292.31 - 302.64\ \text{mL}}{78.5 - 46.5\ \text{psia}}$$

$$c = \frac{0.001067}{psia}$$

Once compressibility had been calculated for each of the steps, it was plotted in a log-log plot. Depending on the fluid whose compressibility was measured, a reference compressibility line was plotted in order to compare the calculated data with the compressibility of an ideal fluid of the same composition.

4.2.4.1 Effect Water/Brine and Apparatus Compressibility

In the first set of experiments where gases or gas + water mixtures (G/W) were to be compressed, the compressibility of the volume of water used to drive the piston and the compressibility of apparatus were assumed to be zero due to their low compressibility relative to gases. In these initial calculations, it was assumed that the entire measured volume change was attributed to the volume being occupied by gas in the system. It was later concluded that this had not been a good assumption. The initial comparison standard was the compressibility of air calculated from data obtained from the National Institute of Standards and Technology (NIST). Since water and the apparatus (system) were disregarded, the compressibility of air, over the pressure range utilized, was very similar to that of an ideal gas c_{IG}. Derived from the ideal gas equation of state, c_{IG} is the reciprocal of the absolute pressure; in a log-log plot, compressibility vs. pressure is a straight line of slope -1.

$$c_{IG} = \frac{1}{P_{abs}}$$

After running a few experiments, the effect of ignoring the system's compressibility became more and more noticeable when compressing gases from atmospheric to pressures between 500-1000 psia and higher, where calculations would sometimes show an inflexion point in compressibility and it would appear to increase instead of decrease linearly. This was recognized to be due to the system's compressibility. It was then decided to break down the measured compressibility into its individual components, gas and/or water in the testing side, and the system. The system's compressibility included the pump, water in pump's reservoir, vessel, lines etc.

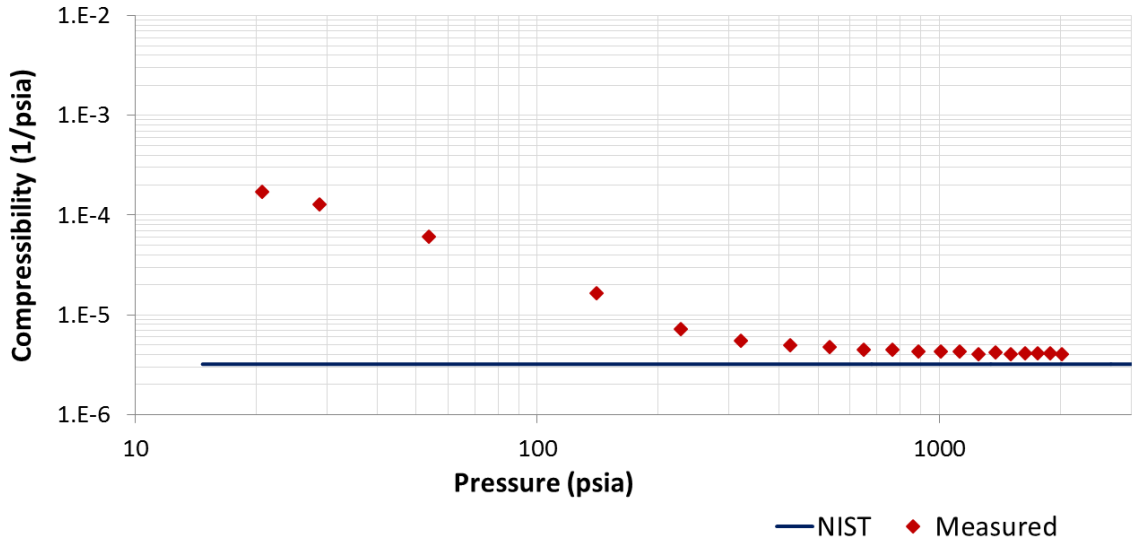

Figure 4.6 Log-log plot comparing the measured compressibility of water in the apparatus used in this research vs. NIST data.

The method to estimate the compressibility of the apparatus was by measuring the compressibility of water in the system and then comparing such values with data available from NIST. Any difference between the available values for the compressibility of water and the measured compressibility was attributed to be the apparatus's compressibility. The average compressibility of water at 68 °F over a pressure range between 14.7 and 2000 psia was calculated to be ~$3.17*10^{-6}$/psia (NIST, 2013). Figure 4.6 shows the difference between the measurements taken in one of the experiments in which water was compressed and the reference value of water compressibility obtained from NIST. The apparatus appeared to have different compressibility contributions at different pressures. In the higher pressure range (>300 psia) the average measured compressibility was found to be ~$4.2*10^{-6}$/psia. The difference between the measured and NIST data was calculated to be ~$1*10^{-}$

^{6}/psia. The compressibility measured across range between 200 and 2000 psia yielded an average value of ~4.6*10^{-6}/psia. These two values were used to adjust for the compressibility of the system in the measured data. The larger value was used for experiments when the initial pressure of the fluid was between 14.7 and 100 psia. The smaller for initial pressures greater than 100 psia.

The reference compressibility utilized for fluids such as foam where gas and water are in direct contact with each other was considered to be that of a G/W mixture of two bulk phases in the same initial volume proportions as the foam. When calculating the compressibility of these reference ideal G/W mixtures, it was critical to know the initial volume fraction and subsequently calculate the new volume fraction and total volume at every pressure step. To account for this compounded effect, the compressibility equation was used in the following form:

$$c_{tot} = f_{water}c_{water} + f_{gas}c_{gas}$$

$$c_{tot} = -\frac{1}{V_o}\frac{(\Delta V_g + \Delta V_{w})}{\Delta P}$$

$$\Delta V_i = f_i * V_o * c_i * \Delta P$$

where V_i is the volume of component *i*, f_i is the volume fraction of component *i* and c_i is the compressibility component *i.* The latter equation means the gas volume decreases rapidly compared to the water volume as pressure increases. Consequently the contribution

of the gas phase to the G/W mixture compressibility eventually becomes small even though the gas phase itself remains much more compressible than the water.

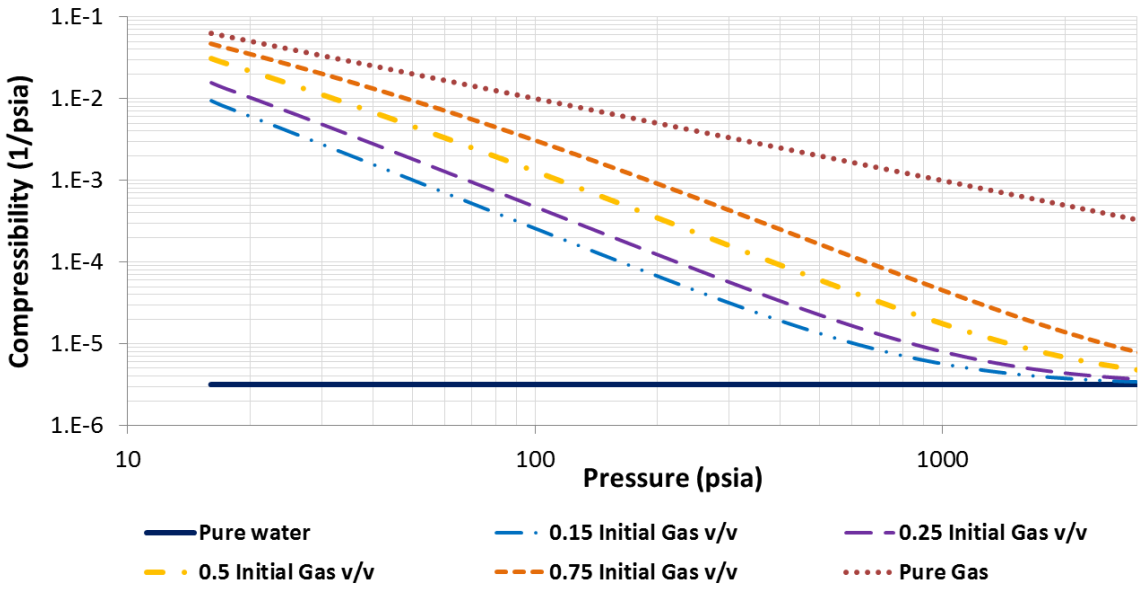

Figure 4.7 Theoretical compressibility of various ideal G/W mixtures initially at P_0=14.7 psia.

Figure 4.7 illustrates the compressibility of G/W mixtures with different initial gas fractions computed from the equations above (recall gas v/v *100 = quality %). In this case, all mixtures are initially at atmospheric pressure and behave ideally upon compression. The compressibility of water for this and all subsequent calculations was considered to be $3.17*10^{-6}$/psia. The effect of gas dissolution into the aqueous phase is not included in this calculation. The common trend toward the compressibility of water at sufficiently large pressure for all the G/W mixtures can be explained by the fact that gas has much more compressibility than water especially at low pressure. The gas volume is therefore greatly

reduced over the displayed pressure range and at large pressure its volume fraction contributes very little and thus the overall compressibility of the mixtures behaves mostly like pure water.

Figure 4.8 show an example of experimentally collected data. In this case air in direct contact with water was compressed inside the vessel. After loading a known water volume at atmospheric conditions, pressurized air was loaded into the vessel and was initially at 89 psia. The red marks represent the measured compressibility of this air/water mixture. In this case the data was compared to an equivalent ideal G/W system in which the initial gas quality at 89 psia was 49.4% = 0.494 gas v/v. The very close agreement shows that the apparatus is behaving as planned and that solubility of air in water has a minor effect in this particular experiment (see next section). It is important to notice that that the reference ideal G/W mixture from Figure 4.8 also has an initial pressure of 89 psia and cannot be directly compared to any of the lines in Figure 4.7.

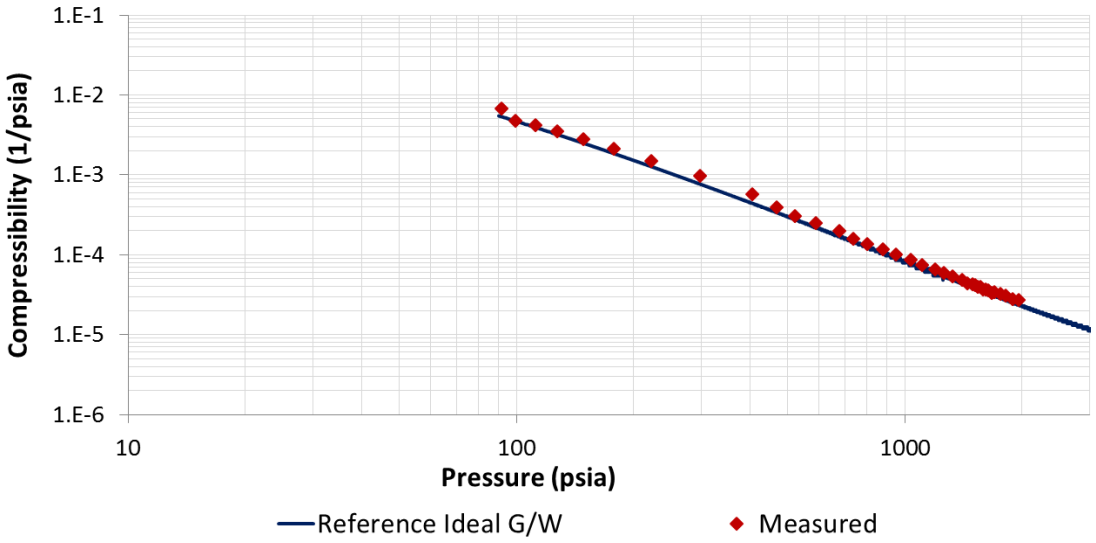

Figure 4.8 Example of comparison between measured data of an air + water system with an initial quality of 49.4% to an ideal system with the same initial component volume fractions

4.2.4.2 Effect of gas solubility

The effect of gas solubility was initially not taken into consideration, but later it became evident that in some experiments it was important whenever gas and water were in direct contact with each other. The effect became most noticeable in stable foams (G/W mixtures) that were generated at atmospheric pressures and were subsequently compressed. It was presumed this occurred due to the much larger G/W contact surface in foams which in consequence increased the rate of mass transfer (dissolution of gas into water). For air + water mixtures, the potential effect of gas dissolution effects was approximated using Henry's Law constants. For the pressurized foam generation experiments in Chapter 5 where pure nitrogen was used, experimental data from Wiebe et al (1933) was utilized. A Henry's constant of $1.3*10^{-3}$ mol/(L*atm) was used for oxygen and a constant of $6.1*10^{-4}$

mol/(L*atm) for nitrogen (Sander, 1999). The constants were converted into cubic centimeters of gas at a standard temperature and pressure (25 °C, 1 atm) per gram of water in order to compare it to nitrogen experimental data from Wiebe et al (1933).

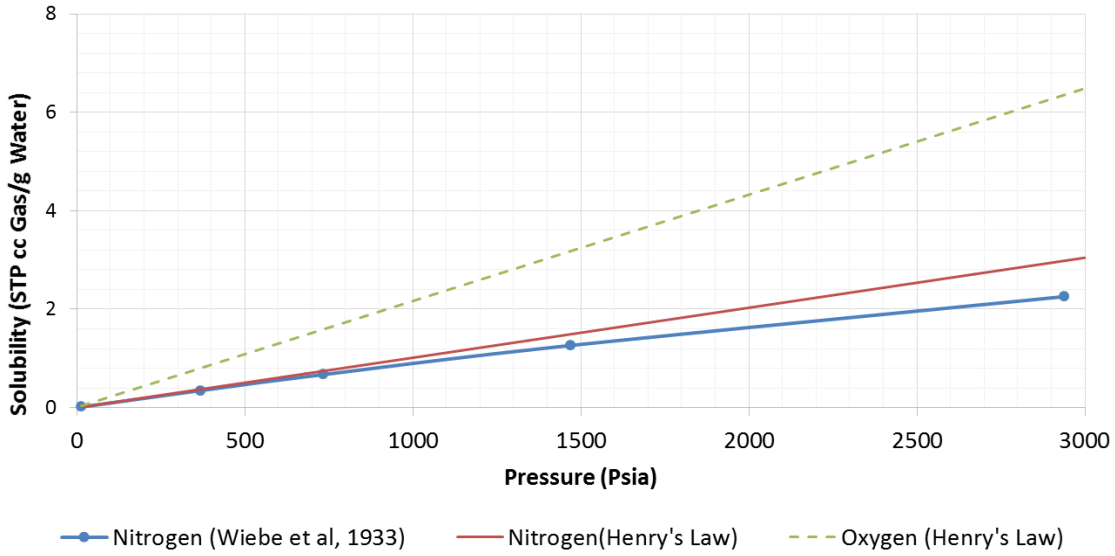

Figure 4.9 Solubility of nitrogen and oxygen in water

Figure 4.9 shows the theoretical maximum amounts of dissolved gas at any given pressure, but since gas dissolution is a mass transport process the exact quantity of dissolved gas at any given time inside the vessel was not exactly known. This is because the time interval between pressure steps was rather short (~ 1 min) and the vessel was not stirred. Thus the time required to reach the equilibrium concentration of dissolved gas was likely longer than the time available. Figure 4.10 illustrates the effects of dissolution in compressibility in the extreme cases where maximum gas dissolution took place, i.e. the time interval before the next increment in pressure was extremely long. Two cases are

presented, one is an air + water mixture of 75% initial quality (purple line) and its corresponding theoretical curve (green line) neglecting dissolution, and a 25% initial quality (orange line) and its reference (blue line). The starting pressure for all these calculation was 14.7 psia. The bounding curves for gas only (red) and water only (blue) are also shown.

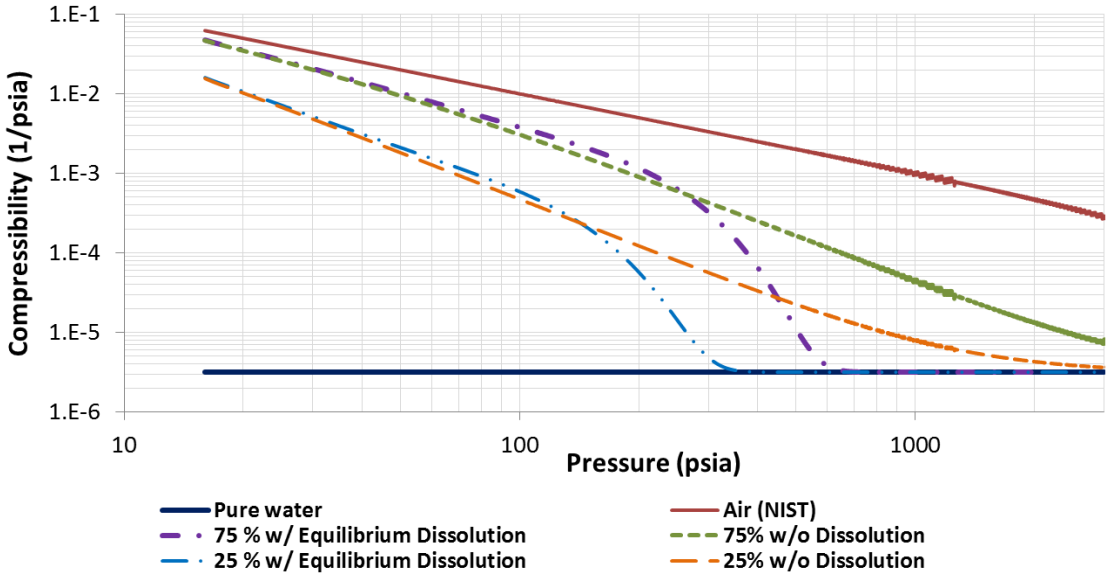

Figure 4.10 Potential effects of air dissolution in compressibility. The Henry's law constant of air is assumed to be 8.032*10^-4 mol / (L*atm). Compressibility with dissolution was calculated at G/W equilibrium conditions.

As figure 4.10 shows, at low pressures air solubility is manifested as an apparent increase in compressibility. The purple and blue dashed curves lie slightly above the green and orange curves respectively at pressures below 250 psi and 150 psi respectively, but as the gas volume fraction decreases due to the combined effects of compression and dissolution, solubility appears as a larger apparent compressibility.

As described in the subsequent results and conclusion sections, in order to minimize solubility effects, the nanoparticle stabilized foams tested in chapter 5 were generated under pressure. The main purpose of considering dissolution was to describe certain trends in the compressibility behavior in specific experiments. These effects will be discussed in section 4.3 and 4.4 will only be compared in a case by case basis and when deemed necessary.

4.3 Results and Discussions

4.3.1 Compression Vessel Volume

Measurement	Volume (mL)
1	377.83
2	377.58
3	378.25
4	377.9
5	378.21
Average	377.95

Table 4.1 Compression vessel volume measured by injecting water inside the vessel

4.3.2 Foam Stability and Viscosity

Three recipes were tested for stability in order to choose a surfactant to make foam and foamed cement. Once a surfactant was chosen, the chosen surfactant's foam viscosity was measured. Subsequently, Cembinder W50 nanoparticles were added to same foam

recipe. The foam with nanoparticles stability and viscosity was also measured to compare its properties to the reference foam.

The three initially tested recipes can be seen in Table 4.2. All surfactant concentrations were based by weight of water (bwow) percent. Any surfactant added, replaced the denoted percentage water weight of the original recipe's water mass. In these recipes where only surfactant and water are the components, % bwow is equal to % wt. In later recipes where cement or nanoparticles were components, this is not the case. The initial quality after mixing was also recorded for each foam.

Foam	Water (g)	AOS Witcolate 1247 H (g)	CAPB Petrostep CG-50 (g)	Amine oxide Aromox APA TW (g)	Initial foam quality (v/v %)
AOS+CAPB 4% bwow	201.6	5.6	2.8	X	83
AOS+CAPB 8% bwow	193.2	11.2	5.6	X	78
Amine Oxide 9% bwow	191.1	X	X	18.9	64

Table 4.2 Foam stability test recipes.

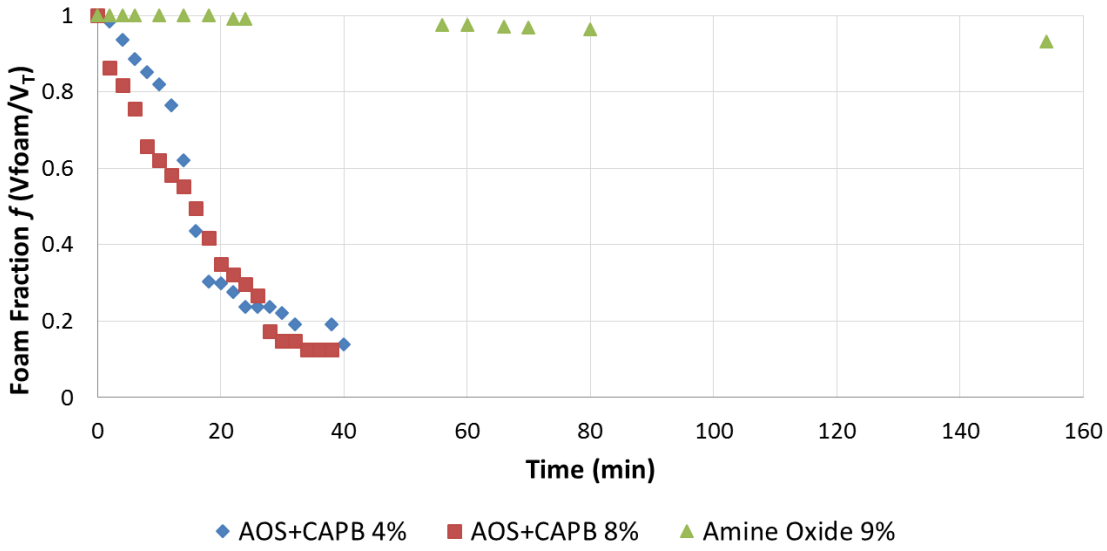

Figure 4.11 Foam stability of recipes from table 4.2 observed at atmospheric pressure. The AOS+CAPB 4% initial foam quality was 83%, the AOS+CAPB 8% foam was 78% and the Amine Oxide 9% foam was 64%.

Figure 4.11 shows the results of the foam stability test. The 4% and 8% bwow AOS+CAPB foams (blue and red series respectively) showed similar large scale aging behavior. Even though it had a lower surfactant concentration, the 4% bwow (blue) did achieve a greater initial quality. Both foams began to significantly break almost immediately after being mixed. At 20 minutes both mixtures were less than 50% foam by volume and the top half of the foam were bubbles that appeared much larger than the ones in the lower half. After around 40 minutes both were less than 20% foam by volume and mostly relatively large bubbles remained. The 9% bwow amine oxide foam (green) had the best long term stability. It was all foam after 20 minutes and at 22 min the first liquid collected at the bottom. The bubbles at the top did appear to have grown relative to the bottom during this period. After 80 minutes it was still 96% foam by volume. At this point

it was decided to use the amine oxide surfactant since the length of a compression experiment was roughly an hour after loading the vessel. Based on the stability of the amine oxide foam, it appeared the foam would endure over the course of the compression experiment and presumably remain a foam during the process.

Cembinder W50 nanoparticles were added to the same amine oxide foam recipe to observe if its stability would be affected. The amount of nanoparticles added was based on recipe "H + 0.5% bwoc Cembinder W50" found in section 3.1.5. Mass of water and amine oxide in the mix remained the same, since the nanoparticles were bwoc, they were just an additional component in the mixture. The amount of water and surfactant totaled 210 grams in the reference recipe, thus the amount of particles was adjusted to maintain the 0.38 water to cement ratio. The amount of Nanoparticles used was 2.76 grams.

As the foam with nanoparticles was being poured into the graduate cylinder for the stability test, it was qualitatively observed to have a distinctive viscoelastic behavior. At this point a sample of the batch was then immediately tested in a rheometer to quantify its rheological properties. Subsequently, a new batch of the reference foam without nanoparticles was mixed in order to quantify its rheological properties as well. Although expected to be relatively similar, the fact that this foam batch and the previously mixed for the stability test had the same quality (64%) was a mere coincidence. However, it was assumed that their rheological properties would be comparable since they were made from the same recipe and had the same initial quality.

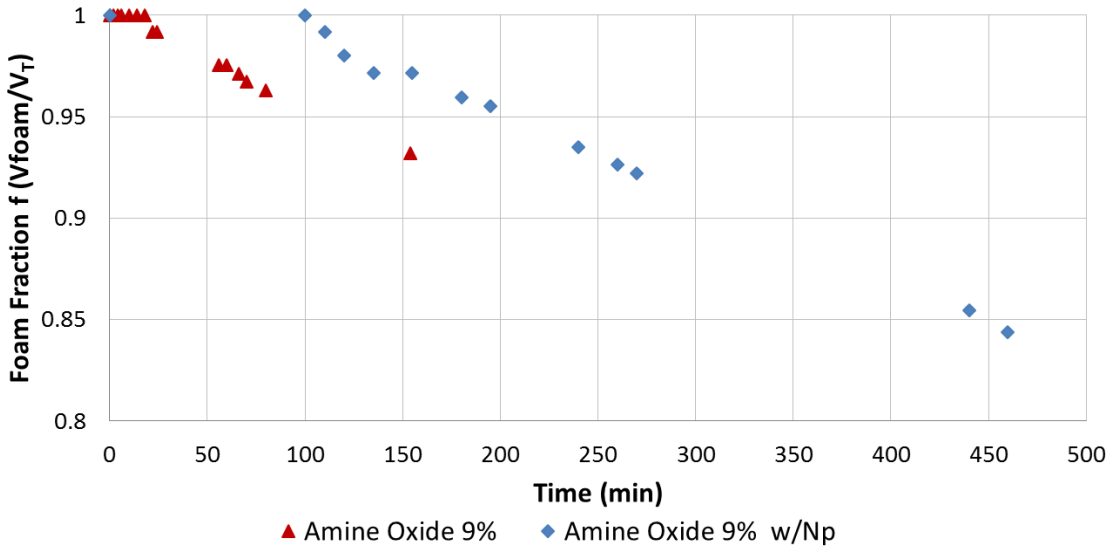

Figure 4.12 Foam stability of Amine Oxide 9% bwow + Cembinder W50 Nanoparticle 0.5% bwoc foam and reference Amine Oxide 9% bwow foam. The foam with nanoparticles had an initial quality of 65% and the reference foam had an initial quality of 64%.

The foam with Cembinder W50 nanoparticles exhibited greater stability than its equivalent without the nanoparticles. The foam without nanoparticles had liquid settle at the bottom after ~22 min vs. the foam with nanoparticles which had the first liquid settle after about ~100 minutes. At ~155 min, the mix with nanoparticles was still ~97% foam and the mix without was ~93% foam. At all points up to ~155 minutes, the foam with showed a consistent larger percentage of foam volume fraction.

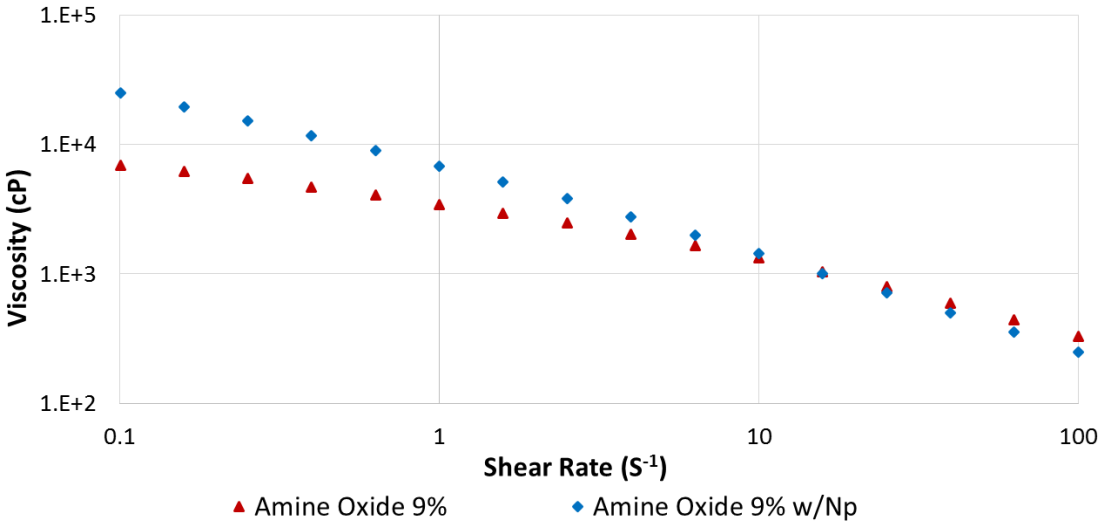

Figure 4.13 Semi-log plot comparing foam bulk viscosities of the Amine Oxide 9% bwow recipe with and without nanoparticles. Rheometer's reference temperature was set 25 °C

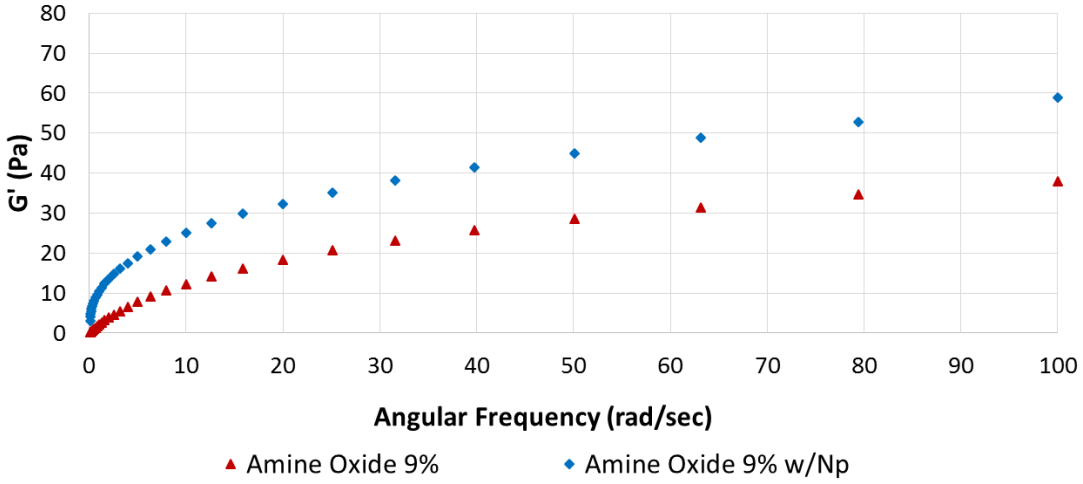

Figure 4.14 Comparison of foam G' (elastic) component of the Amine Oxide 9% bwow recipe with and without nanoparticles. Rheometer's reference temperature was set at 25 °C.

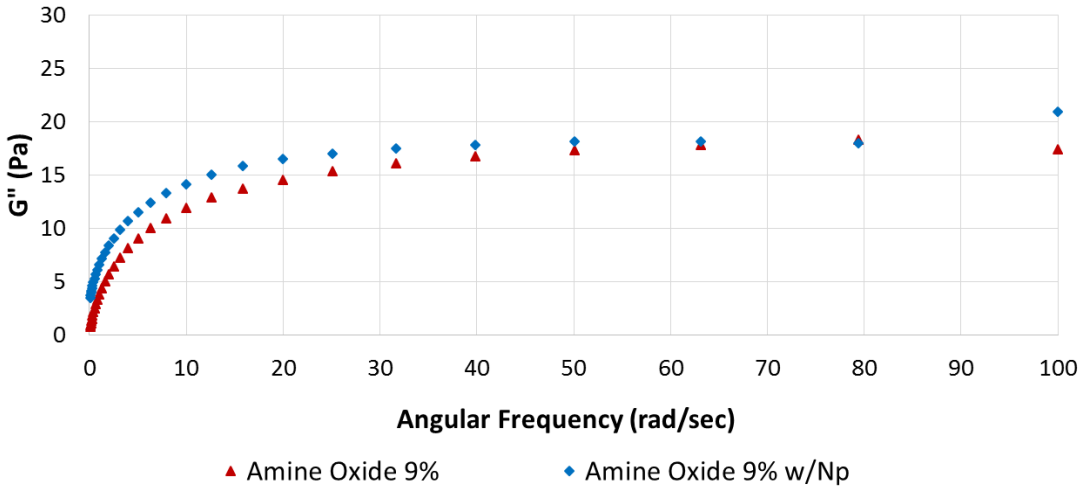

Figure 4.15 Comparison of foam G" (viscous) component of the Amine Oxide 9% bwow recipe with and without nanoparticles. Rheometer's reference temperature was set at 25 °C.

The foam with nanoparticles showed a larger bulk viscosity at shear rates between 0.1 and 20 s^{-1}, at which point the foam without nanoparticles had the larger bulk viscosity put the maximum shear rate of 100 s^{-1}. The elastic component, G', was consistently larger in the foam with nanoparticles. Finally the foam's viscous component, G", was larger in the foam with nanoparticles at shear rates between 0.1 and 80 s^{-1}. Between 80 and 100 s^{-1} the foam without nanoparticles showed a larger G" reading.

The fact that the foam with nanoparticles displayed different rheological properties was not used to conclude that nanoparticles were stabilizing the foam, but to note that distinguishable rheological properties were observed. Combined with the subsequent results found in section 5.3.1, it was concluded that the likely explanation was gelling caused by nanoparticle instability due to surfactant concentration.

4.3.3 Compressibility of Various Test Fluids

4.3.3.1 Compression of Water

The first compressibility measurements were made with DI water as the test fluid. Since the compressibility of water is a value easily found from literature, it was decided it would be a good fluid to test in order to validate the functionality of the apparatus.

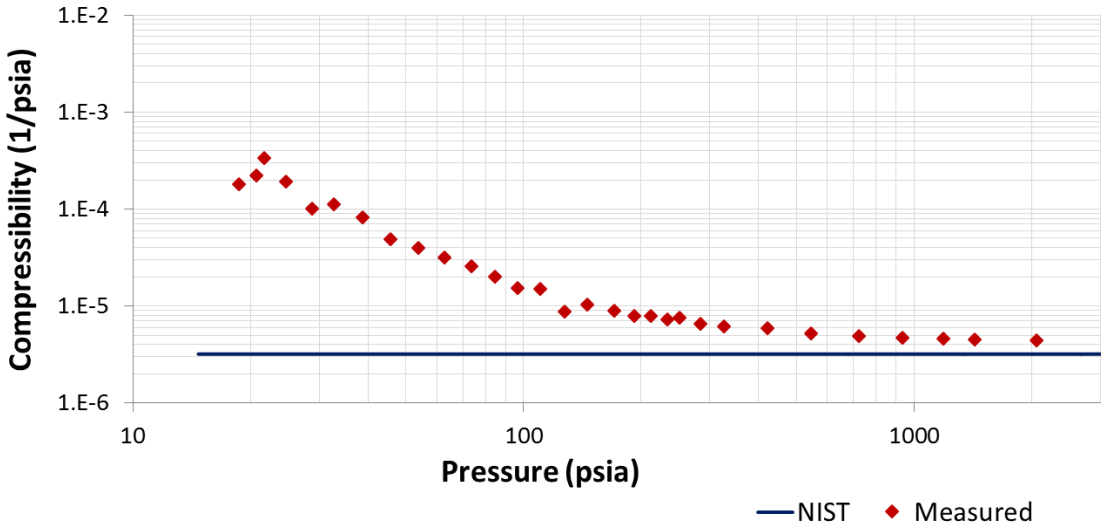

Figure 4.16 Compression of water experiment #1.

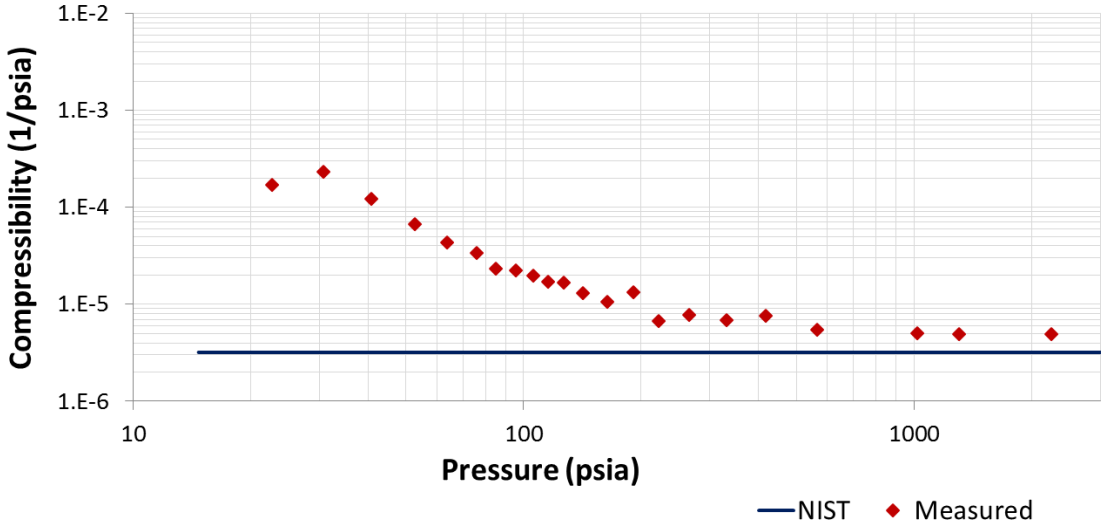

Figure 4.17 Compression of water experiment #2.

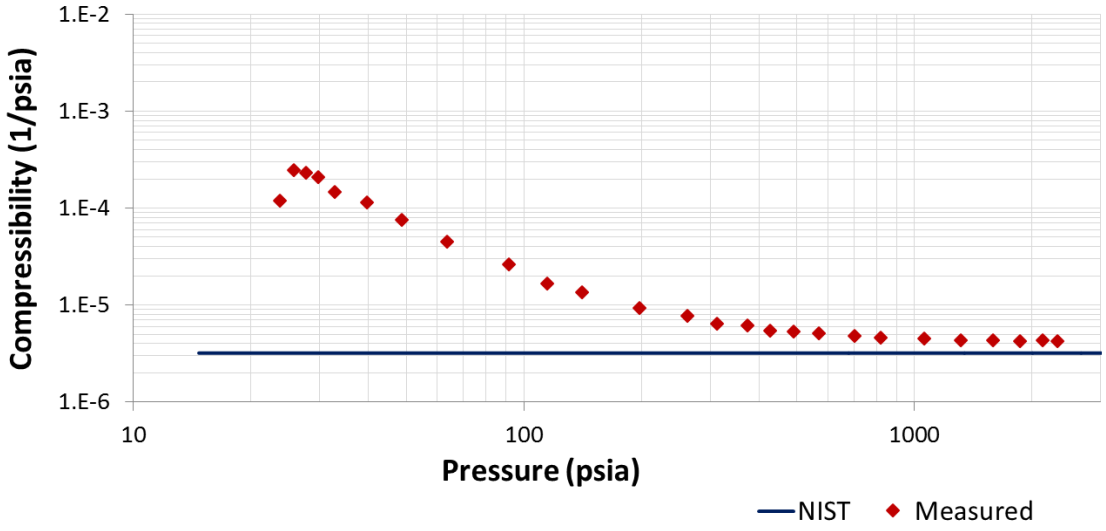

Figure 4.18 Compression of water experiment #3.

Experiments #1 to #3 show a larger compressibility than that researched from NIST, especially at pressures lower than 300 psia; at which point the measured valued begin to converge to the NIST value. This was attributed to the compressibility of the apparatus itself. At this point it was also suspected that running the pump immediately forward after running it in reverse caused some inaccuracies in the measurements.

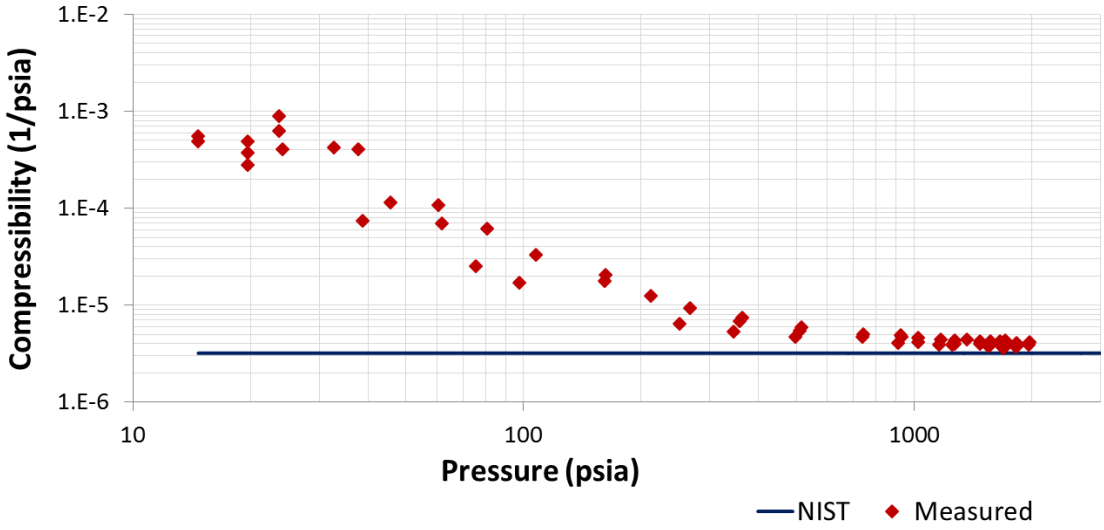

Figure 4.19 Compression of water experiment #4. Experiment performed measuring compressibility every two consecutive pressure increments and then one reduction. Purpose of the experiment was to prove variability of running syringe pump forward and in reverse.

Experiments #4 was done to confirm the suspicion that running the pump in reverse caused some measurement inaccuracies. The measurement variation appeared to diminish at pressures higher than 300 psia. After this point protocol was adjusted to run the pump forward and bleed a few milliliters of water from the pump's reservoir prior to running any experiments.

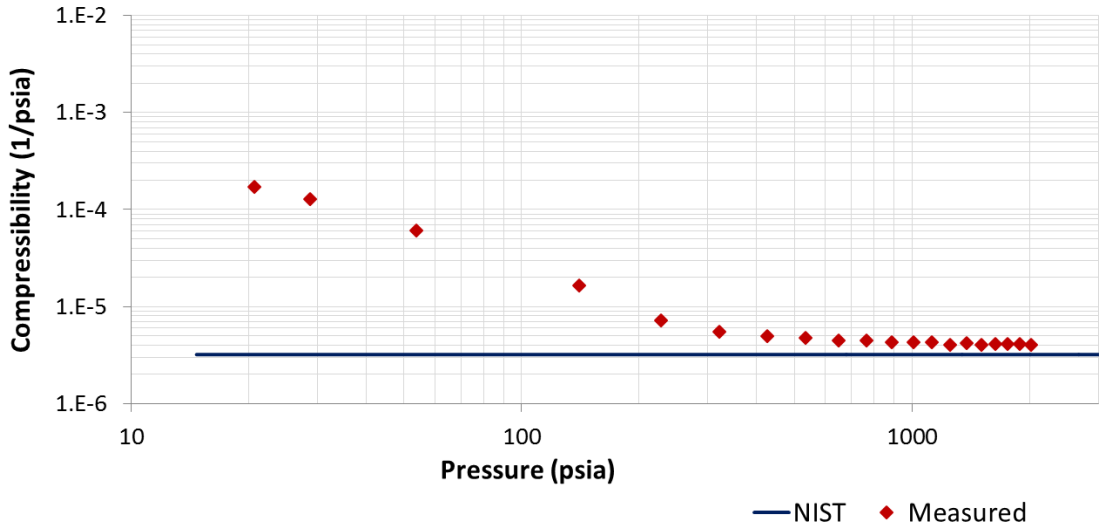

Figure 4.20 Compression of water experiment #5.

The convergence to the value for the compressibility of water from NIST was attained faster in experiment #5 by running the ISCO pump forward and purging a few milliliters of water first and then performing the compression experiment. Experiment shows further proof that running the pump forward immediately after running it in reverse to fill the reservoir caused noise in the measurements. For future experiments it was presumed the gas phase would have relatively much larger compressibility than that of the system at low pressures and thus this difference from the compressibility of water would not be of much significance. Additionally it was concluded this effect could be further diminished by starting the experiments with a pressurized testing fluid.

4.3.3.2 Compression of CO2

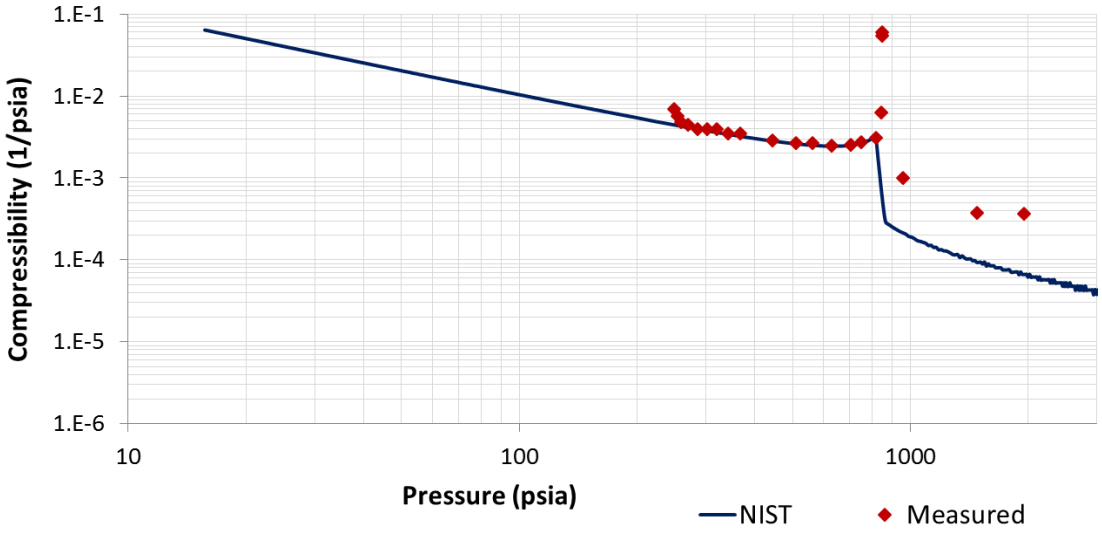

Figure 4.21 Compression of CO_2. NIST CO_2 compressibilities at 68 F (line) are consistent with measurements in the compression cell at room temperature (red dots). Divergence in measured data after phase change was presumed to be to the fact not enough time was given for the system to equilibrate during phase change. Main purpose was to observe if phase change could identified.

4.3.3.3 Compression of Air

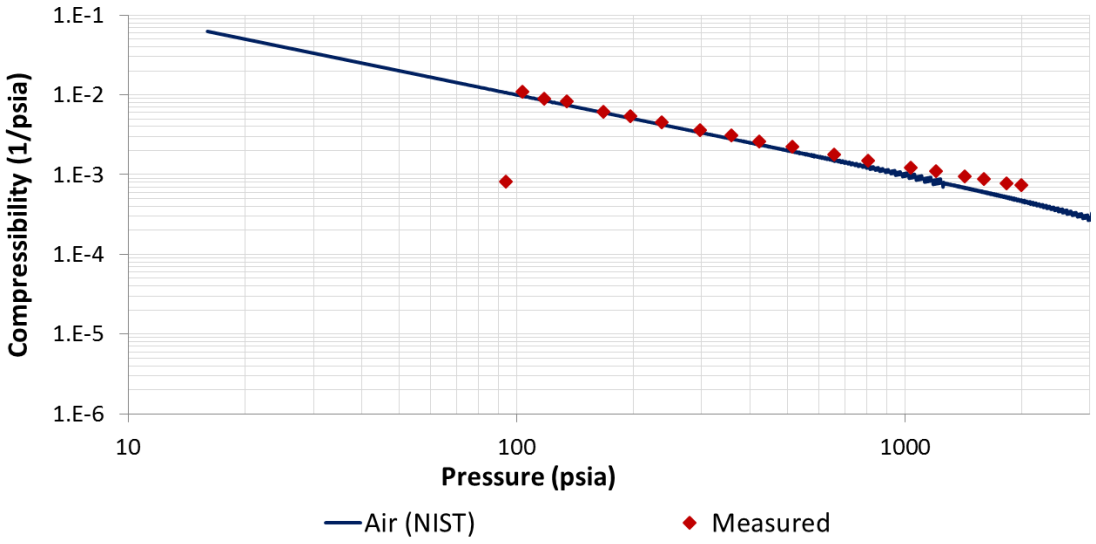

Figure 4.22 Compression of air experiment #1. P_o=68 psia.

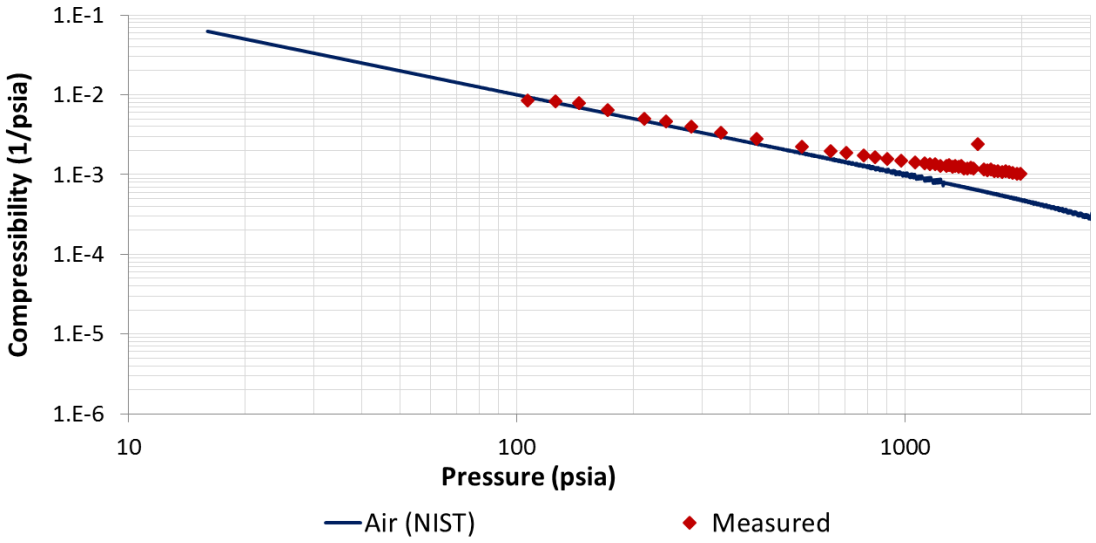

Figure 4.23 Compression of air experiment #2. P_o=91 psia.

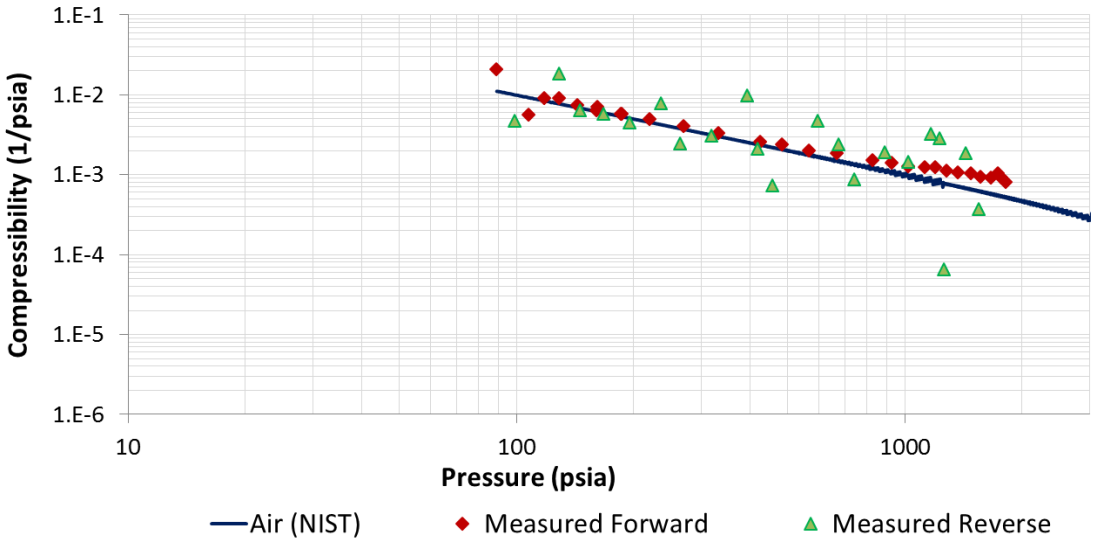

Figure 4.24 Compression of air experiment #3. Air P_o=88 psia. Compressibility was measured by running ISCO syringe pump forward (red marks) and then in reverse (green triangles). The purpose of this experiment was to confirm the effect noticed in compression of water experiment #4 (Figure 4.19) where running pump in reverse showed compressibility measurement inaccuracies.

In the three experiments were air was compressed, there appeared to be a systematic deviation from the NIST data at pressures greater than 750 psia or so. The made it appear as if the compressibility of air was greater than what it should be. This effect was not considered critical for this research as an abrupt reduction in compressibility due to the presence of "armored" bubbles was the sought after behavior. Experiment #3 was done to confirm findings that measurements were inaccurate when running the pump in reverse found when compressing water (Figure 4.19). In experiment #3, the ISCO pump was initially ran continuously forward. Once the measurement at the maximum pressure of ~1800 psia was recorded, the pump was ran in reverse to verify compressibility measurement variation.

4.3.3.4 Compression of Air + Water in Direct Contact

In order to get an idea on how solubility effects on compressibility could be mitigated by increasing the initial pressure of the gas phase in G/W mixtures, a compression of air in direct contact with water was performed. A known volume of water was loaded into the vessel and subsequently the remaining space was filled with compressed laboratory air. The system was left to equilibrate for 5 minutes to let some air dissolve into the water phase.

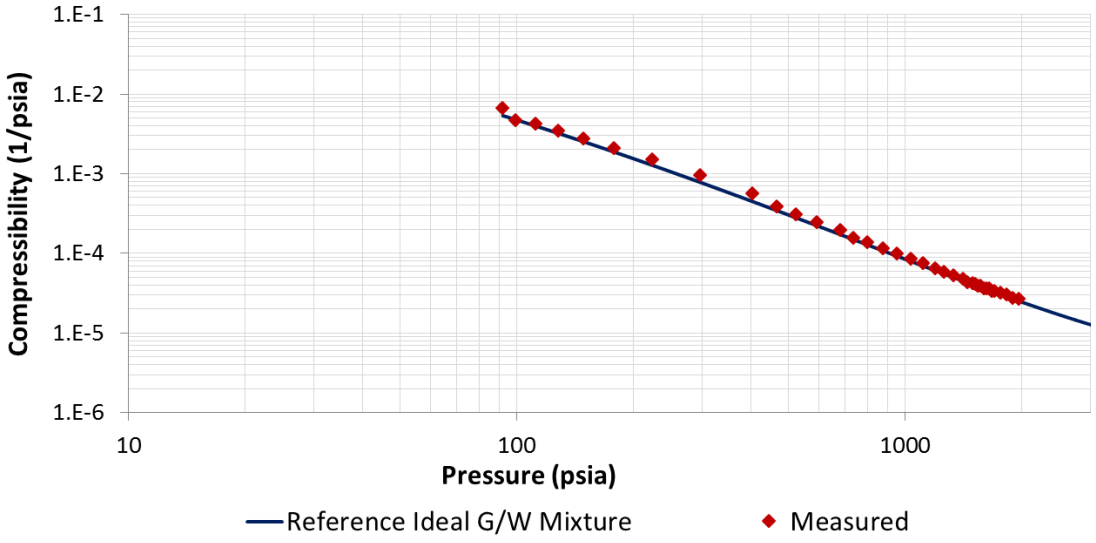

Figure 4.25 Compression of air + water experiment. P_o=89 psia. Initial reference G/W mix initial quality was 49.4%. Air solubility appeared to have minor affects at 1000+ psia, but the overall trend only seemed to have a slight change.

The results of this test show that if the gas phase is initially under pressurized conditions, the effects of gas dissolution will have small effects in compressibility measurements in the chosen time step between measurements of ~1 min.

4.3.4 Compression of Foam and Foam with Nanoparticles

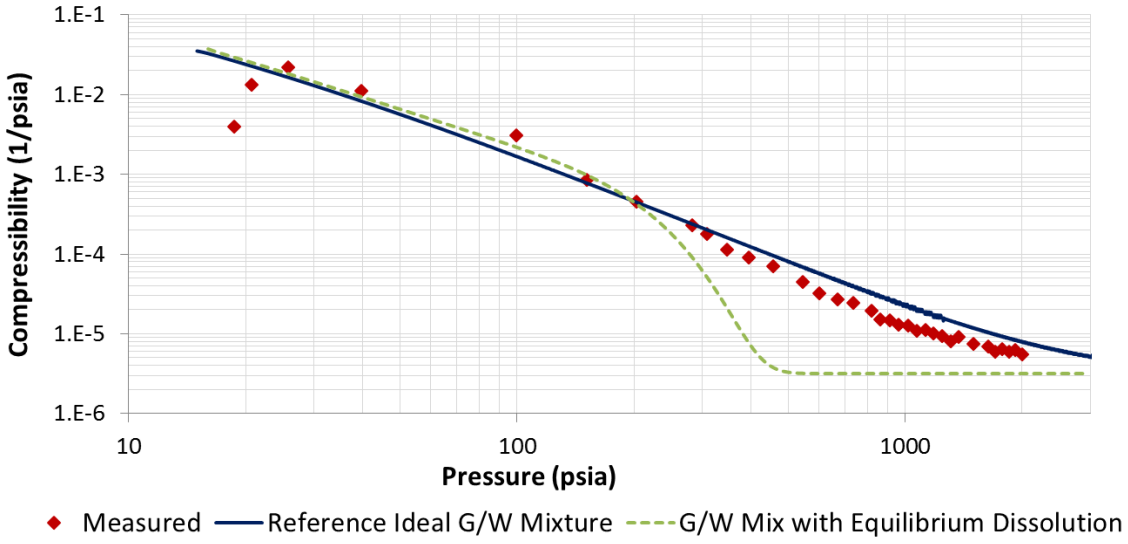

Figure 4.26 Compression of foam experiment #1. P_o=14.7 psia. Amine Oxide 9% bwow recipe used. Initial foam quality 56.3%. Stable foam, some foam remaining at end of compression experiment but was not easily quantifiable. Dissolution effects are noticeable in the experiment (red dots shift toward dashed green curve) presumably due to foam stability which greatly increases G/W interface area and hence the rate of mass transfer during compression experiment time period. In contrast, a simple air/water experiment where air was initially pressurized (larger amount of initial air moles) and there is no foam, thus a small gas/water interfacial area (Figure 4.25). Dashed green curve shows apparent compressibility when gas dissolution goes to equilibrium in the aqueous phase.

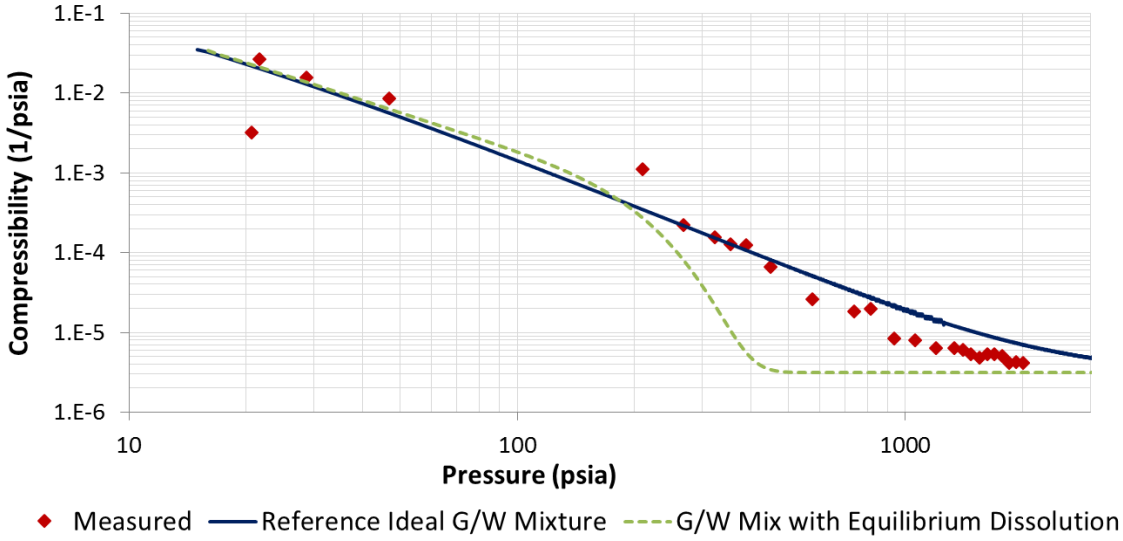

Figure 4.27 Compression of foam with nanoparticles experiment #1. P_o=14.7 psia. Amine Oxide 9% bwow + 0.5% bwoc Cembinder W50 recipe used. Initial foam quality 52.6%. Dissolution effects display a very similar behavior to that in analogous foam without nanoparticles (Experiment #1, Figure 4.26).

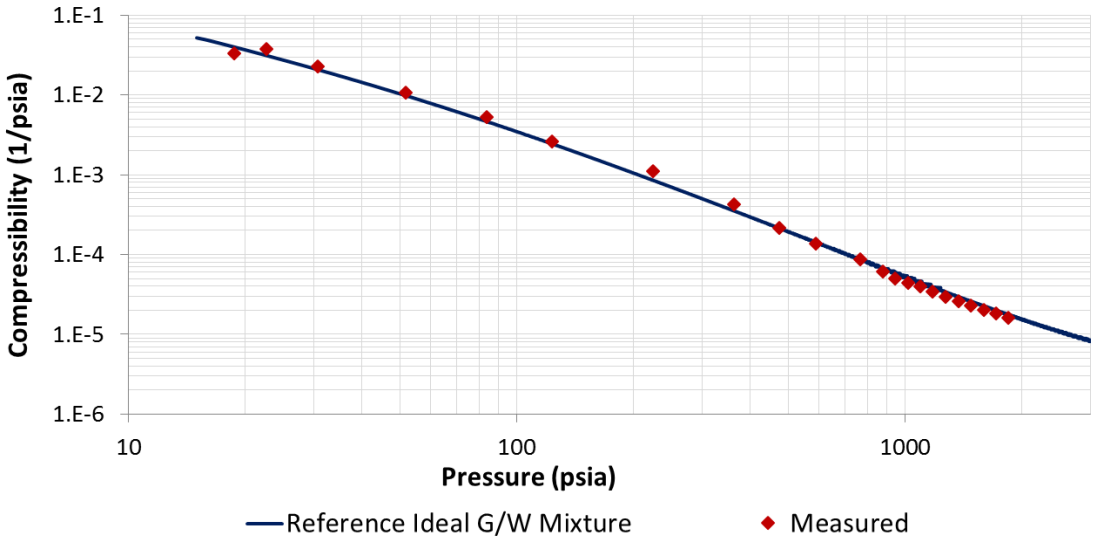

Figure 4.28 Compression of foam with nanoparticles experiment #2. P_o=14.7 psia. AOS+CAPB 8% bwow + 0.6% bwoc Nyacol DP 9711 recipe used. Initial foam quality 77.6%. Known unstable foam recipe used, it all broke during experiment. Dissolution appears to have minor effects likely due to small interfacial area: the foam was unstable, and large relative initial foam quality.

The compressibility of foam made with AOS+CAPB *% bwow + 0.6 Bwoc Nyacol DP 9711 recipe was measured to observe if there was any compressibility behavior difference between the stable and unstable foams, as the foam was not expected to last over the course of the experiment.

Having tested the compression vessel with various fluids, as expected the compressibility data from NIST and the ideal compressibility of a gas/water mixture appears to fit the measured data relatively well. In the tested pressure ranges, the compressibility of most of the G/W mixtures is governed by compressibility of the gas phase, regardless of whether in bubbles or in bulk, until gas volume fraction is so small

that water compressibility dominates. On a log-log plot, for most of these fluids we get a straight line of slope close to -1, recall this is how the compressibility of an ideal gas would behave since $c_{IG} = 1/P$. In the case of G/W mixtures this line begins to flatten almost becoming horizontal as the gas fraction becomes so small that water compressibility begins to dominate. The flattening becomes apparent at relatively low pressures for small initial gas fractions but not until large pressures for large initial gas fraction.

Though gas phase compressibility is the first order influence on gas/water mixture compressibility for much of the pressure range used in these experiments, second order effects become apparent in some situations. When stable foam was compressed, gas dissolution into the aqueous phase accounts for the deviation from the log-log straight line behavior (Figures 4.27 and 4.28). In the experiments where an unstable foam was tested or compressed air was in direct contact with water, dissolution effects over the course of the compression experiments were minor (Figures 4.26 and 4.29). This was likely due to the small G/W interface surface area and lack of time for dissolution to occur (of order 1 min between pressure steps and 1-2 hr total for one experiment).

These observations set the baseline for seeking evidence of armored bubbles, which would be manifested as downward deviations from the trend line between c_{tot} and P. The deviation would arise because a rapid reduction in compressibility of the gas phase, and hence of the gas/water mixture, takes place when the bubbles become rigid. The CO_2 measurements can be used as analogous sought behavior, the phase change (gas to liquid) at the saturation pressure for CO_2 gives a change in compressibility which the apparatus can detect. Nevertheless, assuming the armored bubble effect takes place and the amour's bulk modulus is relatively small, it is possible it could be masked by dissolution.

A last point to recall is that the foams that had nanoparticles had not been determined to be stabilized by the particles. At this point, the most likely explanation was that the foams that did show increased stability was due to the gelling of nanoparticles.

4.3.5 Compression of Foamed Cement and Foamed Cement with Nanoparticles

The same water to cement ratio from Chapter 3 was used (0.38). The presence of cement (cement slurry) greatly reduced the amount of air that could be entrained (foam quality). For reference ideal G/W mixture compressibility, the mass of cement was excluded.

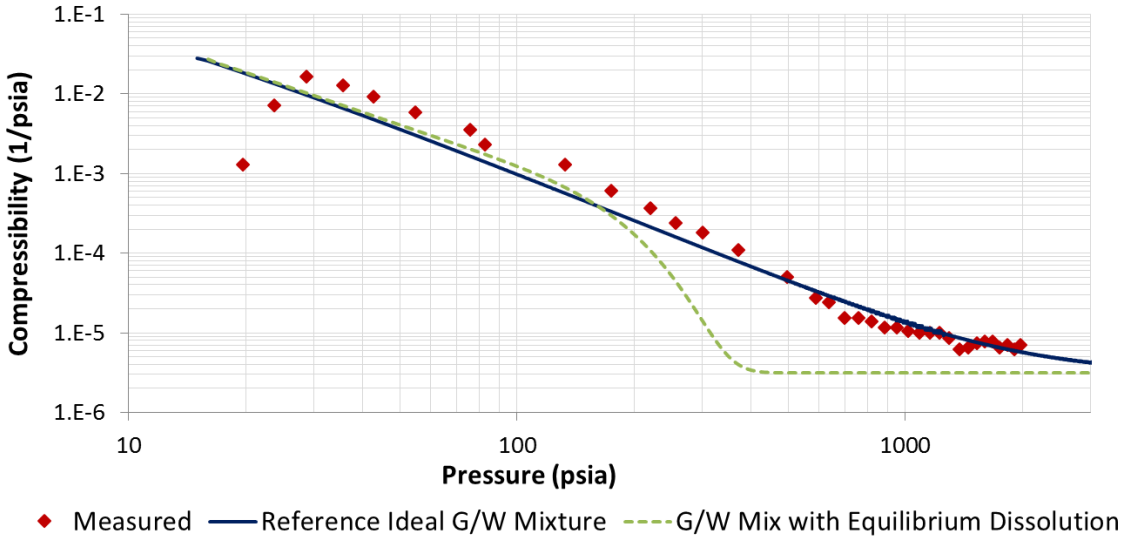

Figure 4.29 Compression of foamed cement experiment #1. P_o=14.7 psia. Amine Oxide 9% bwow foamed cement recipe. Water to cement ratio used 0.38. Including cement mass in slurry, initial foam quality was 21.6%. Once cement mass was excluded, quality was adjusted to 42%. Overall shape of curve appears to show dissolution effects. Exclusion of cement mass/volume in calculations likely caused inaccuracies, but did not appear to change overall trend.

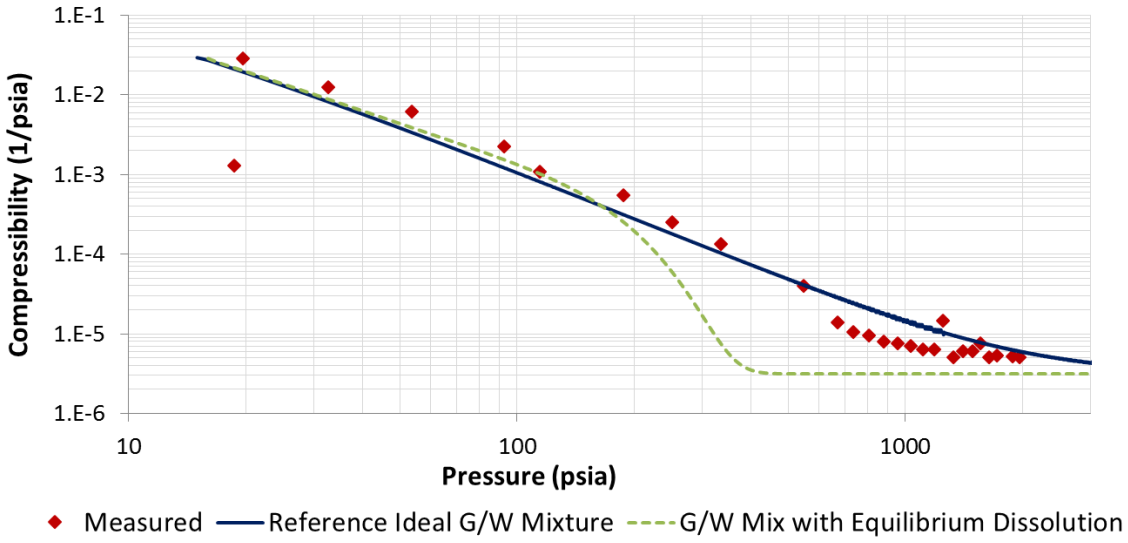

Figure 4.30 Compression of foamed cement with nanoparticles experiment #1. P_o=14.7 psia. Amine Oxide 9% bwow + 0.5% bwoc Cembinder W50 recipe used. Water to cement ratio used 0.38. Initial foam quality 23.04%. Once cement mass was excluded, quality was adjusted to 44%. Overall shape of curve appears to show dissolution effects. Exclusion of cement mass/volume in calculations likely caused inaccuracies, but did not appear to change overall trend.

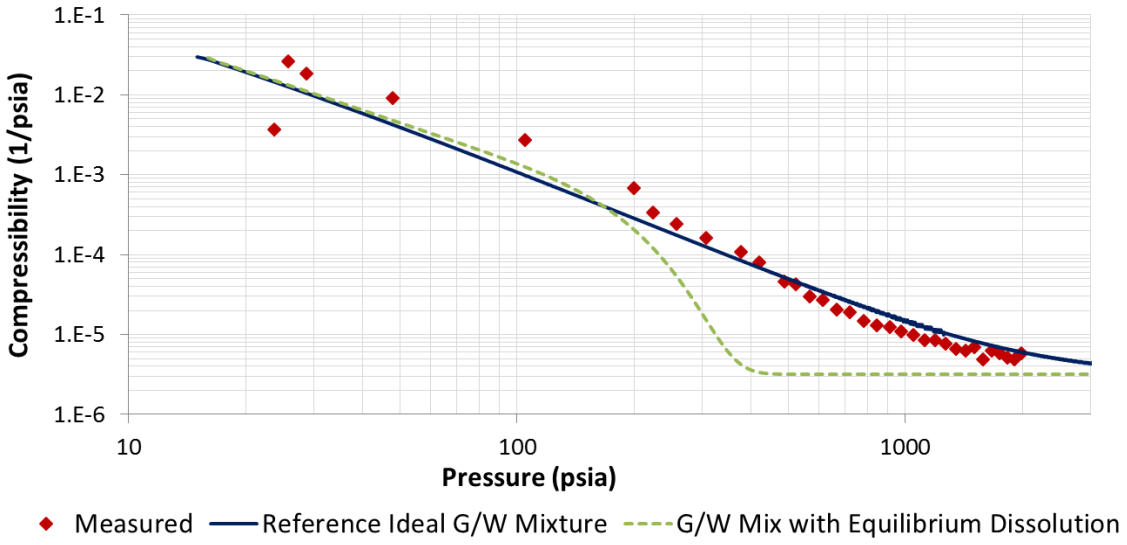

Figure 4.31 Compression of foamed cement with nanoparticles experiment #2. P_o=14.7 psia. Amine Oxide 9% bwow + 1% bwoc Cembinder W50 recipe used. Water to cement ratio used 0.38. Initial foam quality 23.52%. Once cement mass was excluded, quality was adjusted to 44.7%. Overall shape of curve appears to show dissolution effects. Exclusion of cement mass/volume in calculations likely caused inaccuracies, but did not appear to change overall trend.

The presence of cement in foam did not appear to show any significant variations when compared to pure foam. A method to estimate effect in foam compressibility by the presence of cement solids was not developed. As such, it was decided to exclude the cement solids mass/volume in measurements. As a qualitative observation, adjusting the compressibility measurements by excluding the mass/volume of cement appeared to present itself as an overall increase in compressibility. A possible explanation is that the cement solids do have a small contribution to compressibility which is not being taken into account. The contribution may be by the solids themselves compressing, or perhaps a tighter packing of the small solid particles of cement powder.

4.4 CHAPTER CONCLUSIONS

The compressibility of various test fluids was measured in order to validate the functionality of the compressibility measurement apparatus. The fluids tested were water, air and CO_2. The measurements obtained were all compared to data available from NIST. The validation experiments allowed the estimation of the compressibility of the apparatus itself which was found to be between ~$4.2*10^{-6}$/psia and ~$4.6*10^{-6}$/psia depending on the starting pressure of the fluid being tested. Having estimated the compressibility of the apparatus, a method was developed to distinguish the compressibility contribution of the apparatus from the compressibility of the test fluid.

Foam stability experiments were performed in order to select a surfactant to generate foams and foamed cement. The surfactant chosen was an amine oxide (Aromox APA TW), as its foam exhibited sufficient stability to last over the course of a compressibility measurement experiment (1 to 2 hr). Cembinder W50 nanoparticles were added to this foam to observe if stability would be affected by their presence. The Amine Oxide 9% bwow + 0.5% Cembinder W50 recipe displayed increased viscous properties vs. its counterpart which did not have nanoparticles. This was investigated as a potential enhancement of stability by the presence of nanoparticles, although the nanoparticle stability tests performed in Chapter 5 showed this was unlikely. The most reasonable explanation was the gelling effect caused by nanoparticles becoming unstable due to large surfactant concentration.

It was decided that the best compressibility benchmark for a foam, would be that of an equivalent G/W system. A compressibility benchmark was established by calculating the compressibility of an ideal gas + water mixture with the same initial quality and

pressure. In the first experiment where surfactant stabilized foam was compressed, compressibilities higher than the benchmark were observed in the 14.7 to 200 psia range, and compressibilities lower than the benchmark were observed in the 200+ psia range. At this point the effects of gas dissolution at equilibrium in compressibility were also assessed. The equilibrium gas dissolution adjusted compressibility served as a limiting case boundary to explain potential deviations from the ideal gas + water mixture compressibility.

It was determined that mass transport of gas molecules (dissolution into aqueous phase) affected the compressibility measurements of foams or foamed cement that were generated at atmospheric conditions. The effects appeared to be more noticeable in foams/foamed cement that had long term stability. The most likely explanation is that the large surface area between the air and water phases in foams increased the mass transport rate throughout the compression of the fluids. At this point it was recognized that if an armored bubble effect actually occurring and its magnitude was relatively small, the effects would likely be masked by gas dissolution.

Compressing an air + water mixture made with pressurized air showed very minor effects of gas dissolution upon gas/water compressibility. It was concluded that generating nanoparticle stabilized foams under pressurized conditions, and with a maximum quality at which they were stable, would minimize gas dissolution effects in compressibility measurements. Generating the foams with pure nitrogen would also reduce gas dissolution, as nitrogen is roughly 2x less soluble in water than oxygen. As an end result, minimizing dissolution would increase the capability to observe the armored bubble effect.

Chapter 5

Compressibility of Nanoparticle Stabilized Foams

Having validated the functionality of the compression vessel and established a suitable fluid compressibility benchmark, the next step was to compress nanoparticle stabilized foamed cement in search for evidence of the armored bubble effect. The first set of experiments in this chapter investigated the generation of nanoparticle stabilized foams under the ionic and pH conditions that cement slurry presents. After testing the stability of various nanoparticles under cement slurry conditions, none of the nanoparticles available were found to be entirely appropriate. At this point it was decided to instead use a proof of concept approach and test the compressibility of nanoparticle stabilized foams and not foamed cement. That is, evidence of armored bubbles was sought in gas/water foams rather than foamed cement. The Wacker HDK-H30 nanoparticles were used for the majority of the experiments. These nanoparticles were chosen because they have the advantage of generating extremely long term stable foams without the aid of surfactant. Long term stable foam made with Ludox TMA nanoparticles and CTAB surfactant was also tested. This working recipe (Maestro et al, 2014) was discovered towards the end of this research and only a single experiment with this combination was performed. As the conclusions from the previous chapter indicated, solubility can in some cases make it difficult to accurately measure the compressibility of a foam. In order to mitigate potential solubility effects, the majority of the foams generated for the experiments presented in this chapter were generated under pressurized conditions and with nitrogen gas. These foams were produced with the use of a beadpack operated at elevated pressure.

5.1 MATERIALS AND EXPERIMENTAL METHODS

5.1.1 Materials

Materials and equipment previously described in Chapter 3 and/or Chapter 4:

- Blender
- Cembinder W50 and Nyacol DP 9711 nanoparticle dispersions
- AkzoNobel Aromox APA TW, AkzoNobel Witcolate 1247 H and Stephan Petrostep CG 50 surfactants
- Model 500D Teledyne ISCO syringe pump (x3). Two utilized in the foam generation apparatus and one in the compression apparatus
- Compression apparatus including compression vessel, ISCO syringe pump and pressure transducers with LabView software attached to it. The apparatus was slightly modified and such modifications will subsequently be described with more detail

Nanoparticle Dispersions

Wacker–Chemie hydrophobic HDK-H30 silica nanoparticles. These silica nanoparticles have hydrophilic SiOH and hydrophobic methyl-chlorosilane groups attached to surface and were donated by Wacker-Chemie. They have a nominal particle density of ~2.2 g/cm^3. The particles are made by reacting hydrophilic amorphous fumed SiOH covered silica with methyl chlorosilanes. Fumed silica consists of fractal-like particle aggregates synthesized by flame hydrolysis. In this process, primary particles, in the nm-range and with a narrow size distribution, link together forming stable fractal aggregates in the range 100–500 nm (Nordström et al, 2010). Primary particles are approximately spherical of diameter between 5 and 30 nm (Binks & Lumsdon, 2000). They have a 50%

residual SiOH surface coverage and thus a 50% methyl chlorosilane capped surface. Due to their overall hydrophobicity, these particles are originally in dry solid form and need to be dispersed in water. Once in water, the dispersion has a pH between 4 and 4.5. The target particle/aggregate diameter for these dispersions was between 150 and 250 nm. This particle size was considered to satisfy the $r \approx 10^{\wedge -7}$ m parameter established by Binks and Horozov (2005) to assume the particles were permanently adsorbed in the G/W interface.

Nissan Chemical EOR series silica nanoparticle dispersions (EOR-5XS, EOR-12, EOR-25, EOR-50 and EOR-80). These nanoparticle dispersions were donated by Nissan Chemical and have a proprietary surface treatment. The dispersions are between 17-22 wt% silica (20 wt% value used) and have particle diameter ranging between 5 and 80 nm as indicated by the number in their name. Depending on the batch the particles have a pH between 9 and 11.

3M polyethylene glycol (PEG) surface treated silica nanoparticles. These nanoparticles were donated by 3M. They have a particle diameter of 5 nm and came in 20.19 wt% silica dispersion.

Ludox TMA nanoparticle dispersion. Uncoated colloidal silica with a particle diameter of 15 nm. The dispersion has a pH between 4 and 7, density of 1.23 g/mL and are 34 wt% silica.

Nyacol Technologies Nexsil 5000 silica nanoparticles. Uncoated silica nanoparticles with a diameter between 4-6 nm. The dispersion has a pH between 10.5 and 11.5, specific gravity of 1.1 and is 15 wt% silica.

Surfactant

MP Biomedicals cetyltrimethylammonium bromide (CTAB). Anionic surfactant that is originally in a dry powder form. It has a pH between 6 and 7 in water, a solubility of 3 g/L in water, a molecular weight of 364.5, a critical micelle concentration (CMC) of 1mM, an aggregation number of 170. The lot purchased (MR31434) had a 99.5% purity.

AkzoNobel Arquad 2C-75 quaternary ammonium salt (QA) anionic surfactant. It has a pH between 7 and 9, density of 0.882 g/cm^3 and a viscosity of 430 cP. Its composition is 70 to 80 wt% quaternary ammonium compounds, 15-20 wt% isopropanol and 5-10 wt% water.

Sodium Chloride

Fisher Scientific sodium chloride. ≥99.0% purity sodium chloride was utilized to mix brine solutions.

Sodium Bromide

Acros Organics sodium bromide. 99.5% purity sodium bromide was utilized (Lot A0336170).

pH meter

An Oakton Model pH-110 pH meter was utilized to measure pH during nanoparticle stability experiments.

Conductivity meter

A YSI model 3100 conductivity meter was used to measure conductivity during nanoparticle stability experiments.

Compressed Nitrogen Gas

The nitrogen gas used to generate foams under pressure is 99.999% pure and was purchased from Matheson Gas. The nitrogen in the cylinder was at a pressure of 2650 psi and was loaded into an accumulator at the desired pressure for each experiment.

Emerson Industrial Sonifier

A model VW250 Branson Digital Sonifier with a microtip was used to create aqueous dispersions of the Wacker HDK-H30 nanoparticles.

Dynamic Light Scattering (DLS) Particle Size Analyzer

Two different DLS analyzers were used to measure particle diameter due to the demand for utilizing the equipment. Either a Beckman Coulter Delsa Nano C Particle Analyzer or a Brookhaven ZetaPALS instrument was utilized depending on availability.

Beadpack

A high pressure column from HiP (High Pressure Equipment Company) was filled with beads in order to create a "beadpack". The beads were bought from Potters Industries LLC. The inner diameter of the column is 0.44 cm and its length is 15.24 cm. The beads used are made of glass and are spherical in shape. The beads used had a size distribution between 150 μm and 210 μm in diameter, with an average diameter of 180 μm. In order to hold the beads in place, pieces of mesh were put in the end caps of the column to hold the beads from flowing out of the beadpack as fluid passed through it.

Pressure Transducers and Data Acquisition Computer

Rosemount differential pressure transducers (model 3051CD5A22A1A) were used to measure the pressure differential across the beadpack. The transducers have a maximum operating pressure of 3,600 psia and can read pressure drops up to 2,000 psia. They are

connected to a power supply unit and a data acquisition card which sends the data to a computer. The pressure transducer data was then displayed and recorded on a computer using LabView software. The differential pressure transducers were calibrated to operate in a range between 0-210 psi pressure differential.

View Cell

An in-house high pressure vessel with sapphire windows was used to qualitatively observe the foam and foam bubble size during experiments. The sapphire view cell windows were manufactured by Swiss Jewel Company and have a 1" diameter and a thickness of 3/8". The case that holds the windows in place has a 2” diameter. Once assembled, only a portion of the windows can be seen. This portion has a 15.4 mm diameter.

Figure 5.1 Photograph of view cell with scale bar.

Pressure Regulator (Back Pressure Relief Valve)

Spring loaded back pressure relief valves were used to keep the system at a desired pressure during experiments. The model SS-4R3A valves were manufactured by Swagelok. In the apparatus, the back pressure relief valve maintains an almost constant pressure by preventing flow until the upstream pressure becomes greater than the set pressure. The operating pressure range can be changed by using different springs of different stiffness. For best performance, the back pressure relief valve should not be used in the presence of solids. A waste accumulator is used to prevent the flow of nanoparticles and displaced sand from cores into the back pressure relief valve. It is also recommended to use DI water in the waste accumulator to avoid scale deposition in the relief valve orifice.

Waste Accumulator

A 400 mL floating-piston accumulator was used at the outlet of the foam generation apparatus to collect the effluent of the experiments. The piston is pushed all to way to either end and the void chamber is loaded with DI water. The opposite end is then connected to the back pressure regulator. Effluent from experiments flows into the other end, moving the piston and displacing the water. This setup protects the back pressure relief valve from solids that can clog the orifice and also allows for "smoother" backpressure control since relatively incompressible water flows through the pressure regulator and not foam. The waste accumulator was fitted with Swagelok Quick-Connects in order to be able to be removed and reset easily after every experiment.

Foam Generation Apparatus

The same apparatus utilized by Hariz (2012) and Worthen et al (2013b) to generate carbon dioxide and water emulsions or foams was utilized to generate the air and water or

nitrogen and water foams described in this research. The apparatus was modified so that it could be lined up to an additional gas accumulator and either utilize compressed nitrogen or compressed air to generate foams under pressure. Additional modifications were built in order to bypass certain parts downstream of the beadpack used to generate foam. A final set of modifications were also constructed in the apparatus so that the compression vessel could be connected and loaded with pressurized foam. Slight adjustments were also made to the compression vessel so that it could be loaded with pressurized foam being generated as close to steady state as possible. For simplification purposes, the schematic presented will only displays the lines and parts of the apparatus that were utilized in this research.

Refractometer

Fisher Scientific Abbe Benchtop Refractometer. A model 334620 refractometer was used to measure refractive index of nanoparticle dispersions.

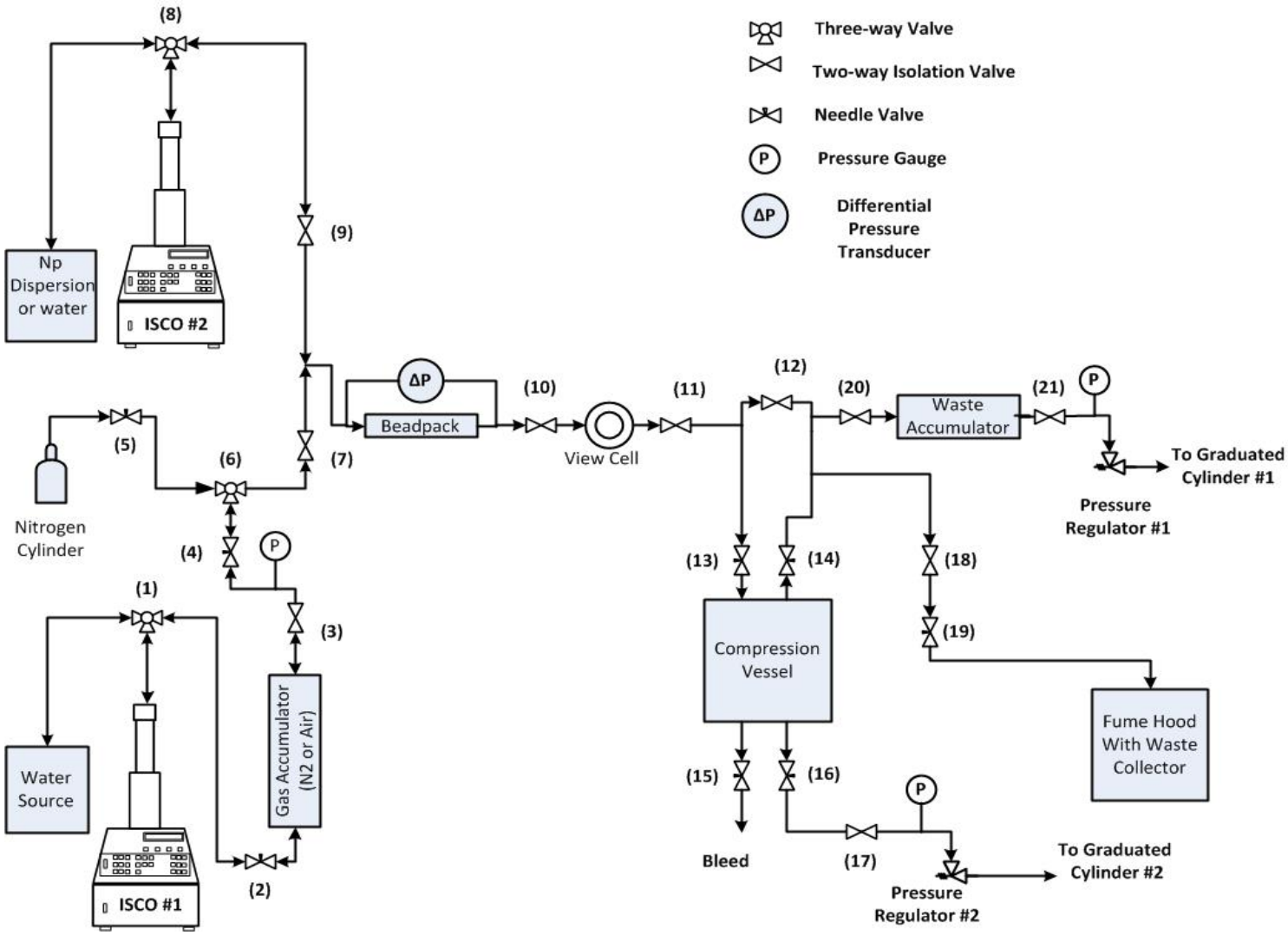

Figure 5.2 Schematic of the pressurized foam generation apparatus with compression vessel attached to it

Compression Vessel Modifications

The modifications built into the compressibility vessel in order to load it with foams generated under pressure did not change its functionality/procedure once the vessel was filled. After loading with foam, the vessel is disconnected from the foam generation apparatus and reconnected to the ISCO pump and associated pressure transducers used to perform the compression segment of the experiment as described in Chapter 4.

In order to connect and disconnect the vessel as quickly as possible, Quick-Connects fitting were utilized. The fitting were placed next to the needle valves associated with the vessel, valves 13, 14, and 16. When the vessel is not connected, corresponding Quick-Connects plugs are placed in the foam generation apparatus so that it can still operate. The plugs basically replace valves 13 and 14. A pressure regulating device was built to be coupled with the vessel when being filled with pressurized foam. The regulating device includes the line segment in the schematic which includes valve 17, a pressure gauge and pressure regulator #2. A Quick-Connects fitting was also added to the pressure transducer that connects to the top cap in figure 4.4. The transducer can be connected to either valve 13 or 14.

5.1.2 Nanoparticle Stability Experiments

The aqueous phase in cement slurries has large ionic strength and high pH, conditions at which some dispersions of nanoparticles become unstable, typically by aggregation of individual nanoparticles into colloid-sized clusters. Aggregates of nanoparticles will not attach to bubble surfaces as effectively and reduce the number of individual nanoparticles available, so nanoparticle stability tests were performed in order to determine which nanoparticles or nanoparticle/surfactant combination to use to generate

nanoparticle stabilized foams and foamed cements. The experiments consisted in titration experiments. The different nanoparticle dispersions were titrated with surfactant, sodium hydroxide (NaOH) solution, sodium chloride salt solution (brine) and cement filtrate. Cement filtrate was obtained with a Büchner funnel vacuum filtration setup.

1. Pour a known mass of nanoparticle dispersion into a beaker. Be sure to know the initial nanoparticle wt%
2. Add a few drops of either surfactant, brine, NaOH or cement filtrate (titrant).
3. Measure the mass of titrant added with the use of a scale. In order to be able to do this it is critical to record the solution mass prior to adding the titrant
4. Stir until evenly mix with a glass stir rod
5. Record any observations such as cloudiness, precipitation of solids or gelling
6. (Optional) measure pH and/or conductivity
7. Repeat steps 3 to 5 until particles precipitate/gelate, this indicates the particles no longer have colloidal stability
8. Record total titrant added to reach unstable nanoparticle conditions

5.1.3 Beadpack Preparation Procedure

In order to create the beadpack, the following procedure was utilized:

1. Securely lodge mesh inside both end caps of the beadpack
2. Use vise grip to secure one of the end caps vertically
3. Add graphite lubricant to threads and then place column on top of end cap and tighten with wrench
4. Use a disposable plastic pipette to fill beadpack column with beads from top to bottom

5. Once beads reach top of column, temporarily place a piece of paper on top and apply slight pressure with finger to paper
6. Tap the side of the beadpack with a wrench so that the beads pack as closely as possible and void spaces are minimized and eliminate the potential of fluid "channeling" through large void spaces
7. Remove paper and observe bead level, if beads subsided add additional beads until top level is reached
8. Repeat steps 5 to 7 until beads no longer subside
9. Add graphite to top end cap and very carefully screw on top of column. Make sure the column remains vertical and no beads are spilled.
10. Now that the beads are secured in place, the beadpack can be turned 180° and the second end cap secured in the vise so that it can be tightened with a wrench
11. Connect beadpack to foam generation apparatus

If the beadpack is being re-packed, additional steps will be required prior to adding new beads

1. Remove both end caps of beadpack
2. Use 1/8" tubing as a metal rod to push-out/remove beads in beadpack
3. Rinse all the parts in DI water
4. Either use compressed air or let the pieces dry. If column is not completely dry, it will be difficult to properly re-pack because beads will get stuck in moist places and minimizing void space will be difficult

During this research project, the beadpack beads were often replaced depending on the experiment being performed. The Wacker HDK-H30 particles and foam generated with them appeared to be "sticky" and would sometimes partially obstruct the beadpack. None of the other nanoparticles, surfactants or nanoparticle/surfactant combination appeared to have this effect. The pressure drop across the beadpack was used as a proxy to know if any blockage was occurring in the beadpack. If flushing the beadpack with DI water did not eventually show a pressure drop across the beadpack equal to when initially calibrated with DI water, the beadpack was considered to have blockage. For reproducibility purposes, the beads were replaced for every experiment in which the HDK-H30 nanoparticles were utilized. It was decided the variability in permeability obtained every time the beads were replaced was preferable to using the same beads with blockage.

5.1.4 Obtaining Beadpack Reference Pressure Drop

Reference beadpack pressure drop data was obtained every time the beads in the beadpack were replaced. This data was used as reference at the end of each experiment in order to determine if the beads had to be replaced or if the beads appeared to be in their original state and could be reused. The compression vessel does not have to be connected for this procedure. At this point it is recommended pressure regulator #2 is connected in the place where pressure regulator #1 appears in Figure 5.2. This will save time overall throughout the experiment. In this procedure such component will just be referred as "pressure regulator" as either #1 or #2 can be connected in such location.

1. The compression vessel does not have to be connected for this procedure. Valves 13 and 14 need to be closed or if disconnected, Quick-Connects plugs need to be in their place
2. Reset and refill the waste accumulator
3. Fill the fluid reservoir of ISCO pump #2 with DI water
4. Line up valve 8 so that ISCO pump #2 is connected to the reservoir
5. Fill ISCO pump #2 with water , be sure to purge any trapped air
6. Verify valves 7 and 18 are closed
7. Verify valves 9, 10, 11, 12, 20 and 21 are open
8. Set the pressure regulator at minimum backpressure
9. Line up valve 8 towards the beadpack
10. If desired start recording pressure drop data
11. Run pump at 5 mL/min
12. Monitor pressure regulator setup until water flows out of it
13. Tighten pressure regulator, water flow should stop. Pressure will build up until set pressure it reached
14. Using this technique tighten/loosen pressure regulator until desired pressure is reached. Use pressure gauge next to regulator to set such pressure
15. Monitor pressure drop in LabView, once it reached steady state (does not change) record the pressure drop for the specified flow rate
16. Increase flow rate to 10 mL/min and repeat steps 11-15. Continue doing this in 5 mL/min flow rate increments until 25 mL/min is reached (In a few cases, 30 mL/min was the highest value used)

17. Decrease flow rate to 20 mL/min and set pressure regulator to desired pressure. Subsequently foam will be generated at ~20 mL/min total flow rate, thus defining this rate as the final setting
18. Stop pump
19. Open valves 18 and 19 to relieve the pressure built up in the system.

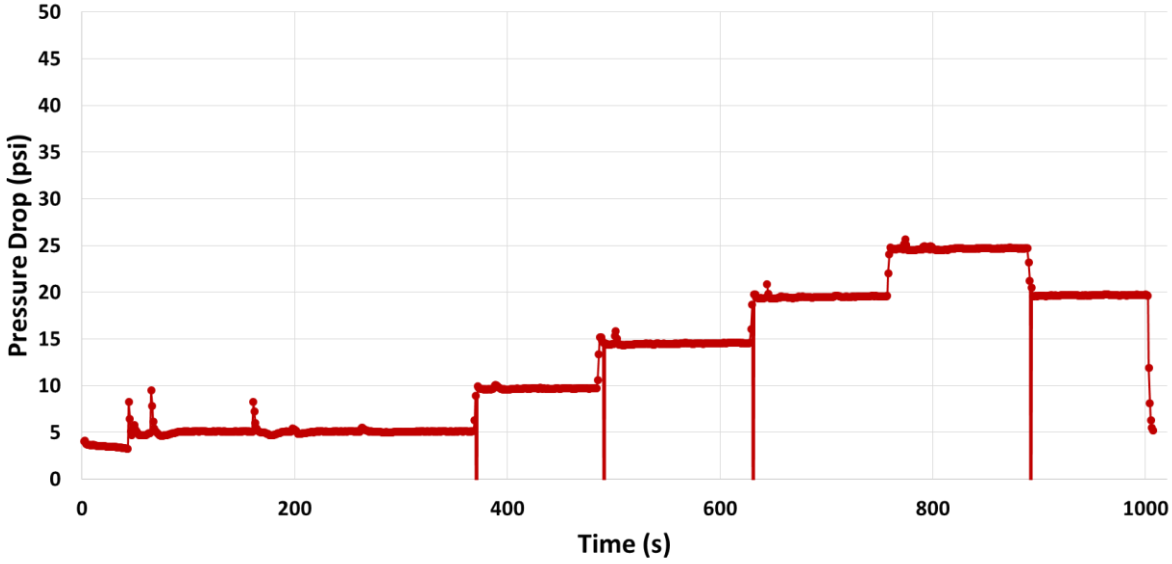

Figure 5.3 Example of pressure drop behavior throughout beadpack reference pressure drop data collection. Sudden drops indicate missing data which occurred while changing experiment parameters, in this case flow rates.

Figure 5.3 is used as an example of determining when the steady state pressure drop for any given flow rate was achieved. Until about time t=200 the apparatus is in a transient state. Between t=200-380 the system reached its 5 mL/min steady state. Then, flow rate was increased to 10 mL/min until a new steady state was reached. In this manner the experiment continued until the 25 mL/min steady state was reached. Finally at roughly t=900 the flow rate was decreased to 20 mL/min in order to lock in place the pressure

regulator desired setting. The data was then captured in table form and permeability was calculated. Pressure drop should have a linear relationship with flow rate. After having plotted the data, an R^2 value was found using software.

5.1.6 Preparing Wacker HDK-H30 Aqueous Dispersion

Due to their hydrophobicity, The HDK-H30 nanoparticles cannot be dispersed in water simply by mixing the two components. The particles have to be first dispersed in ethanol. After being dispersed in water, the ethanol can be removed and the particles will remain dispersed in water. The described procedure to create the aqueous dispersions was adapted from Binks & Horozov (2005). Due to their hydrophobicity, the maximum stable concentration achieved during this research was 4.5 wt%.

1. Mix a maximum of 0.9g HDK-H30 per 20 mL of ethanol in a 50 mL centrifuge tube. The most common quantity used in this research was 0.8g per 20 mL of ethanol. Once the final dispersion in water was made this equals to approximately a 4 wt% particle dispersion
2. Centrifuge at 7000 RPM for 6 minutes
3. Decant and dispose of ethanol
4. Add DI water to 40 mL mark
5. Stir solids into water
6. Place in the sonifier and run for 1 minute. Set sonifier at 30% amplitude and 0.2 seconds on per 0.5 seconds off interval
7. Centrifuge at 8000 RPM for 7 minutes
8. Decant and dispose of water
9. Repeat steps 4-6

10. Centrifuge at 8000 RPM for 7 minutes
11. Decant and dispose of water
12. Add DI water to 40 mL mark
13. Place in sonifier for 30 min
14. Measure particle aggregate diameter
15. Repeat 13&14 until desired particle aggregate diameter is reached.

In this research the target particle diameter was between 150-250 nm. More commonly the smallest aggregate diameter achieved was around between 200-250 nm. During the sonifying process, the dispersion can significantly rise in temperature to the point that some water evaporates. It is important to account for such potential losses or replace evaporated water so that the concentration is known at all times. If the dispersion has to be sonified for longer than 30 min, the dispersion should be allowed to cool down in between the 30 min intervals. If the dispersion gets too hot, especially in the zone around the tip, it appears some silica particles permanently will fuse together. When this seemed to occur, the fused particles were no longer be able to be reduced in size. It is believed this was not due to particles being joined as aggregates. This problem was only commonly observed when creating dispersions with concentrations greater than ~2wt%.

5.1.7 Preparing Foam Generation Apparatus

This section describes all the preparations made prior to running the foam generation experiment

5.1.7.1 Compression Vessel Preparations

During the pressurized foam generation process, the compression vessel will basically function in the same way the waste accumulator during the studies of foam generation with this apparatus in other projects. The piston will be fully displaced to one side and the void vessel chamber will be filled with DI water. The opposing chamber with a near zero-volume will be lined up towards the generation apparatus. The chamber does have a small pathway through which fluid can go through without moving the piston. When a foam generation steady state is reached, valves will be closed so that foam will push on the opposite side on the piston and fill the vessel while displacing the water out. The preparation procedure is very similar to Section 4.1.3.1 "Loading of a Fluid at Atmospheric Pressure". In this case the fluid is DI water

Open the needle valves in the top cap

1. Assuming both caps are currently screwed in, unscrew/remove the top cap of the vessel
2. Open the needle valves in the bottom cap of the vessel
3. Use a plastic rod to push the piston all the way down. Use a rubber hammer to lightly strike the plastic rod to make sure the piston is all the way to the bottom
4. Load the top of the vessel with DI water. Add enough water so that it fills the vessel right under the threads into which the top cap screws into.
5. Remove any bubbles stuck to the vessel walls with a 1 mL syringe
6. Slowly screw back in the top cap, towards the end a small amount of fluid will spill out of both of the top needle valves.
7. Lock both of the needle valves

8. Turn over vessel 180°. The water side of the vessel will be at the bottom
9. Connect compression to the foam generation apparatus. Quick-Connects next to valves 13 and 14
10. Connect pressure regulator #2 to the bottom needle valve with a Quick-Connects fitting next to it (Valve 16 in Figure 5.2). Recall that if the procedure in Section 5.1.4 Obtaining Reference Beadpack Pressure Drop was done in its entirety, pressure regulator #2 will be already be set at the desired pressure
11. Place a 500 mL graduated cylinder at the water outlet of pressure regulator #2. This will help monitor when the vessel is full of foam

5.1.7.2 Filling Gas Accumulator with Compressed Nitrogen or Air

1. (Optional) If compressed air is going to be used, disconnect nitrogen cylinder and connect the lab's instrument air instead
2. Make sure valves 4, 5 and 7 are closed
3. Open regulator valve in cylinder, or open laboratory air valve if air is to be used (gas source)
4. Line up valve 6 so that the gas source connects to the gas accumulator
5. Open valve 5
6. Open valve 3
7. Slowly open valve 4 slowly. Monitor pressure gauge in gas accumulator until desired pressure is reached.
8. Close valve 4
9. Close valve 4 then valve 5 and finally the regulator valve from the gas source
10. Line up valve 6 towards the foam generation apparatus

11. Line up valve 1 so that ISCO Pump#1 is connected to the DI water source
12. Refill pump making sure all air is purged
13. Line up valve 1 towards the gas accumulator
14. Open valve 2
15. Run ISCO Pump#1 at a low flow rate (~5 mL/min) until pressure equilibrium is reached between pump and gas in accumulator. The pump should display the pressure reading of the gas phase to the nearest psi

*The following steps might also be necessary if air is to be used as gas phase. Lab air is at 100 psi and if needed the pressure can be increased by compressing the air prior to the foam generation

16. Run pump until initial gas phase pressure has been reached
17. Close valve 2 and line up valve 1 towards the water reservoir
18. Refill pump
19. Line up valve 1 towards the gas accumulator
20. Open valve 2 and run pump until pressure equilibrium/connectivity is reached

If a single load of water injection is not enough to reach initial desired gas pressure, the pump can be refilled and more water injected by repeating steps 17-20

5.1.7.3 Preparing and Loading Nanoparticle Dispersion

The nanoparticle dispersions were mixed with brine prior to being used to generate foams. The presence of salt, in this case NaCl, enhances the ability of the nanoparticles to reach the G/W interface (Paunov et al, 2002). Depending on NaCl concentration, the salinity might also destabilize the particles short or long term. Due to this reason the particles were mixed with brine just prior to generating the foams. The NaCl was not

directly added to the nanoparticle solution, but instead dissolved in water and then added to the nanoparticle dispersion. Adding the solid NaCl directly can in some cases also cause nanoparticle aggregation. Having described this, it is important to consider that in order to achieve a target NaCl wt% in the dispersion, the brine solution being mixed into the particle dispersion has to have higher NaCl wt% than the target because the concentration will be reduced as the brine mixes with the originally NaCl free dispersion. For example if the target is to have 200 g of 4 wt% NaCl, then a possibility would be to add 100 g of 8 wt% NaCl to 100 g of NaCl-free nanoparticle dispersion. In the same manner, the NaCl-free dispersion must have higher nanoparticle wt% than the final target concentration.

A 1 mM sodium bromide (NaBr) concentration was used in the foams generated with the CTAB + Ludox TMA mixture, so no NaCl was present in this case. Most of the dispersions used had a final NaCl concentration of 4 wt%. An additional advantage from the presence of salt is that it reduces the solubility of both oxygen (MacArthur, 1916) and nitrogen (Smith et al, 1962).

1. Measure desired NaCl and DI water mass
2. Pour NaCl into water
3. Mix until all salt has dissolved
4. Slowly add brine into nanoparticle dispersion. For these experiments a minimum of roughly 200 g of prepared dispersion were needed per run
5. Line up valve 8 so that the nanoparticle dispersion container and ISCO Pump #2 are connected
6. Be sure that pump is completely empty otherwise whatever is inside the pump will mix with the dispersion

7. Fill the pump with the dispersion and purge any trapped air
8. Be sure valve 9 is closed and then line up valve 8 towards the foam generation apparatus

5.1.7.4 Foam Generation

If replicating this type of experiment read this procedure in full prior to running the experiment. Foam was generated with a target quality of 75%. With the compression vessel prepared and the gas and nanoparticle aqueous dispersion phases loaded and lined up, the following steps were performed:

1. Be certain the source gas phase has a pressure between 60-100 psi greater than the foam outlet target pressure (pressure regulator set point). If the foam outlet target pressure is 100-350 psi, then a pressure greater by 100 psi is needed. If the foam outlet target pressure is between 350 and 800 psi, a pressure greater by 60 psi is needed. This will work as an initial "push" to accelerate the foam generation process. The reasoning behind this will be described with more detail in the discussion in section 5.4
2. Ensure once more waste accumulator has been refilled and reset
3. Pressure regulator #1 should be tightened so that there is some flow restriction. It will be set in a later step
4. Be certain valves 1, 6 and 8 are lined up to the beadpack
5. Valves 7, 12, 15, 16, 18 and 19 should be closed
6. Valves 2, 3, 4, 9, 10, 11, 13, 14, 17, 20 and 21 should be open
7. Begin recording beadpack pressure drop data with LabView software
8. Place a 500 mL graduated cylinder at the water outlet of pressure regulator #1

9. Run ISCO pump #2 with the aqueous dispersion at desired flow rate (5 mL/min) The aqueous dispersion will begin to flow through the apparatus and purge the system
10. Pressure will begin to build up, at this point set Pressure regulator #1 at the desired foam target outlet pressure. The pressure set point should be the same as the Pressure regulator #2. Recall pressure regulator #2 had already been set in the procedure described in section 5.1.7.1
11. Run ISCO pump #1 at desired flow rate (15 mL/min) and quickly open valve 7. At this point gas and the aqueous phase should begin mixing downstream of the beadpack
12. Readjust set pressure regulator #1 as the increased flow rate will slightly alter the outlet pressure
13. Monitor pressure drop and the view cell to observe when foam is being generated
14. When foam is detected, carefully monitor pressure drop. It should gradually increase as the whole system is filled with foam and finally reaches steady state. Although unlikely, it is possible that the initial pressure "push" is greater than the steady state pressure drop. If this is the case, pressure regulator #1 should be tightened slowly. Pressure drop should decrease at this point. Continue doing so until pressure drop increases without adjusting the regulator and finally reaches a steady state. pressure regulator #2 will later also have to be adjusted if this occurs
15. During this period monitor water volume in graduated cylinder #1, it should never exceed ~400 mL, which means the accumulator is full. If steady state is not reached by this point the experiment will have to be reset

16. Once steady state is reached, wait 2 minutes. This will allow for any foam generated under transient conditions to be purged. 2 minutes is enough for this system based on line size between the beadpack and the waste accumulator. It might be different for a different system
17. (Optional) Take photographs or video of the foam flowing through view cell
18. Close valve 14 and quickly open valve 16. This will begin filling the compression vessel with foam
19. In the unlikely case that pressure regulator #1 had to be adjusted, perform adjustments to pressure regulator #2. If minor adjustments were needed and steady state is reached quickly (~10s), then the small transient time was deemed acceptable. Otherwise if continued it should be noted that foam was generated under transient conditions.
20. Monitor graduated cylinder #2 water volume until ~375 mL are collected. This is roughly the chamber size of the compression vessel (Section 4.3.1) and any water stuck in the line
21. Once full, the following steps should be performed in a rapid succession
    a. Close valve 13 isolating the compression vessel
    b. Close valve 10 and 11 isolating the view cell
    c. Close valve 7 blocking gas flow
    d. Stop ISCO pump #1
    e. Stop ISCO pump #2. At this point there should be no flow and all equipment should be stopped
22. Close valve 9

23. Stop recording pressure drop data
24. Close valve 16
25. Open valves 12 and 18
26. Slowly open valve 19. This should relieve the pressure of the waste accumulator as well as the lines leading to it and the compression vessel. Wait until fully depressurized
27. (Optional) Take a photograph of the foam in the view cell. This will later be used to determine is the foam stability during the foam compression experiment timespan
28. Disconnect pressure regulator #2 from the compression vessel
29. Disconnect the compression vessel from the foam generation apparatus (Quick-Connects near valves 13 and 14)
30. Plug lines where valves 13 and 14 where connected

5.1.7.5 Foam Compression

In order to measure the foam compressibility, a combination of sections 4.1.3.3 "Connecting the ISCO Syringe Pump to the Compression Vessel" and 4.1.4 "Compression Data Collection Procedure" was utilized. Some additional changes were required for the procedure

Connect the available pressure transducer to either valve 13 or 14, which are now at the bottom, and open the valve

1. Carry out the procedure in section 4.1.3.3. Since the vessel is already loaded, there is no need to flip it over to perform the compression experiment. The only thing that will be different is that the top and bottom of the vessel will be inverted.

The symmetry of the vessel allows to do this without a problem. Water will push and displace the piston from the top instead of the bottom. The connection to the pump will be made using valve 16 which is now equipped with a Quick-Connects fitting

2. Perform steps 1 to 9 from section 4.1.4 (At this point the pressure/volume data collection is complete)
3. Open valve 15 and bleed any remaining water pressure if needed. Recall valve 15 will now be in the top
4. Disconnect the ISCO pump from the compression vessel
5. Measure and record the mass of a beaker or other container. The container should have a minimum capacity of 300 mL
6. Place the container at the bottom of the vessel so that any fluid coming out of either valves 13 or 14 can be collected
7. Close the valve to which the bottom transducer was connected to and carefully disconnect the transducer. Be sure any liquid trapped in the line section and transducer is collected in the collection container
8. Slowly and carefully open either valve 13 or 14 and collect the liquid that comes out
9. Open the remaining valve and collect any additional liquid
10. Carefully invert the compression vessel
11. Open the top cap
12. Use syringe and spatula to collect any liquid/foam stuck to the walls and bottom of the vessel and put it in the collection container

13. Measure the mass of the liquid in the collection container
14. Disassemble and clean the compression vessel
15. Take a second photograph of the foam originally trapped in the view cell

5.1.7.6 Depressurizing and Flushing the Foam Generation Apparatus

If no changes have been made after the procedure in section 5.1.7.4, the foam generation apparatus should be lined up towards the fume hood with waste collector

1. Close valve 20 and disconnect the waste accumulator
2. Open valve 11 and 10 and 9. Any pressure built up in the view cell, beadpack and ISCO pump #2 will be relieved
3. If desired line up valve 8 towards the nanoparticle dispersion source. Run the pump and recover any remaining nanoparticle dispersion. Usually the remaining amount was so small the pump was just run forward towards the foam generation apparatus
4. Refill ISCO pump #2 with DI water
5. Line up valve 8 towards foam generation apparatus
6. Run pump at relatively high rate 50-100 mL/min. this will flush the whole system
7. Repeat steps 4-6 at least 4 times. Monitor effluent in waste collector until it appears clear/pure DI water is coming out
8. Execute the procedure in section 5.1.4 “Obtaining Reference Beadpack Pressure Drop”
9. If beadpack shows the same pressure drop vs. flow rate then the setup is clean and ready to be used again. If it is close to the reference, repeat steps 4-6 until apparatus is clean
10. If pressure drop continues to be different the beadpack will have to be repacked

5.1.7.7 Collection of Pressurized Fluid Samples

In order to attempt to observe if nanoparticle concentration in the aqueous phase changed with pressure, foam compression experiments were performed where fluid samples were collected at different pressures. Compressibility data was not collected for these experiments since it would be very difficult to account for the sample fluid removed from the vessel. The procedure utilized was almost the same one described to test the compressibility of the foam. The same equipment preparation, foam generation and compression vessel connection procedures were used. Once connected to the ISCO pump used for the compression, the following steps were taken

1. Measure the mass of 6-10 sample tubes
2. Record the initial pressure of the foam
3. Connect a 1/16" piece of tubing of 1 or 2 cm in length to either valve 13 or 14, whichever does not have a pressure transducer connected to it
4. Carefully and slowly open the valve and take a small sample. A couple of drops was enough in this case. Close the valve as soon as the sample is collected
5. Run the ISCO pump to pressurize foam and record new pressure. Interval of roughly 500 psi were used
6. Wait 30 min to so that liquid has the opportunity to drain to the bottom of the vessel.
7. Open the valve and purge a few drops (about 5 in this case) in order to have a representative sample. Be sure to collect the liquid
8. Obtain a new sample
9. Repeat steps 4-7 until all samples are collected at the target pressures

10. Follow the same procedure previously described to depressurize, disconnect and collect/measure the liquid in the vessel (Section 5.1.7.6)
11. Calculate the mass of the samples and add the collected waste liquid mass to know initial mass of liquid in vessel

5.2 DATA ANALYSIS

5.2.1 Mitigation of Dissolution Effects

To mitigate solubility effects, a pressure of 200 psi was selected to generate foams. Pure nitrogen replaced air as the gas phase except for the first few experiments performed in this chapter. By calculating the maximum percentage of STP nitrogen moles that would be dissolved starting from initial pressures ranging from 100 to 500 at 100 psi increments and ending at 2000 psi. Using the solubility data from Wiebe et al (1933) and assuming a foam quality of 70% the table 5.1 was calculated. A quality of 70 % was used as it closely represented the measured quality for most experiments presented in the results section.

Foam generation pressure (psi)	% of original bubble mass dissolved at 2000 psi
100	10.1
200	5.0
300	3.4
400	2.5
500	2.0

Table 5.1 Percentage max gas dissolution capacity of a 70% initial quality foam starting from different pressures up to 2000 psi.

It is implied the calculated values would dissolve over the complete pressure differential range between the listed values and 2000 psi, and not as a single concentrated event. These values do not include the solubility reduction by the presence of NaCl. Also, it is believed the time period of the compression experiment which at a maximum was 3 hours, was also likely not enough for saturation to take place. This had previously been observed in the results of the compressed air + water experiment, shown in Figure 4.25, where air and water initially at 89 psia were compressed. During this experiment dissolution showed very minor effects in compressibility. Effects that for the purpose of potentially detecting the presence of an armored bubble would be negligible.

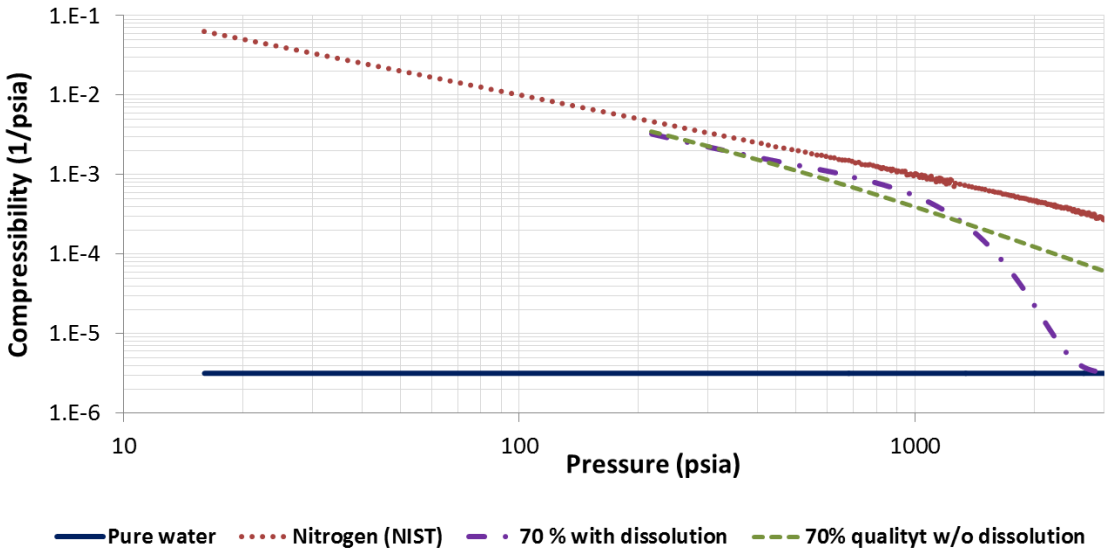

Figure 5.4 Maximum effect of nitrogen dissolution in compressibility of a foam generated at 200 psi (214.7 psia) at quality of 70%.

5.2.2 Bead Pack Porosity and Permeability

The porosity ϕ of the beadpack was assumed to be 0.36. According to Zhang et al (2006), that is the lowest porosity value found in literature for a random closed packing of spheres with a uniform size. Using this value, the beadpack dimensions and the equation for the volume of a cylinder, the pore volume of the beadpack was found to be 0.834 mL.

$$V_{cylinder} = \pi r^2 L$$

$$Pore\ Volume = \phi V_{cylinder}$$

where r is the radius of the beadpack and L is the length

The permeability k of the beadpack was found using Darcy's Law in combination with the flow rate Q and pressure drop ΔP data recorded while flowing DI water through it. Measured room temperature was usually 68-69 °F. Thus the value used for the viscosity μ of water was 1 cP (Korson et al, 1969). The circular cross-sectional area A was calculated from the radius of the beadpack. Gravity was not taken into account since the beadpack was positioned horizontally for the experiments.

$$k = \frac{\mu L Q}{A \Delta P}$$

5.2.3 Stable Foam Generation Criteria

Two factors were utilized to confirm the generation of a stable foam. The first one was an increase in pressure drop through the beadpack, the second was the actual presence of foam flowing through the view cell downstream of the beadpack. One additional

criterion was used to determine if the foam was stable during the length of the compression experiment. After being generated and the compression vessel filled, foam was isolated in the view cell. At this point the view cell was photographed. Once the compression experiment was finished (~2 hours), a second photograph was taken and the two were compared. If the foam remained the same, it was determined to have the necessary stability for the compression experiment. However, it is important to mention that this cannot be used as proof that the foam was stable while being compressed inside the solid steel compression vessel, but rather an indication that it was at least stable at the conditions it was generated.

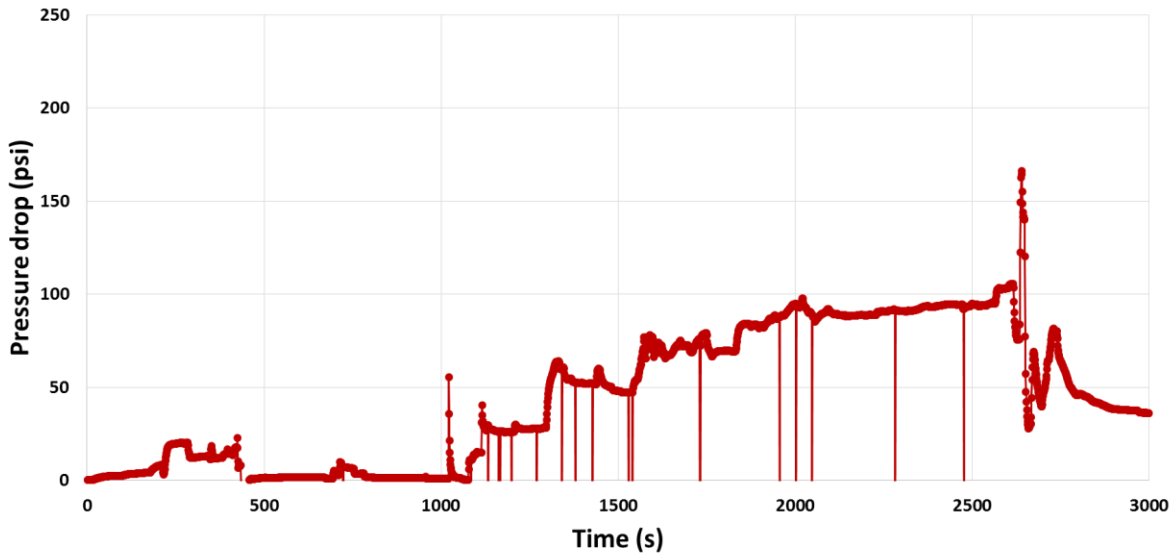

Figure 5.5 Example of beadpack pressure drop increase during foam generation. In this experiment foam generation begins at roughly t=1250 s (Sudden drops represent data gaps when experimental parameters were being changed and not actual pressure drop data).

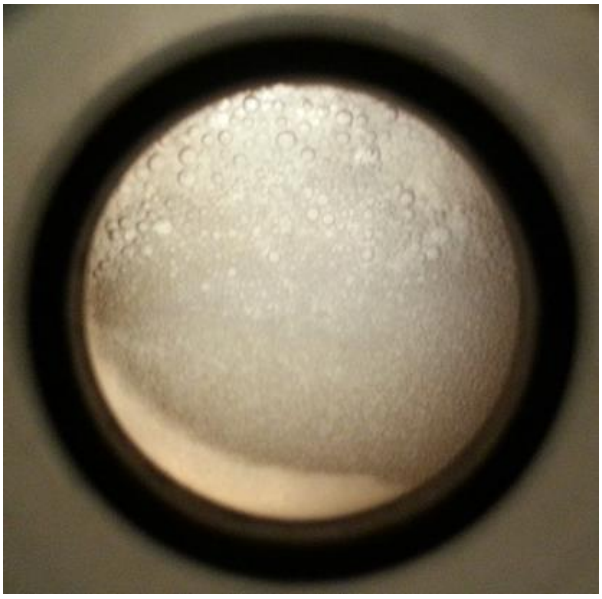

Figure 5.6 Example of stable foam flow observed through the view cell.

Of note is that the stable foam flow example shown in figure 5.6 does not correspond to the pressure drop data from figure 5.5. The two images were chosen as they were deemed to be some of the best examples observed during the various experiments that will subsequently be described.

5.2.4 Foam Quality Measurements

The flow rates at which stable foams were generated and compressed, were customarily 5mL/min aqueous dispersion + 15 mL/min gas phase. Ideally this would generate foams with exactly 75% quality (or a proportional quality when the flow rates were slightly different). It was later proved that this was not exactly the case. The quality of the foam that filled the compression vessel was measured by collecting all the liquid in the vessel after the compression experiment. The mass of the liquid *m* was subsequently

measured. Using this measurement and assuming the density ρ_w of the dispersion was the same of 4 wt% brine, 1.0253 g/mL (Green & Perry, 2008), the volume fraction occupied by the aqueous phase f_w was calculated as follows.

$$V_w = \frac{m}{\rho_w}$$

$$f_w = \frac{V_w}{V_T}$$

where V_w is the volume occupied by the aqueous phase and V_T is the total vessel volume, (Quality = f_w*100). Assuming the aqueous phase has the same compressibility of water, the volume was adjusted for pressure prior to calculating the volume fraction. Recall that the measured total vessel volume was 377.95 mL.

5.2.5 Bubble Size Measurements

A Nikon Digital Sight DS-Fi1 camera was used to photograph the view cell and capture foam images. Image Processing and Analysis in Java (ImageJ), a public domain image processing software, was used to analyze the images and estimate average bubble diameter. Bubble diameter used to estimate total bubble/liquid interfacial area and the mass of nanoparticles necessary to form a single layer (monolayer) covering the summed surfaces of the bubbles in a foam.

5.2.6 Nanoparticle Coverage of Bubble Surface

One of the conditions earlier described so that the armored bubble structure could potentially be formed was that enough nanoparticles must be present to cover total bubble surface area. The particles must completely cover the bubble surface either after pressure

is applied or, in the ideal case, at the pressure at which foam is made. To calculate the bubble surfaces, the bubbles were assumed to be spherical. The volume occupied by gas in the compression vessel was then divided to find the number of bubbles with diameter D_b that could fit in such volume. Once this total number of bubbles was found, their total surface area was added.

To approximate the amount of nanoparticles needed to cover such surface, the bubble surfaces were taken to be flat relative to the nanoparticles covering them. The results section will show the measured bubble diameter was conservatively at least 700x larger than the nanoparticle diameter, and usually around 1000x or more. This size difference justifies the flat bubble surface assumption. All nanoparticles used including the HDK-H30 fumed silica nanoparticle aggregates were assumed to be spherical for this calculation. Figure 5.7 displays the spherical nanoparticle 2-D packing structure assumed to cover the flattened bubble surfaces. Examination of the suggested tessellation shows that trigonometry can be used to calculate the area occupied per nanoparticle. Each of the overlaid red rhombuses drawn includes the area occupied per nanoparticle including void space. The approximation also assumed the formation of monolayers with no additional particles on top. The sharing of surfaces between bubbles in a foam was not taken into account.

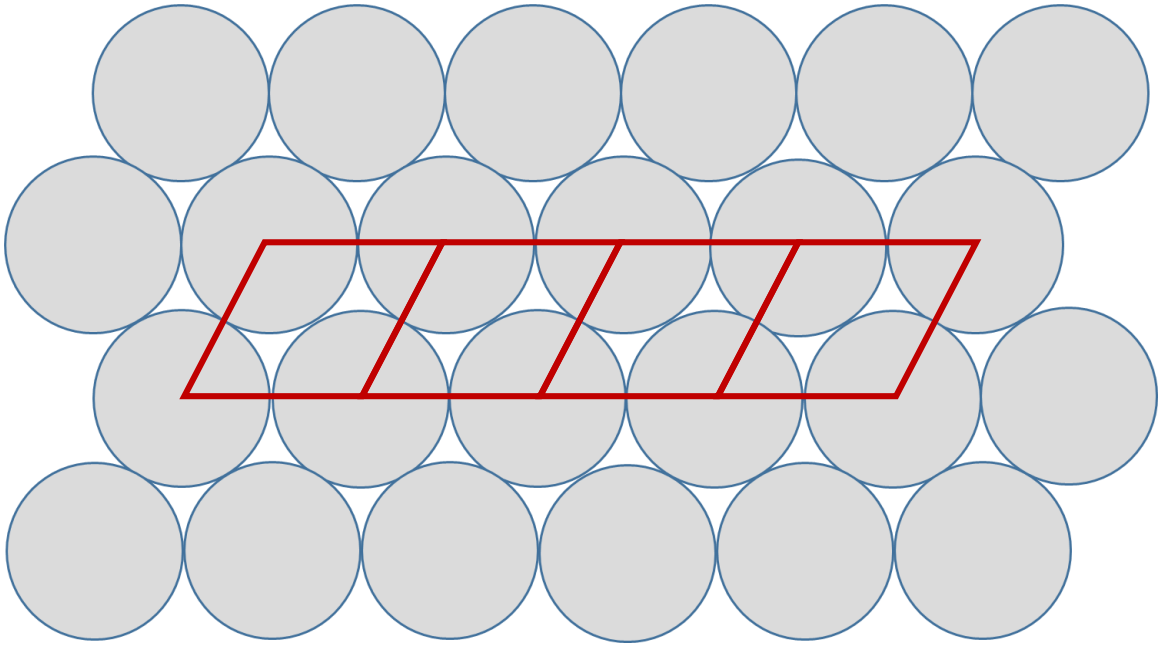

Figure 5.7 Assumed nanoparticle 2-D packing structure covering foam bubble surfaces. Contiguous rhombuses delimit the unit area occupied per nanoparticle.

The following trigonometry derived equation was used to calculate the area occupied per nanoparticle:

$$A_{Np} = \frac{D_{Np}^2\sqrt{3}}{2}$$

where A_{Np} is the area of bubble surface occupied per nanoparticle and D_{Np} is the diameter of the nanoparticle.

Having calculated A_{Np}, the total bubble surface area was divided by this number. This would equal the necessary amount of nanoparticles needed to cover all surfaces. Subsequently using the equation for the volume of a sphere, the volume occupied by all

these nanoparticles was calculated. The next step involved finding how much mass was needed to comprise this volume by multiplying by the nominal particle density of 2.2 g/cm^3. Finally, using this mass and the fact that the remainder of the volume in the vessel was occupied by the aqueous dispersion, a target nanoparticle dispersion wt % concentration to guarantee sufficient particles for monolayer coverage was calculated.

5.2.7 Bubble Volume and Surface Area Compression Calculations

Charts were created in order to visualize how the volume and surface area of the foam might have changed with pressure. Comprehending surface area change with pressure was imperative in order to predict the possible increase in nanoparticle bubble surface density as a function of pressure. The volume and surface area change of a single bubble was plotted. Volume and surface area were normalized relative to an arbitrary initial magnitude. The bubble was assumed to be spherical and to undergo compression as an ideal gas. If this assumption holds, than the area of a sphere scales with volume by the following relationship.

$$A_{sphere} \sim V_{sphere}^{2/3}$$

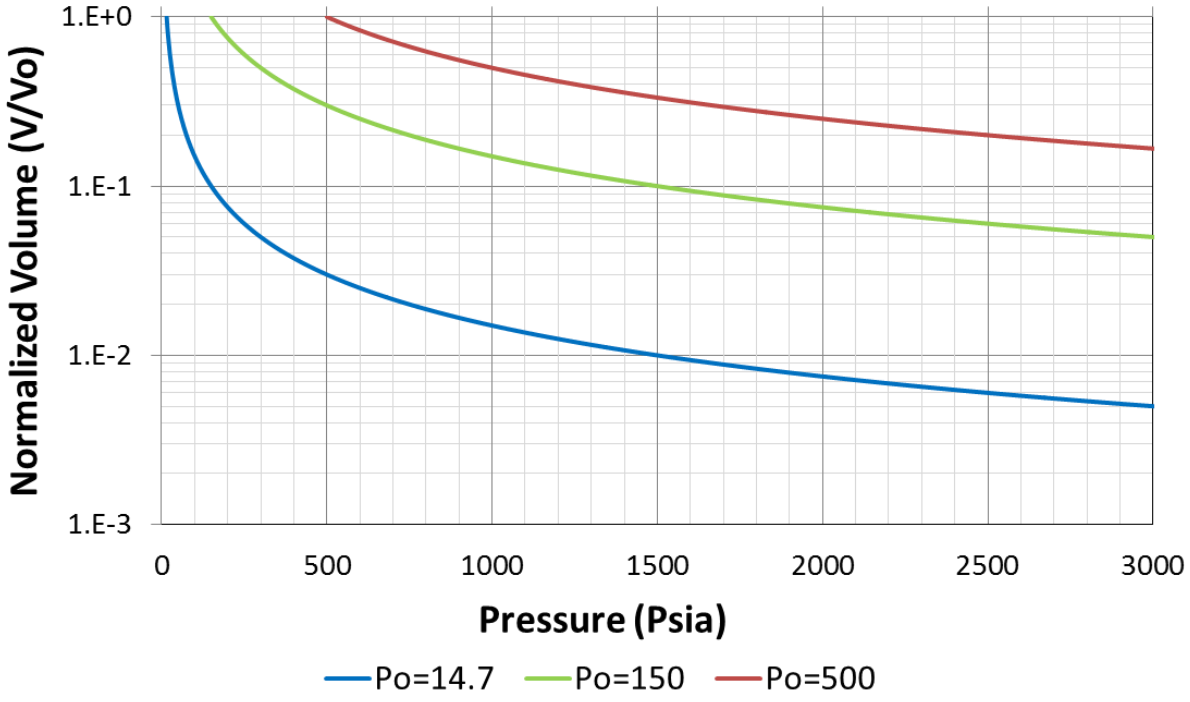

Figure 5.8 Semi-log plot illustrating how the volume of a single spherical bubble changes with pressure. The volume was normalized relative to an arbitrary initial magnitude.

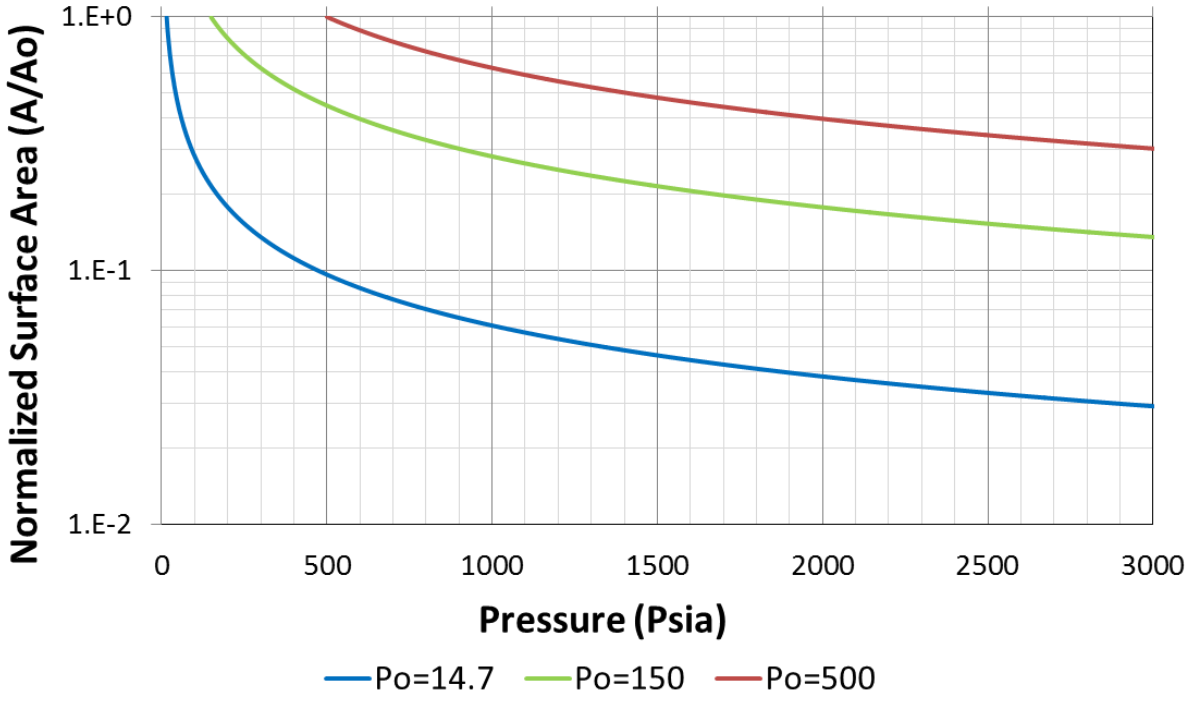

Figure 5.9 Semi-log plot illustrating how the surface area of a single spherical bubble changes with pressure. The surface area was normalized relative to an arbitrary initial magnitude.

5.2.8 Refractive Index Measurements

Refractive index (RI) measurements were taken of the drained liquid samples of from the compressed HDK-H30 stabilized foams. The purpose of these measurements was to attempt to detect/infer if any nanoparticle concentration changes in the liquid phase were occurring as the foam was being pressurized. If nanoparticles were being ejected from the bubble surfaces as the bubble surface area decreased, then the aqueous phase should exhibit an increased nanoparticle concentration. Conversely, if initially attached nanoparticles

remain attached to bubbles during compression, the concentration of dispersed nanoparticles in the aqueous phase should not change during compression.

Prior to taking the foam compression experiment's refractive index measurements, a reference experiment was performed. The RI of different wt% HDK-H30 aqueous dispersion was measured. The purpose of this benchmark experiment was not to have an absolute concentration comparison, but to determine if RI did change as a function of wt% concentration. The reason this experimental data could not be used as an absolute references was because, (1) every batch of HDK-H30 aqueous dispersion had different average particle aggregate sizes, (2) even if an identical aggregate size could be obtained per batch, aggregate size could potentially change as the brine was added to the dispersion and foam was generated in the apparatus. As the results section will show, it was found that RI changed as a function of concentration in the benchmark experiment.

5.3 Results and Discussions

5.3.1 Nanoparticle Stability Tests

The nanoparticle dispersion stability tests involved titrating surfactant, NaCl, NaOH and cement filtrate. During the nanoparticle stability titration experiments, mostly a qualitative analysis was performed. The tests involved observing cloudiness, precipitation or gelling of the sample. The first two sub-sections display images, Figures 5.10 and Figure 5.11, as examples of how gelling/precipitation appears. Changes in particle size due to aggregation or Zeta potential, which is often used to quantify nanoparticle dispersion colloidal stability, was not measured.

5.3.1.1 Cement Filtrate pH

Cement filtrate from three different batches was collected. The filtrate was extracted at slightly different times after mixing.

Batch	Time until filtrate extraction (min)	pH
1	35	12.63
2	50	12.83
3	75	12.74

Table 5.2 pH of cement filtrate extracted after different mixing times. Water to cement ratio used was 0.38.

5.3.1.2 Amine Oxide (Aromox APA TW) Titration into Cembinder W50 Nanoparticles

In this experiment the Cembinder W50 nanoparticle dispersion was used as it came from the manufacturer (15 wt %).

Amine Oxide wt%	Stability observations
1	No change
2	No change
3	Cloudiness
4	Heavy cloudiness
4.5	Gel

Table 5.3 Cembinder W50 nanoparticle stability test. Titrant was amine oxide surfactant. Initial nanoparticle dispersion concentration was 15 wt%.

Figure 5.10 Gelled Cembinder W50 nanoparticle dispersion after reaching a 4.5 wt% amine oxide surfactant concentration.

5.3.1.3 Cement Filtrate Titration into Cembinder W50 Nanoparticles

Cement filtrate collected from each of the different batches was titrated into the Cembinder W50 dispersion. pH was recorded when precipitation/gelling occurred.

Filtrate pH	Amount added (g)	Final solution pH
12.63	8.46	11.61
12.83	8.44	11.63
12.74	8.46	11.65

Table 5.4 Cembinder W50 nanoparticle stability test. Titrant was cement filtrate. Initial nanoparticle dispersion concentration was 15 wt%.

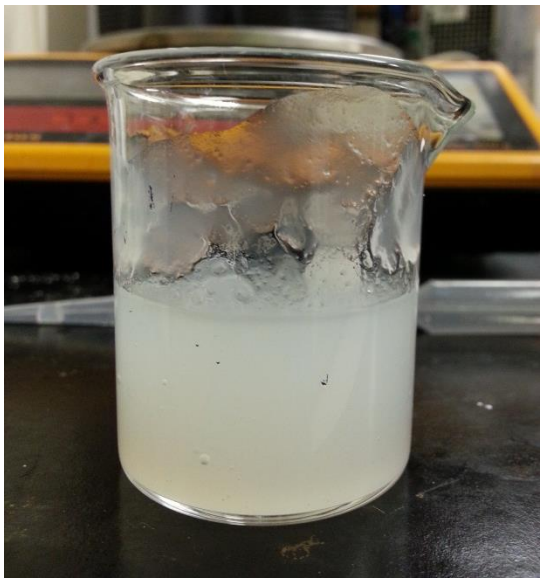

Figure 5.11 Precipitated/gelled Cembinder W50 nanoparticle dispersion after being destabilized by addition of cement filtrate.

From the results of these two test, it was decided to attempt to generate nanoparticle stabilized foams with a combination different than the cembinder W50 particles and the amine oxide surfactant.

5.3.1.4 Surfactant Titration into Nanoparticle Dispersions

Two surfactants used in the oil and gas industry to generate foamed cement., Arquad 2C-75 (QA) and Witcolate 1247 H (AOS), were titrated into 3 types of silica nanoparticles. The surfactants were titrated into the stock solutions. Surfactant was added up to a maximum concentration of 20 wt% or until nanoparticle instability was recorded. If the particles remained stable at 20 wt% concentration a “did not gel” note was recorded.

Type of nanoparticles	QA surfactant wt% at which nanoparticle instability was observed
Nexsil 5000 (uncoated)	8
3M (PEG coated)	20
EOR 5XS (proprietary coating)	10

Table 5.5 Maximum QA surfactant concentration at which different nanoparticle stock solutions displayed nanoparticle instability.

Type of nanoparticles	AOS surfactant wt% at which nanoparticle instability was observed
Nexsil 5000 (uncoated)	20
3M (PEG coated)	Did not gel
EOR 5XS (proprietary coating)	Did not gel

Table 5.6 Maximum AOS surfactant concentration at which different nanoparticle stock solutions displayed nanoparticle instability.

Up to this point the AOS surfactant appeared to be the best fit for future nanoparticle stabilized foams generation experiments. The tested particles seemed to remain stable at high AOS wt% concentrations vs. the QA.

5.3.1.5 Titration of NaOH, NaCl and Cement Filtrate into Nanoparticle Dispersions

The same nanoparticle dispersions from section 5.3.1.5 were utilized. The stock solutions were utilized without any adjustments in concentration. Even though the initial concentration of the nanoparticle dispersions was somewhat different, concentration was not considered to be one of the most important factors for the stability of colloidal silica (Martin et al, 1990). For these summary plots the variables shown are pH and conductivity.

Conductivity was used as an indication of ionic activity. It was used solely as an indication since it cannot be used as a direct comparison due to different ion species conductivity, including the combination of monovalent, divalent and trivalent ions in cement filtrate. In the case when particle instability was observed, it has been marked in the plots as either cloudy or gel depending of the physical appearance of the dispersion. The data from which the plots were generated can be found in the appendix section in Tables A.1 through A.9.

The cement filtrate batch utilized for all of these titrations was the batch that had a pH of 12.74 from section 5.3.1.1. The filtrate had a conductivity of 36.2 milliSiemens/cm. The reason for choosing this cement filtrate batch was because the collected amount was the most abundant and would allow for a larger number of titrations with identical filtrate.

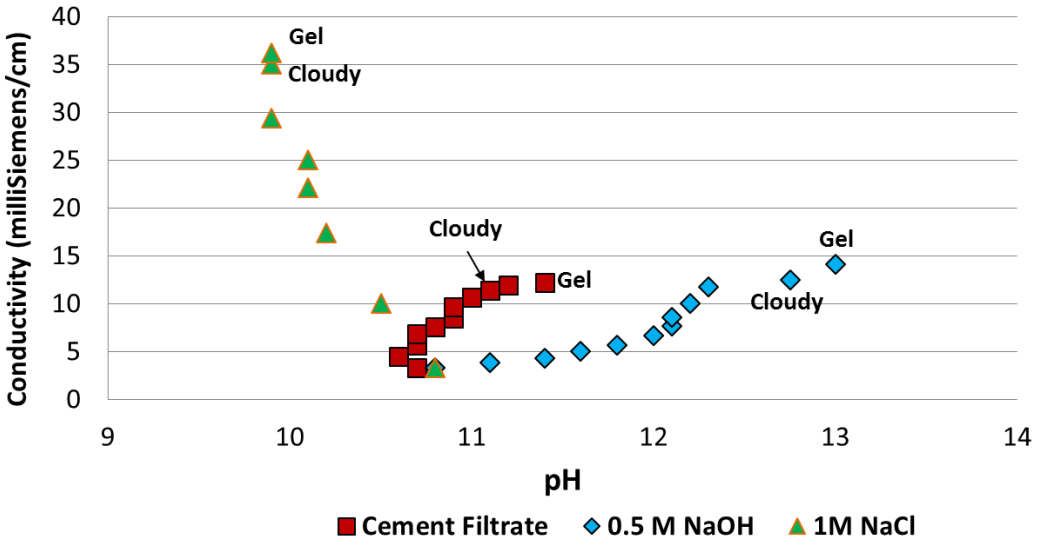

Figure 5.12 Titration of cement filtrate, 0.5M NaOH and 1M NaCl into Nexsil 5000 uncoated silica nanoparticles. Qualitatively, the particles showed ultimate instability in all three titrated substances.

By analysis of figure 5.12 it was concluded that cement slurry had a combination of pH and ionic conditions that were harsh for the Nexsil 5000 and likely the Cembinder W50 nanoparticles (both of which were uncoated).

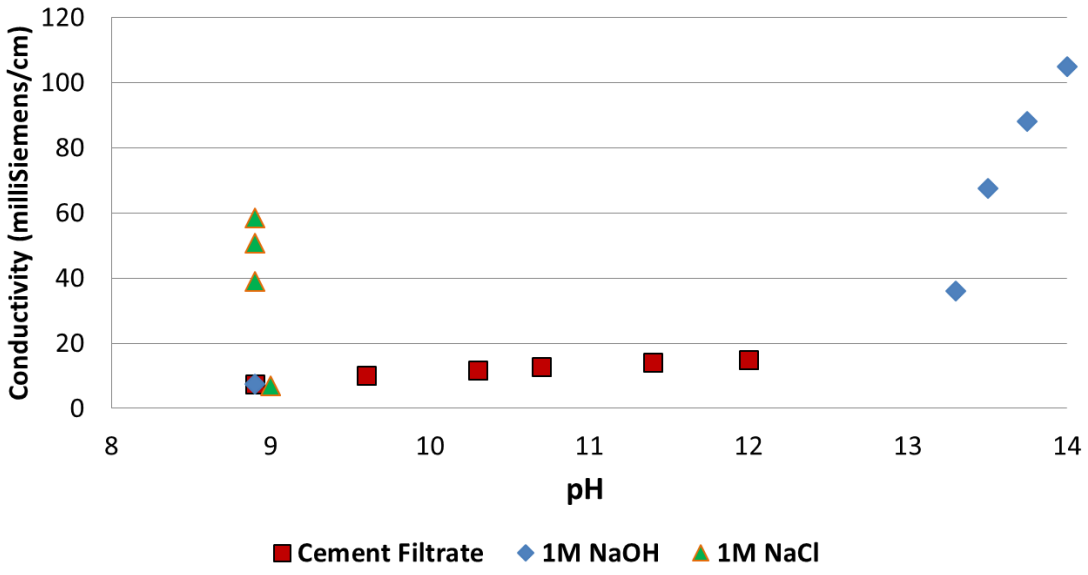

Figure 5.13 Titration of cement filtrate, 1M NaOH and 1M NaCl into 3M PEG coated nanoparticles. Qualitatively, the particles displayed constant stability during all concentrations of the titrated substances.

After the highest concentration of 1M NaCl was titrated, salt was added directly to the solution up to ~9 wt% concentration. The particles remained stable at these conditions. The data point was not recorded in the chart since the conductivity meter had pegged out at the 120 milliSiemens/cm value.

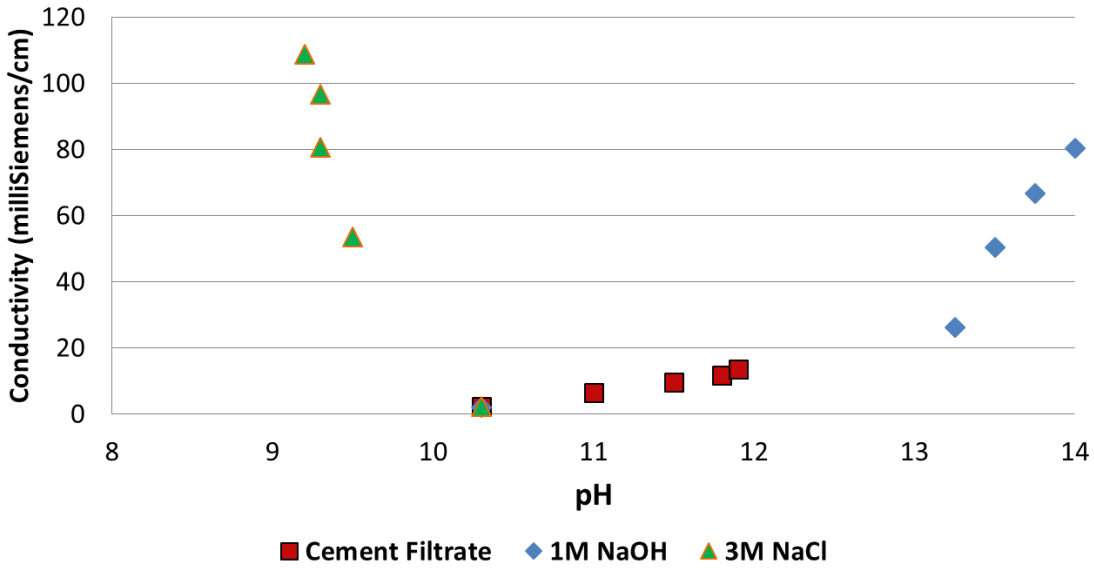

Figure 5.14 Titration of cement filtrate, 1M NaOH and 3M NaCl into EOR 5XS nanoparticle stock solution. Qualitatively, the particles displayed constant stability during all concentrations of the titrated substances.

The reason 3M NaCl instead of 1M NaCl was titrated into the 5XS nanoparticle solution was because it was thought they would should similar behavior to the 3M particles which has already exhibited resistance to high NaCl concentrations.

At this point it was thought that as a general tendency, coated silica nanoparticles in an originally alkaline solution would have higher stability in cement ionic and pH conditions vs. their uncoated counterparts. The next steps would be to try and generate foams with these particles with and without surfactant. At this time, the surfactant that was planned to be tested was the AOS surfactant. However, due to time constraints it was decided that a proof of concept approach would be advantageous. Instead, the partially hydrophobic HDK-H30 silica nanoparticles were chosen to generate long term stable

foams. These particles had the advantage of stabilizing air/water and likely nitrogen/water foams without the need for surfactant.

5.3.1.6 HDK-H30 Foam Generation and Stability Tests

Following the work of Binks & Horozov (2005) and Worthen et al (2013a) foams were successfully generated and stabilized by the partially hydrophobic HDK-H30 nanoparticles. The foams were generated with a 1 wt% HDK-H30 and 4 wt% NaCl concentration. The foams displayed stability over the course of 4+ days (an image of this is unavailable). A new batch of particle dispersion was generated and NaOH was added into to various samples to create solutions with pH ranging from 10 to 14 in increments of 1. Afterwards the samples were sonified in order to generate foams. Foams were successfully generated, except for the pH 14 solution where very little foam was created. After three days the foams presented substantial stability up to a pH of ~13 as can be seen in Figure 5.15. Since a proof of concept approach had been decided on at this point, the stability of these foams in cement filtrate was not tested. It was from these results that the base recipe to generate nanoparticle stabilized foams under pressure was established. However, the HDK-H30 dispersion concentration was higher in the following experiments (~2wt %) to attempt to ensure full nanoparticle coverage of the bubble surface as described in section 5.2.6.

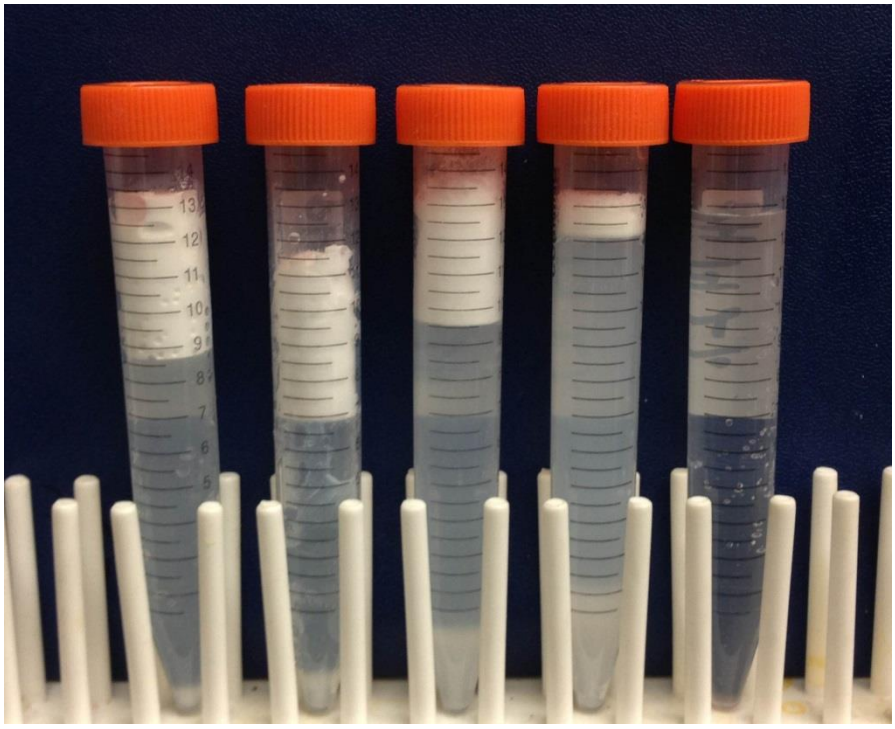

Figure 5.15 HDK-H30 stabilized foams in NaOH solution with pH ranging from 10 to 14 from left to right. Photograph was taken 3 days after foams had been generated by sonifying.

5.3.2 Pressurized Foam Generation Tests

The 3M PEG, HDK-H30 and EOR-50 nanoparticle types where used to attempt and generate stable foams under pressure. The increased beadpack pressure drop recorded of some tested nanoparticles (3M PEG & EOR-50) did demonstrate foam generation in the beadpack, but when it was observed flowing through the view cell it did not appear to be stable enough for the purposes of this research. The 3M PEG and EOR-50 foams did not appear as stable as the HDK-H30 and would break passing through the view cell. These nanoparticles were not investigated with further detail once a type of nanoparticle was identified to be able to generate a stable foam (HDK-H30). The higher outlet pressure

setting for these experiments was due to the initial familiarization on how to achieve steady foam generation with the apparatus. The pressure outlet set point was decreased once there was higher confidence in steadily generating foams at the target outlet pressure of 200 psi in the apparatus. The reasoning can be found in the overall chapter discussion section.

5.3.2.1 3M PEG Coated Particles

DI water flow rate (mL/min)	Pressure drop (psi)
5	5.46
10	11.05
15	15.75
20	20.45
25	25.07
30	29.65

Table 5.7 Reference beadpack flow data. Outlet pressure was set at 800 psi. Calculated permeability was 24.9 Darcy. R^2 value of data fit was 0.9988.

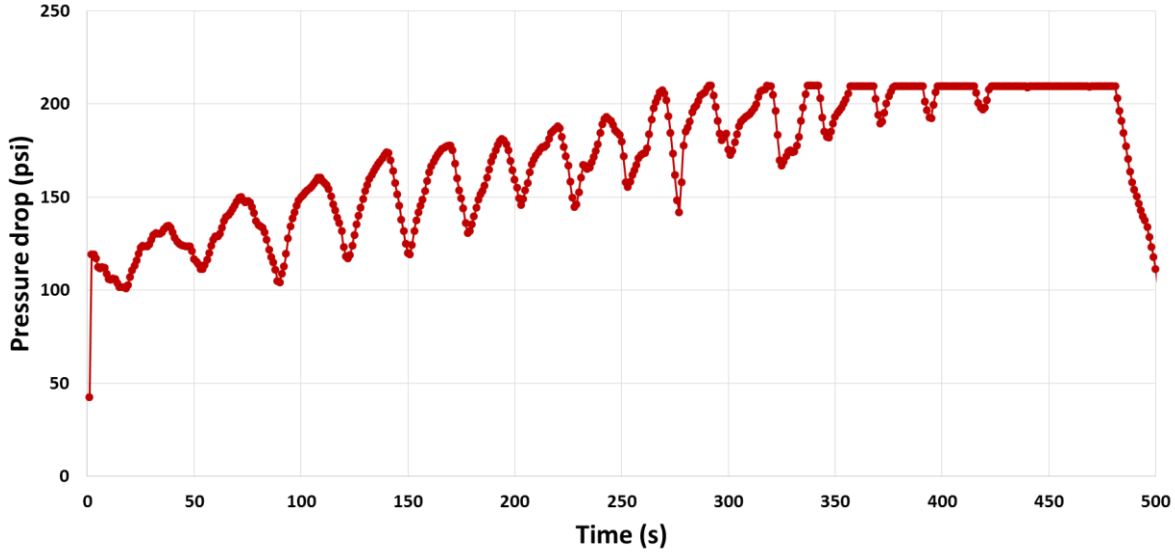

Figure 5.16 Beadpack pressure drop of foam generated with compressed air+2 wt% 3M PEG aqueous dispersion. NaCl concentration was 4 wt%. Outlet pressure was set at 750 psi. Pressure drop data was not recorded until first foam flow was observed through view cell. Flow rates were 5mL/min aqueous dispersion and 15 mL/min compressed air. Pressure drop reached 210 psi calibration limit and pegged out at t=335 s.

The pressure drop oscillation of the foam generated with the air+3M PEG nanoparticles is likely due to the foam generation intervals, followed by limited flow and gas phase compression and then a new slug of foam being generated. This process is described with more details in the overall chapter 5 discussion section. The foam appeared to be of relatively high apparent viscosity since pressure drop across the beadpack went higher than the pressure drop measurement calibration maximum of 210 psi.

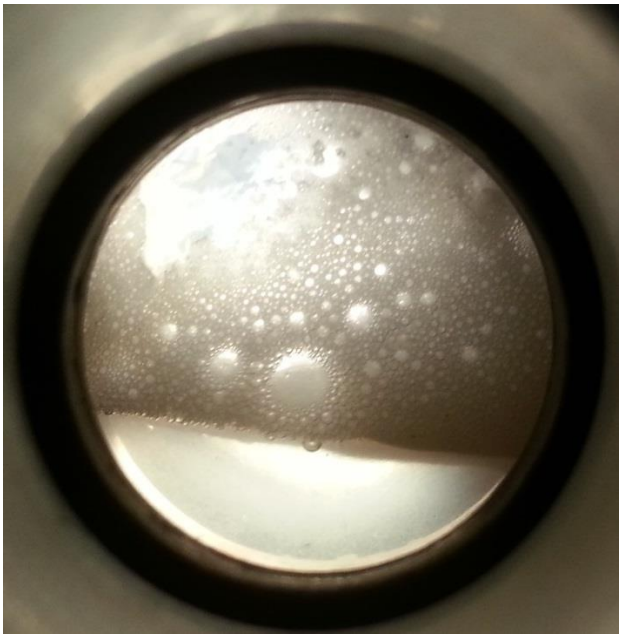

Figure 5.17 Foam generated with air + 3M PEG nanoparticles. Large bubble size variation, foam channeled flow and bubble breaking were observed.

Although the foam appeared to have a relatively high apparent viscosity, the bubbles appeared to break as they were passing through the view cell. When flow was stopped in the experiment and the foam trapped in the view cell was observed, the foam seemed to quickly break into its air and water components. After waiting a few minutes, qualitatively most of the foam appeared to be gone.

5.3.2.2 HDK-H30 Particles

Two runs in the DLS machine showed an average particle aggregate diameter of 362 nm for this batch. Prior to this experiment the beadpack was flushed back to its original state and did not have to be repacked. The same beadpack reference flow data used for section 5.3.2.1 applies.

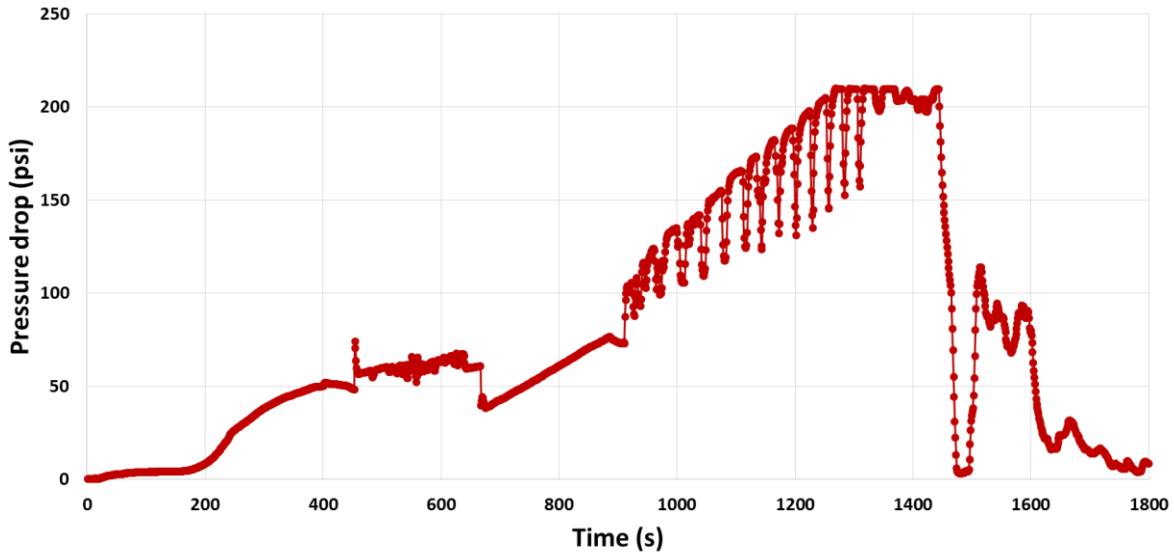

Figure 5.18 Beadpack pressure drop during first successful HDK-H30 foam generation experiment. Foam generated with compressed air+3 wt% HDK-H30 aqueous dispersion. NaCl concentration was 4 wt%. Outlet pressure was set at 700 psi. From t=0 to 642 s a 5 mL/min aqueous dispersion flow rate was used; at t=642 air flow rate was initiated at 15 mL/min. At around t=910 s foam generation appears to take place, this was confirmed in the view cell. At t=1420 s flow rates were changed to 3 mL/min dispersion and 9 mL/ min air. At t=1590 s experiment was stopped.

Pressure drop increase during exclusively aqueous dispersion flow from t=200 to 642 s was attributed to the sticky nanoparticles gradually clogging the beadpack. The steep pressure drop slope during foam generation pressure drop oscillation intervals, is attributed to a combination of foam being generated and saturating the apparatus, as well as gradual blockage in the beadpack. Blockage was found after stopping flow and flushing out the apparatus with DI water. When the waste effluent showed no traces of components other than water, and beadpack pressure drop was continuously larger than the reference pressure drop data, blockage was suspected. The beadpack was dissembled and particle lumps were

found sticking to the beads. After this first successful foam generation experiment with the HDK-H30 particles, it was decided to replace the beadpack beads for every experiment where the HDK-H30 particles were to be utilized.

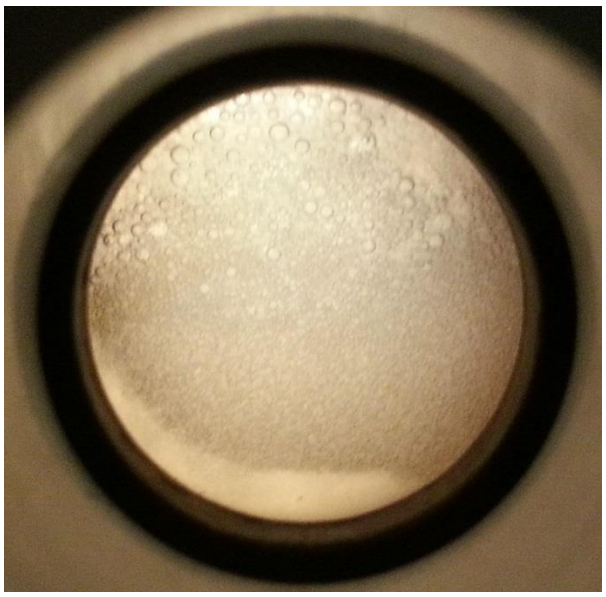

Figure 5.19 Foam generated with compressed air + HDK-H30 nanoparticles. The photograph in Figure 5.6 was captured during this same experiment.

Included to long term dispersion stability, this was an additional reason a smaller aggregate diameter was used in future experiments.

5.3.2.3 EOR Series Particles

DI water flow rate (mL/min)	Pressure drop (psi)
5	4.91
10	9.42
15	14.12
20	18.85
25	23.92

Table 5.8 Reference beadpack flow data. Outlet pressure was set at 220 psi. Calculated permeability was 25.8 Darcy. R^2 value of data fit was 0.9996.

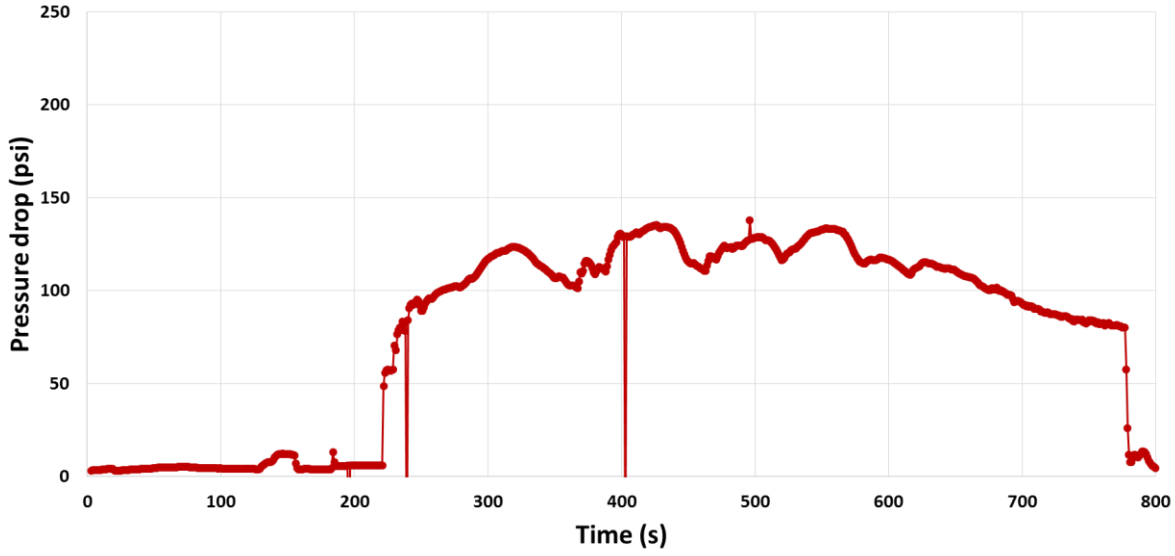

Figure 5.20 Beadpack pressure drop of foam generated with compressed N2+2 wt% EOR-50 aqueous dispersion. NaCl concentration was 4 wt%. Outlet pressure was set at 250 psi. From t=0 to 220 s, system was being pressurized with a 5 mL/min aqueous dispersion flow rate. At *t*=220 s flow rates were 5 mL/min aqueous dispersion and 15 mL/min compressed nitrogen.

Chronologically, this experiment was performed much later after having chosen the HDK-H30 particles for foam generation. It was performed to search for alternatives for stable foam generation with nanoparticles in combination with surfactant. This was the no-surfactant baseline experiment. At this point pure nitrogen was being used as the gas phase and foams were being generated at lower target outlet pressures (100-250 psi), two criterion previously explained.

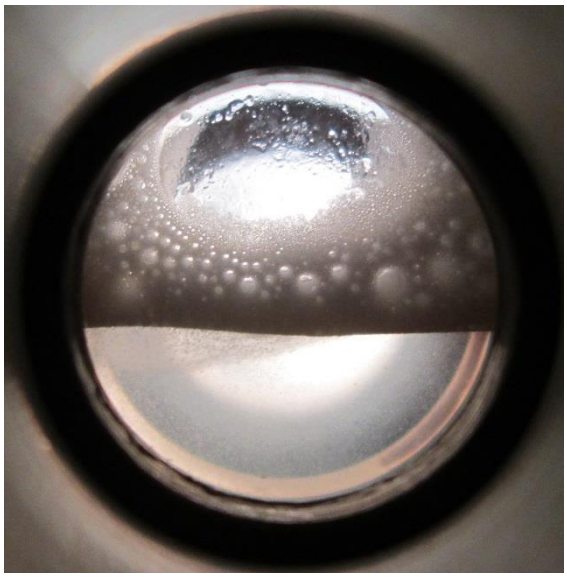

Figure 5.21 Foam observed with EOR-50 nanoparticles. Gas phase was pure nitrogen. Aqueous phase concentrations were 2 wt% nanoparticles, 4 wt % NaCl.

5.3.2.4 Optimal Flow Rates for Foam Generation

Once the HDK-H30 particles were chosen to generate long term stable air + water foams, various G/W flow rates and/or proportions were tested to find optimal/consistent foam generation parameters. For the purpose of this research, it was believed the optimal foam quality would be that where just enough water needed to stabilize all the foam G/W

interfaces was present. This would maximize the foam's specific surface and thus total nanoparticle covered G/W surface throughout the compression experiment. This also means excess water would not occupy the compression vessel. A maximized volume occupied by foam, would likely make the compressibility measurements more accurate. Minimizing excess water would also minimize the extent of gas dissolution during the experiment. To attempt and find such G/W flow conditions a qualitative analysis was performed. Various flow rates were tested and view cell observations were recorded. The target was to reach the maximum gas phase flow rate at which foam appeared stable. Pressure drop data is not available for the presented results

DI water flow rate (mL/min)	Pressure drop (psi)
5	5.7
10	12.35
15	18
20	22
25	28.9
30	32.9

Table 5.9 Reference beadpack flow data. Outlet pressure was set at 600 psi. Calculated permeability was 21.9 Darcy. R^2 value of data fit was 0.9946.

Settings	HDK-H30 flow (mL/min)	Air flow (mL/min)	Ideal quality (%)	Observations
a	5	5	50	Foam was observed, many disconnected bubbles were seen
b	5	10	66.6	Foam observed. Thick aqueous layers between bubbles
c	4	11	73.3	Stable foam flow. Complete foam coverage in view cell
d	3	15	83.3	Foam with large bubbles, gas slugs and channeled flow
e	3	12	80	Foam with relatively larger bubble size
f	4	16	80	Foam with relatively larger bubble size. Bubble size appeared to oscillate less than in setting e
g	4	12	75	Stable foam flow, complete view cell foam coverage
h	5	15	75	Stable foam flow, complete view cell foam coverage

Table 5.10 Summary of qualitative observations of during foam generation experiments varying G/W flow rates. All tests were performed with air+2.5 wt% HDK-H30. Batch average particle diameter was 184 nm. 4 wt % NaCl concentration used. Outlet pressure was set at 600 psi. Ideal quality assumes proportional flow rates do not change throughout apparatus.

This data was gathered over two experiments. After the first (Settings a-d), the apparatus was flushed, but a small amount of enduring clogging was observed in the beadpack. All the reference pressure drops from table 5.5 were roughly ~4 psi greater. The beadpack was not repacked for the second experiment (settings e-h). The increased flow restriction might have skewed the results of the second run, but this was not further investigated. The chosen flow rate for most future experiments was 5 mL/min HDK-H30 and 15 mL/min gas phase (setting h). No noticeable differences were observed between settings g and h. Setting h was chosen due to the shorter waiting time to achieve steady state.

The main purpose of this research was to measure the compressibility of foams. Thus a quantitative study including shear rates, pressures, temperature etc. was not performed to find the absolute best ideal foam quality. However, the setting chosen (h) was consistent with the work performed by Worthen et al (2013b) using the experimental setup from which this one was derived. In CO_2/water particle stabilized foams and emulsions, Worthen et al observed a maximum viscosity at a quality of 0.75 for various nanoparticles tested including the HDK-H30. The explanation presented the authors was that when the foam quality too small, bubbles are very dilute and do not touch each other to form films. When this occurs viscosity does increase but only by a few times relative to the pure solvent. When the quality is too high, the films between bubbles are thin and break or might not form at all. The viscosity of the foam is expected to reach a maximum as quality is increased and then drop to the gas phase viscosity as the quality approaches 100%.

Having found that nanoparticle stabilized air + water foam generation was feasible and optimal flow rates were found, air was replaced with pure nitrogen to further minimize dissolution effects.

5.3.3 Bubble Size and Adequate Particle Dispersion Concentration

Two photographs were processed to find an approximate average foam bubble diameter. The two images were analyzed from the HDK-H30 experiments. The first was chosen since it qualitatively appeared to have smallest bubble size of all experiments and thus the largest specific surface area. The second image was chosen to represent one of the larger qualitatively observed bubble size. For both images, the bubbles chosen were from the mid-section. Since the inlet and outlet of the view cell were located right through the middle, it was regularly observed that fluid would get trapped in the top and bottom sections. This trapped fluid was not thought to be representative of the foam being generated, especially since some got stuck there while the system was reaching steady state.

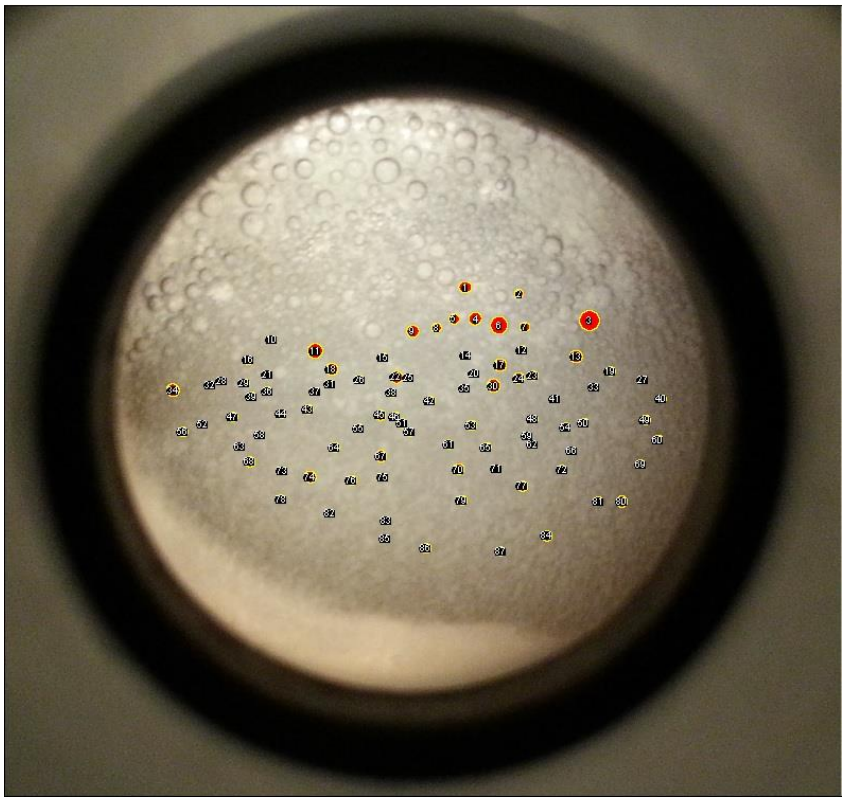

Figure 5.22 Smallest observed bubble size. Image captured during experiment in section 5.3.2.2. Outlet pressure set at 700 psi. Red circles outlined by yellow lines represent bubbles selected to estimate bubble diameter through image analysis. Average bubble diameter was found to be 221 microns.

The sample size was 87 bubbles chosen from different locations in the middle section. The complete analysis can be found in the appendix of this thesis. The average bubble diameter was found to be 221 microns.

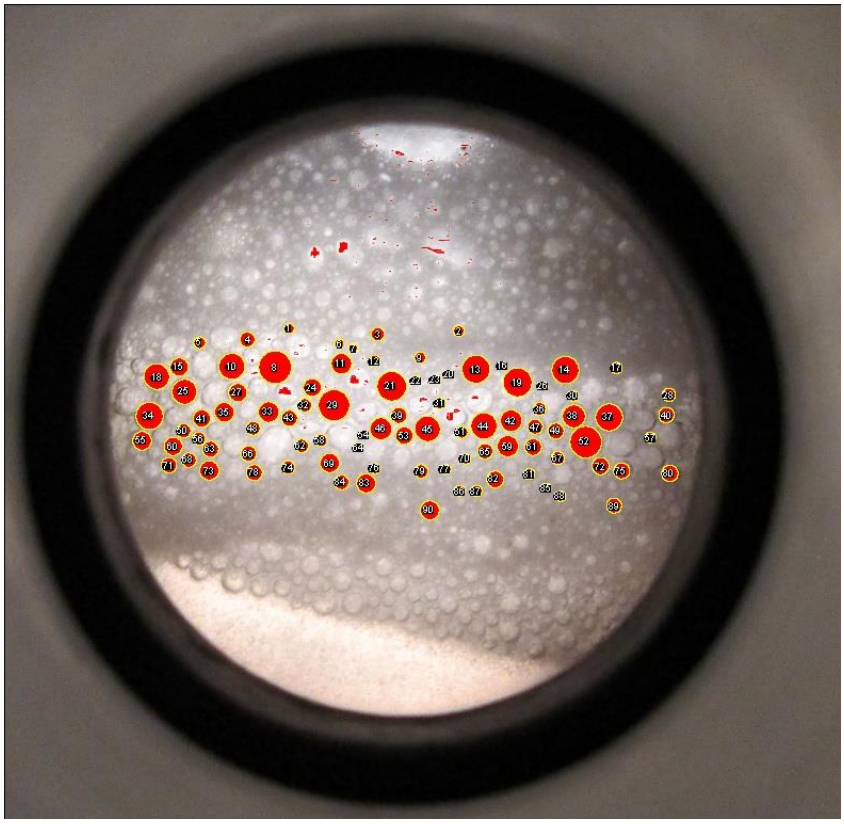

Figure 5.23 Qualitatively larger bubble size example. Red circles outlined by yellow lines represent bubbles selected estimate bubble diameter through image analysis. Average bubble diameter was found to be 383 microns.

The sample size was 90 bubbles chosen from different locations in the middle section. The complete analysis can be found in the appendix section. The average bubble diameter was found to be 383 microns.

Three cases were considered to approximate an adequate nanoparticle dispersion concentration to form a monolayer at foam generation pressure. The three cases represented the anticipated largest and smallest concentrations needed and also a point in between. The first was the smallest observed average bubble diameter (~220 microns) and the largest

HDK-H30 aggregate diameter used (300 nm). The second was the largest bubble diameter (~380 micron) and smallest HDK-H30 aggregate diameter obtained/used (~150 nm). The last point, with a 300 micron bubble diameter and a 250 nm aggregate diameter, was chosen as the in between case. The reasoning for choosing the first case was that smaller bubbles have higher specific surface area and larger nanoparticles the opposite, thus the largest anticipated concentration. The opposite holds true for the second case. An average bubble diameter D_b to HDK-H30 aggregate D_{Np} was also calculated.

Quality (%)	Concentration needed (wt %)
60	1.63
65	2.02
70	2.54
75	3.26
80	4.35

Table 5.11 Required nanoparticle dispersion concentration to create monolayer during foam generation. Average bubble diameter 220 micron, average HDK-H30 aggregate diameter 300 nm. $D_b/D_{Np} = 733$.

Quality (%)	Concentration needed (wt %)
60	0.47
65	0.59
70	0.74
75	0.95
80	1.26

Table 5.12 Required nanoparticle dispersion concentration to create monolayer during foam generation. Average bubble diameter 380 micron, average HDK-H30 aggregate diameter 150 nm. $D_b/D_{Np} = 2533$.

Quality (%)	Concentration needed (wt %)
60	1.00
65	1.24
70	1.55
75	2.00
80	2.66

Table 5.13 Required nanoparticle dispersion concentration to create monolayer during foam generation. Average bubble diameter 300 micron, average HDK-H30 aggregate diameter 250 nm. $D_b/D_{Np} = 1200$.

The calculation results from case three were used to choose a dispersion concentration for all HDK-H30 future foam generation experiments. The 75% quality required concentration of 2 wt% was targeted. This concentration was also considered sufficient for any other nanoparticle type described in this study, since they all were much smaller than the HDK-H30 aggregates and thus had larger specific surface area.

A final observation was that qualitatively there appeared to be a relationship between bubble size and set foam generation outlet pressure. This was not investigated with more detail.

5.3.4 Compression of HDK-H30 Stabilized Foam

The main variable change from the experiment results in this section was the pressure at which foam was generated/loaded into the compression vessel. The foam in the first experiment was generated at atmospheric pressure to have a comparison point to the data obtained in chapter 4.

5.3.4.1 Experiment #1 (Generated at Atmospheric Pressure)

The foam in experiment #1 was generated using the blender previously described and procedure previously described in Chapter 4 and 5

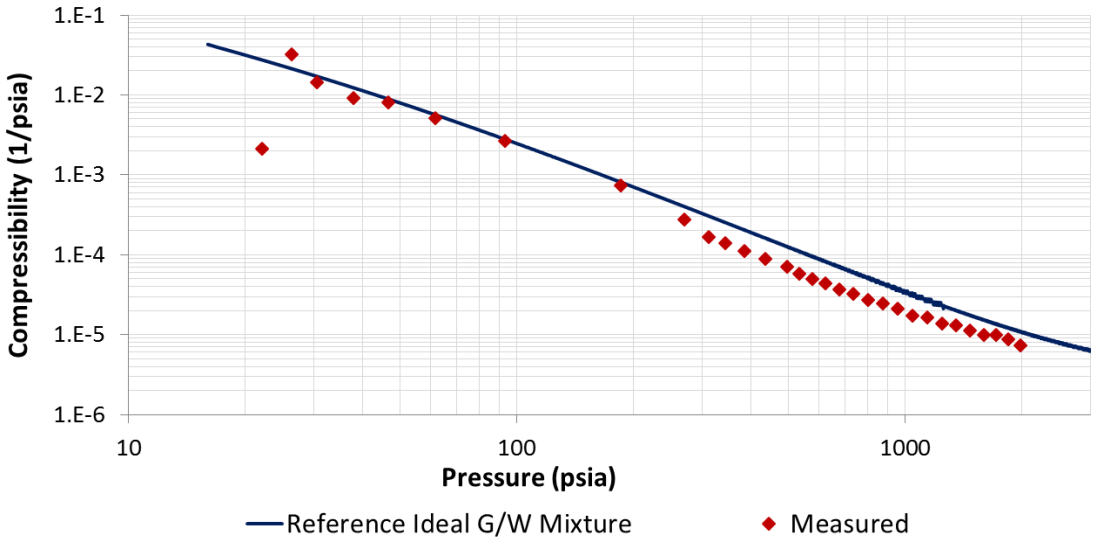

Figure 5.24 Compressibility of 2 wt% HDK-H30 stabilized foam experiment #1. Batch average particle aggregate diameter was 233 nm. NaCl concentration was 4 wt%. P_o=14.7 psia. Initial foam quality 68.7%. Gas dissolution appears to have some effects, but not enough to change the overall trend of the data.

Considering the observed pressure range, 14.7 to ~2014.7 psia, and following the calculations methods discussed in section 5.2.7; the volume of a bubble in this system would have been reduced to ~0.73% of its original size. The foam bubble area would have been reduced to ~3.76% of its original size. If the nanoparticles stay in the G/W interface this would increase the nanoparticle surface density 26.6 times.

5.3.4.2 Experiment #2

Foam target outlet pressure was set at 500 psi, actual pressure was 478 psi. The higher pressure setting for this experiment was due to the initial familiarization on how to achieve steady foam generation with the apparatus.

DI water flow rate (mL/min)	Pressure drop (psi)
5	4.7
10	9.32
15	14.3
20	19.43
25	24.68

Table 5.14 Reference beadpack flow data for experiment #2. Calculated permeability was 25.7 Darcy. R^2 value of data fit was 0.9994.

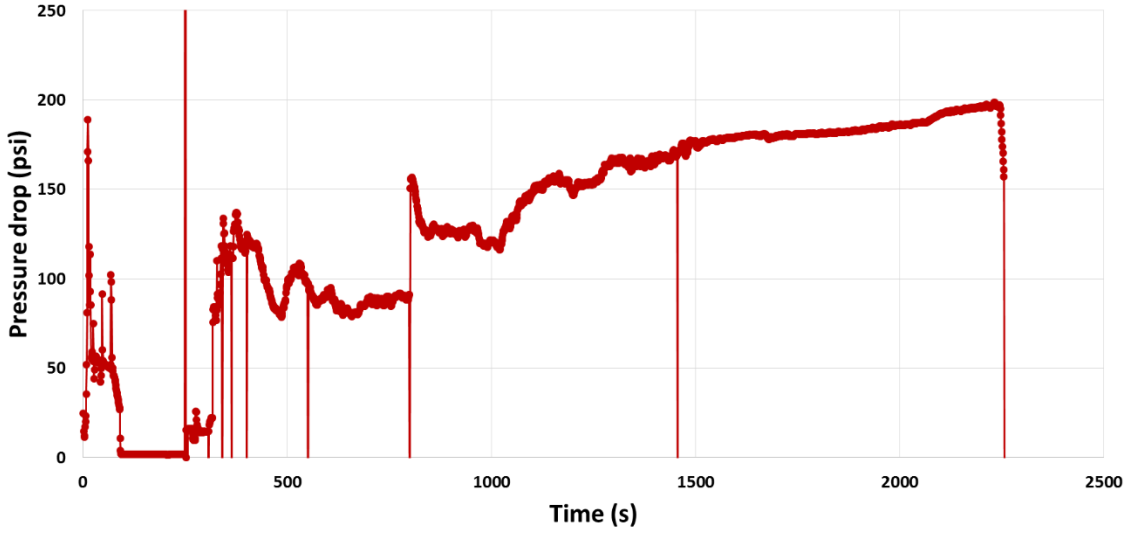

Figure 5.25 Experiment #2. Beadpack pressure drop during foam generation with compressed N2+1.95 wt% HDK-H30 aqueous dispersion. Batch average particle aggregate diameter was 201 nm. NaCl concentration was 4 wt%. Outlet pressure was set at 500 psi. From t=0 to ~250 s, system was being pressurized with a 5mL/min aqueous dispersion flow rate. At *t*~250 s flow rates were 5mL/min aqueous dispersion and 15 mL/min compressed N_2. Steady state assumed at around *t*=~800s, time at which compression vessel loading began.

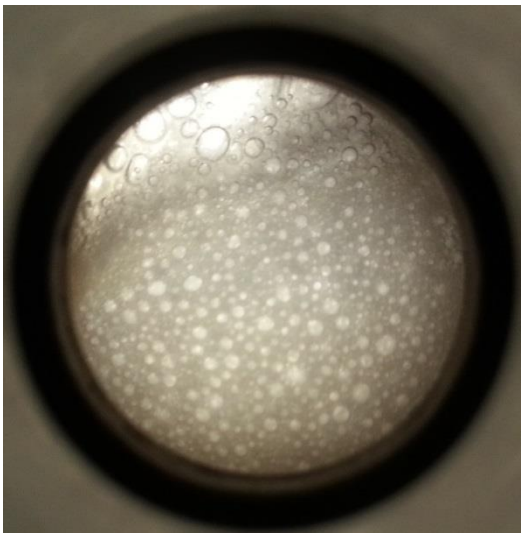

Figure 5.26 Foam generation observed during experiment #2.

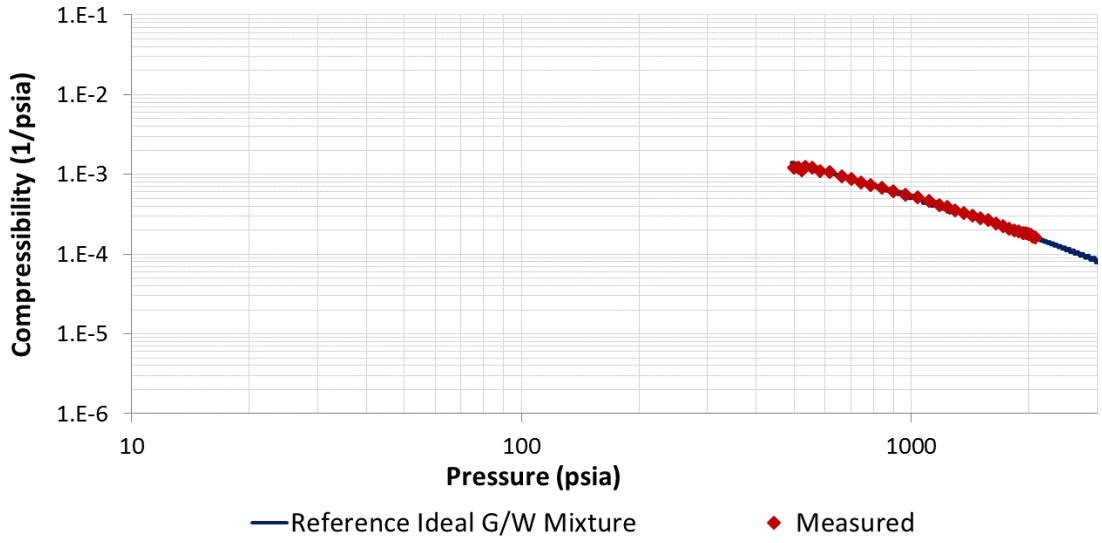

Figure 5.27 Compressibility of foam generated in Experiment #2. Measured P_o=493 psia. Measured initial foam quality 69.2%.

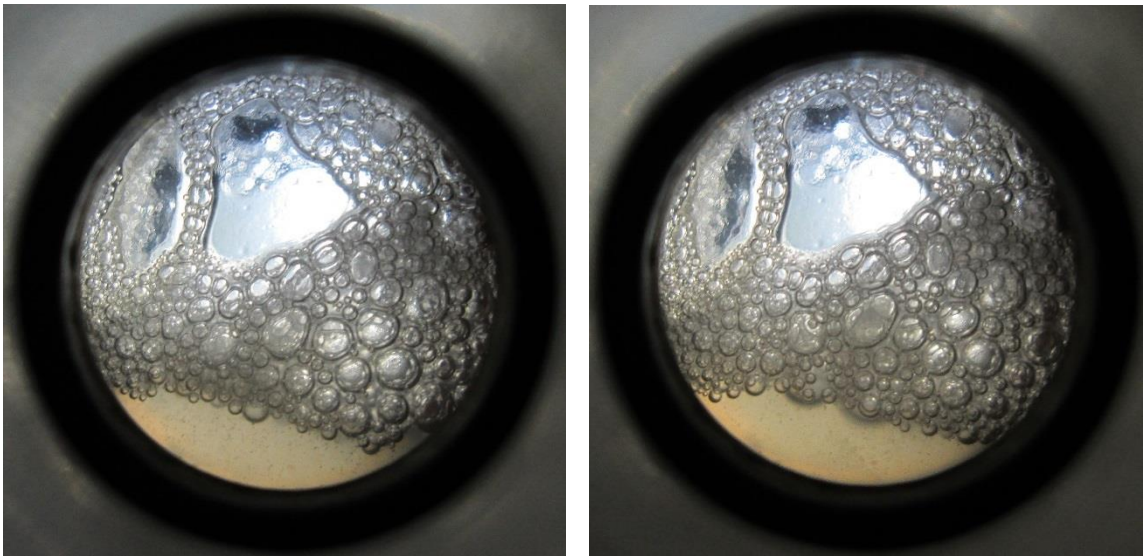

Figure 5.28 Experiment #2 foam long term stability test. Photograph on the right was taken 154 minutes after photograph on the left.

Considering the observed pressure range for experiment #2 was 493 to ~2014.7 psia, foam gas volume would have been reduced to ~24.5% of its original volume and the area to 39.1% of its original size. This would equal to an increase in nanoparticle surface density of roughly 2.6x.

5.3.4.3 Experiment #3

**During this experiment the pressure regulators were set at ~100 psi. It took longer to reach a point where steady state could be assumed. One of the ISCO syringe pumps fully emptied its reservoir and the experiment was stopped without the compression vessel being fully loaded. The foam inside was expanded so that the initial foam volume could be known. The pressure prior to the expansion was not measured. After the expansion, the pressure was measured at 40 psi. It was assumed the foam remained stable after being

expanded. The quality after expansion was measured at 78.8%. Had the foam been originally at 100 psi the foam quality would have been ~60%.

DI water flow rate (mL/min)	Pressure drop (psi)
5	4.93
10	9.29
15	13.78
20	18.54
25	23.4

Table 5.15 Reference beadpack flow data for experiment #3. Outlet pressure was set at 150 psi. Calculated permeability was 26.2 Darcy. R^2 value of data fit was 0.9995.

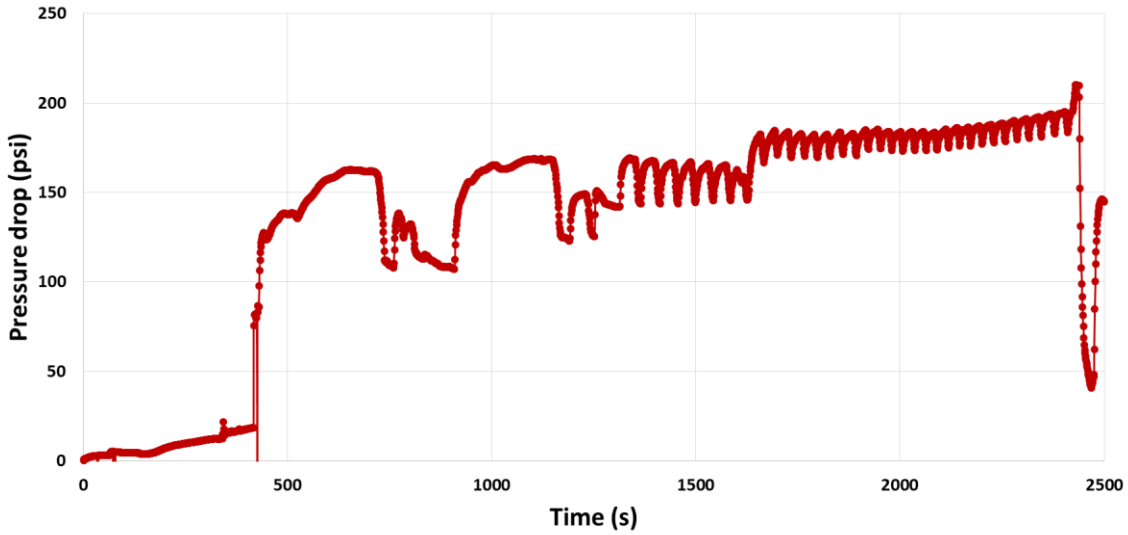

Figure 5.29 Experiment #3. Beadpack pressure drop of foam generated with compressed N_2+1.95 wt% HDK-H30 aqueous dispersion. Batch average particle aggregate diameter was 192 nm. NaCl concentration was 4 wt%. Outlet pressure was set at 100 psi. From t=0 to ~400 s, system was being pressurized with a 5mL/min aqueous dispersion flow rate. At *t*~400 s flow rates were 5mL/min aqueous dispersion and 15 mL/min compressed N_2. Steady state assumed at around *t*~1650s, time at which compression vessel loading began.

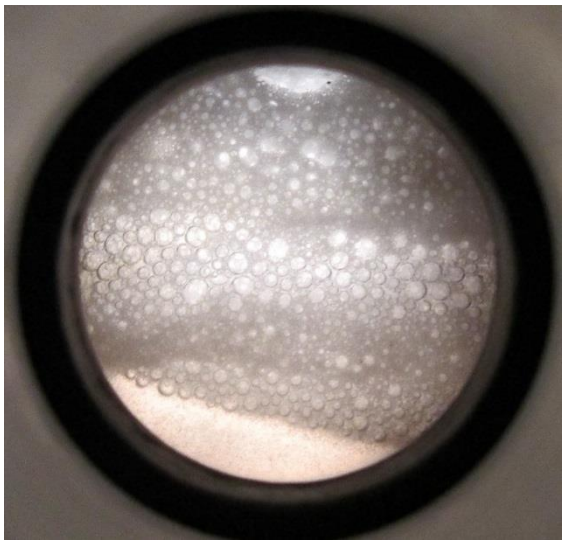

Figure 5.30 Foam generation observed during experiment #3.

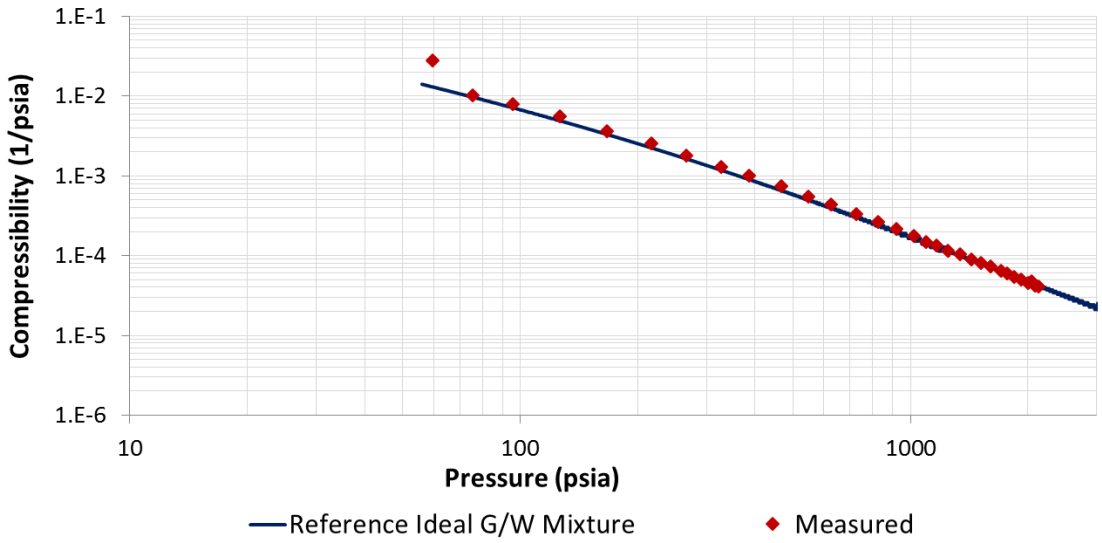

Figure 5.31 Compressibility of foam generated in Experiment #3. Measured P_o=54.7 psia. Measured initial foam quality 78.8%.

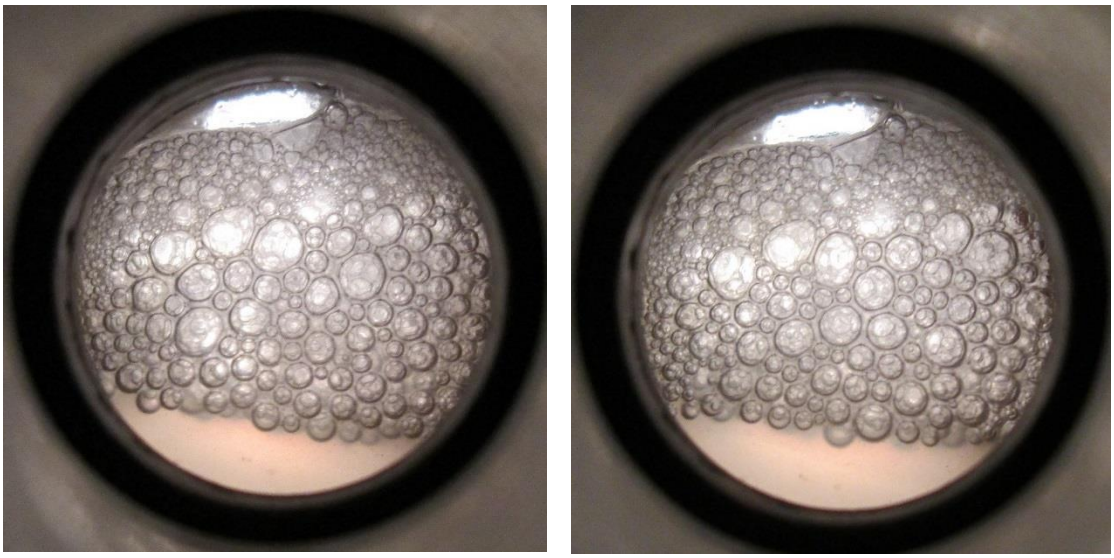

Figure 5.32 Experiment #3 foam long term stability test. Photograph on the right was taken 123 minutes after photograph on the left.

Adjusted to the assumed initial pressure of 100 psi, observed pressure range for experiment #3 was 114.7 to ~2114.7 psia. Foam gas volume would have been reduced to 5.24% of its original size and the area to 14.33% of its original size. This would equal to an increase in nanoparticle surface density of roughly 7x. This case would likely better represent the change in nanoparticle surface density as there is no reason to believe additional nanoparticles would migrate to the G/W interface after the expansion.

Post expansion observed pressure range for experiment #3 was 54.7 to ~2114.7 psia, foam gas volume would have been reduced to 2.59% of its original size and the area to 8.75% of its original size. This would equal to an increase in nanoparticle surface density of roughly 11.42x.

5.3.4.4 Experiment #4

Foam target outlet pressure was set at 200 psi, actual pressure was 170 psi.

DI water flow rate (mL/min)	Pressure drop (psi)
5	5.54
10	10.53
15	15.6
20	20.79
25	26.11

Table 5.16 Reference beadpack flow data for experiment #4. Outlet pressure was set at 200 psi. Calculated permeability was 23.2 Darcy. R^2 value of data fit was 0.9998.

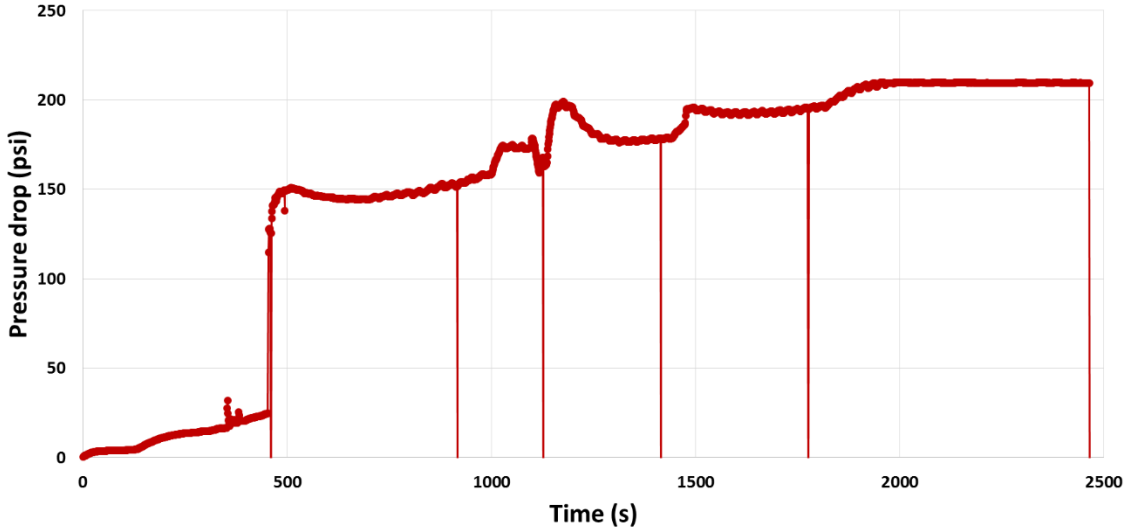

Figure 5.33 Experiment #4. Beadpack pressure drop of foam generated with compressed N_2+1.9 wt% HDK-H30 aqueous dispersion. Batch average particle aggregate diameter was 238 nm. NaCl concentration was 4 wt%. Outlet pressure was set at 200 psi. From t=0 to ~480 s, system was being pressurized with a 5mL/min aqueous dispersion flow rate. At *t*~480 s flow rates were 5mL/min aqueous dispersion and 15 mL/min compressed N_2. Steady state assumed at around *t*~1200s, time at which compression vessel loading began. Pressure differential signal pegged out (210 psi) at *t*~1900 s.

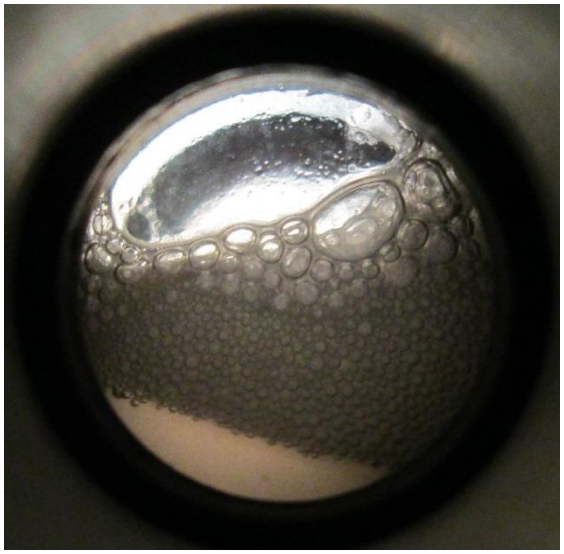

Figure 5.34 Foam generation observed during experiment #4.

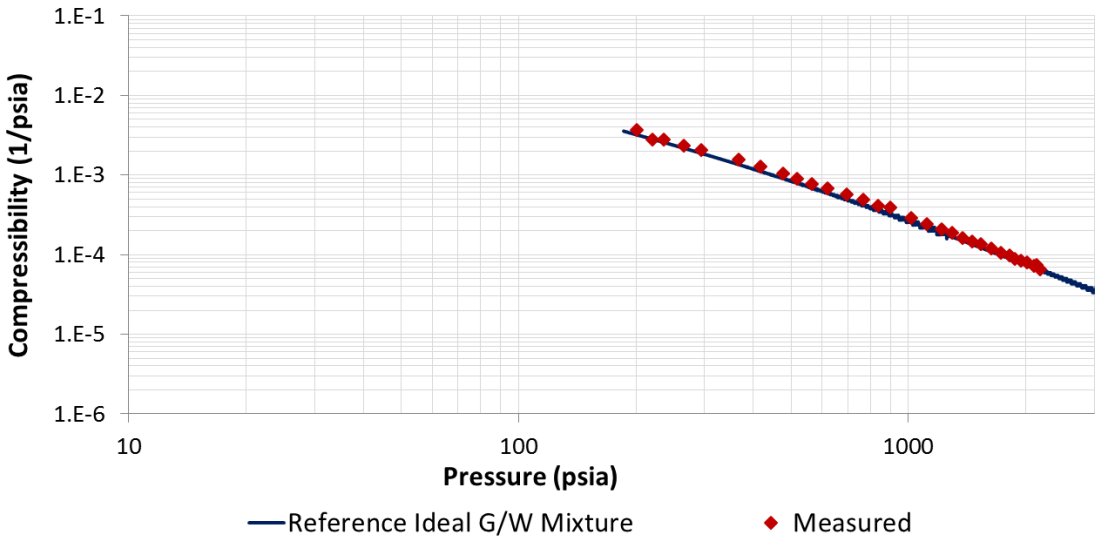

Figure 5.35 Compressibility of foam generated in Experiment #4. Measured P_o=184.7 psia. Measured initial foam quality 66%.

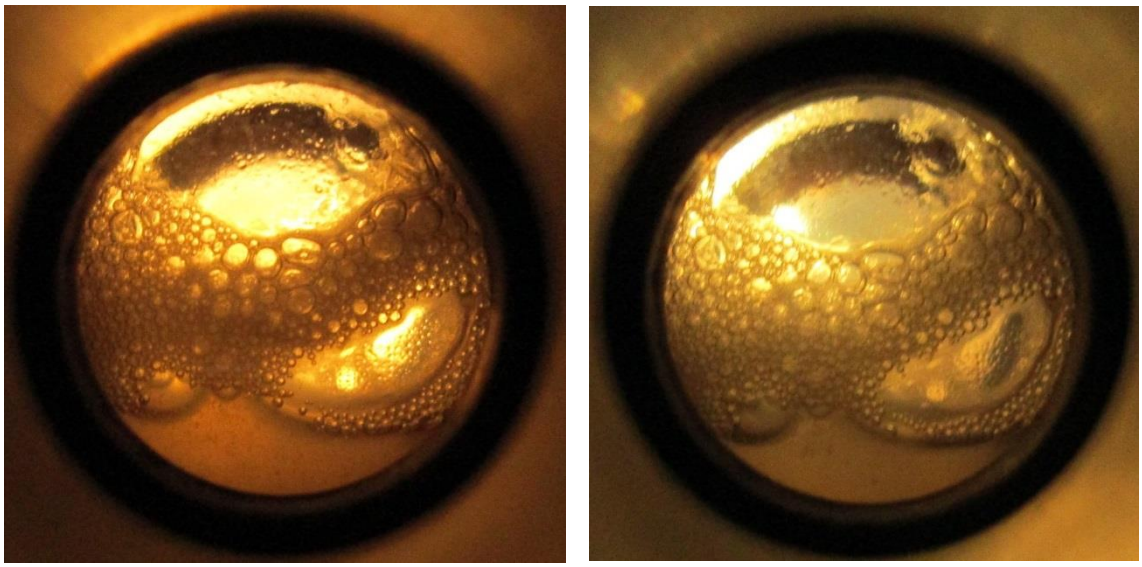

Figure 5.36 Experiment #4 foam long term stability test. Photograph on the right was taken 110 minutes after photograph on the left.

Considering the observed pressure range for experiment #4 was 184.7 to ~2150.7 psia, foam gas volume would have been reduced to ~8.59% of its original volume and the area to 19.46% of its original size. This would equal to an increase in nanoparticle surface density of roughly 5.13x.

The results in this section show that air + water and nitrogen + water foams stabilized solely by HDK-H30 were successfully generated at pressures ranging from 14.7 to ~500 psia. Subsequently, the compressibility of these foams was measured. The foams in all of these experiments were shown to be stable over the time period that the compressibility measurements took place. The armored bubble effect did not appear to be present in any of the four HDK-H30 stabilized foam compressibility measurement experiments. The foam generated at atmospheric pressure did show a reduced

compressibility, an effect that was attributed to gas dissolution as previously concluded in Chapter 4.

Depending on the initial nanoparticle bubble surface density, it is possible that a closed packed was never attained after compression. However, since a direct measurement of nanoparticle concentration in the G/W interface is not available, this is only a conjecture.

5.3.5 Compression of CTAB + Ludox TMA Stabilized Foam

During the course of this research, another foam recipe was found in a research study performed by Maestro et al (2014). The foam was made using a combination of CTAB surfactant and Ludox TMA silica nanoparticles. The concentrations used were $2*10^{-4}$ M CTAB, 1.5 wt % Ludox TMA and 1mM NaBr. The foam recipe was used to confirm the results obtained by using the HDK-H30 nanoparticle stabilized foams.

Foam target outlet pressure was initially set at 200 psi. The nitrogen initial pressure was set slightly too high and the pressure regulator set point had to be increased 250 psi. After adjusting pressure regulator #2 to 250 psi while loading the compression vessel, the measured foam pressure was 231 psi.

DI water flow rate (mL/min)	Pressure drop (psi)
5	5.1
10	9.7
15	14.55
20	19.7
25	24.65

Table 5.17 Reference beadpack flow data for experiment for CTAB + Ludox TMA experiment. Outlet pressure was set at 200 psi. Calculated permeability was 24.9 Darcy. R^2 value of data fit was 0.9996.

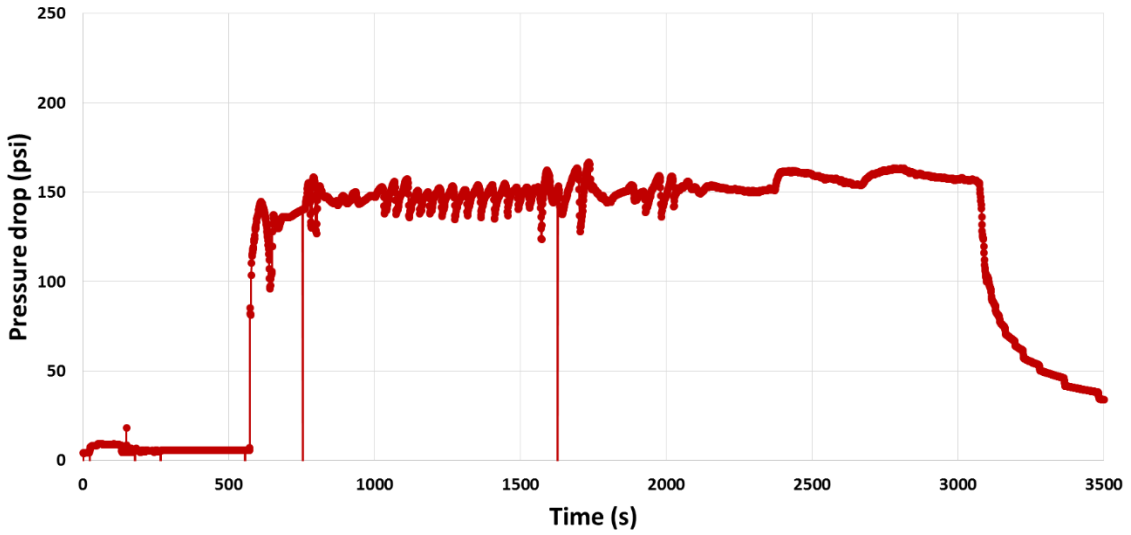

Figure 5.37 Beadpack pressure drop of foam generated with compressed N_2 and a 2*10^-4 M CTAB+1.5 wt% Ludox TMA aqueous dispersion. NaBr concentration was 1 mM. Outlet pressure was set at 250 psi. From t=0 to ~600 s, system was being pressurized with a 5mL/min aqueous dispersion flow rate. At *t*~600 s flow rates were 5mL/min aqueous dispersion and 15 mL/min compressed N_2. Steady state assumed at around *t*~1600s, time at which compression vessel loading began.

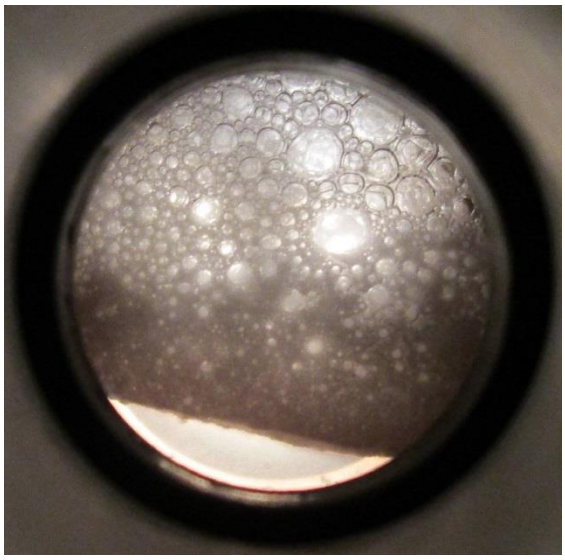

Figure 5.38 Foam generation observed during CTAB + Ludox TMA experiment.

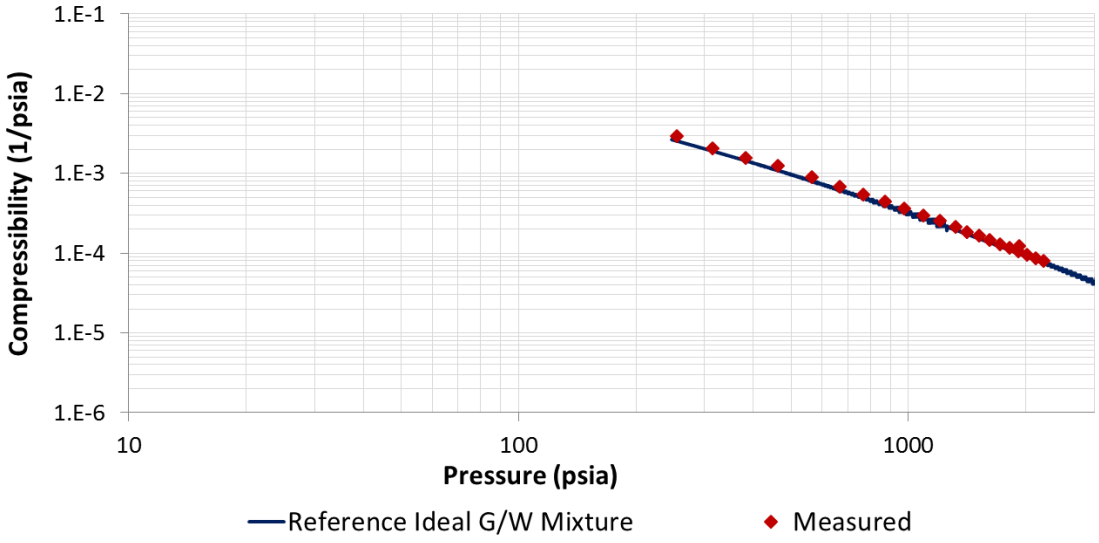

Figure 5.39 Compressibility of CTAB + Ludox TMA foam. Measured P_o=245.7 psia. Measured initial foam quality 65.38%.

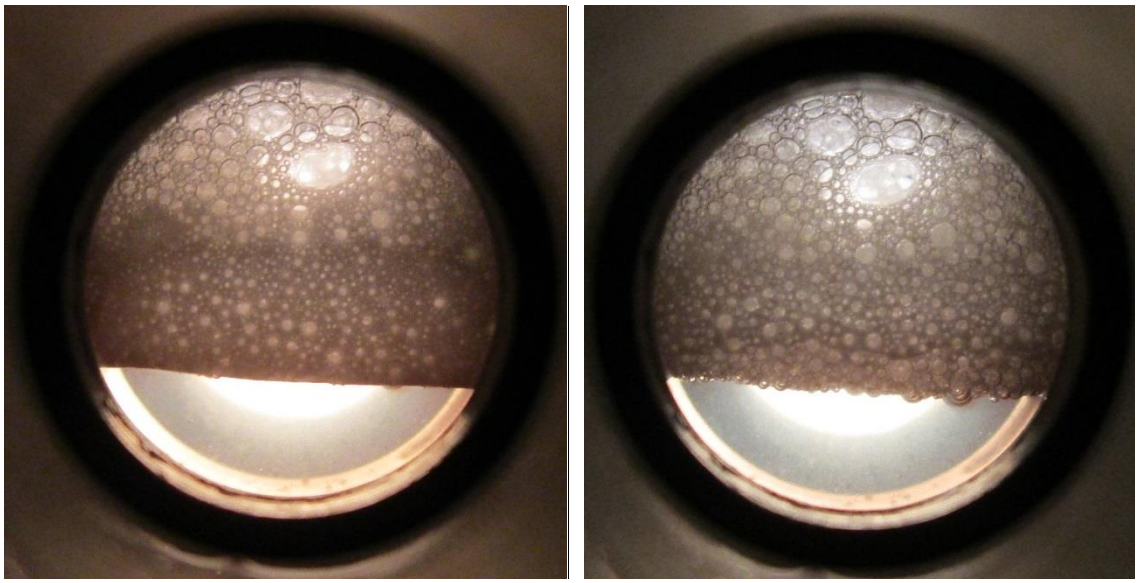

Figure 5.40 CTAB + Ludox TMA foam long term stability test. Photograph on the right was taken 233 minutes after photograph on the left.

Considering the observed pressure range was 245.7 to ~2214.7 psia, foam gas volume would have been reduced to ~11.09% of its original volume and the area to 23.08% of its original size. This would equal to an increase in nanoparticle surface density of roughly 4.33x.

The compression of the foam generated at 245.7 psia with the CTAB + Ludox TMA recipe showed practically the same results as the compression of the foam made with HDK-H30 particles at the most comparable pressure of 184.7 psia. The compressibility of both foams behaves extremely similar to that of its ideal G/W mixture counterpart.

5.3.6 Foam Liquid Phase Refractive Index vs. Pressure

The thought behind these experiments was to look for indications if nanoparticles were remaining at the G/W interface or were popping during compression. The theory was

that as the gas volume compressed excess liquid in the G/W interface would drain during the process. RI could then potentially be used to measure if nanoparticle concentration changes in this drained liquid phase was occurring at different pressures.

5.3.6.1 RI Benchmark Experiment

The benchmark experiment consisted in measuring the RI of various HDK-H30 dispersions with known concentrations. All the dispersions were made from the same batch. The batch had an aggregate diameter of 348 nm. The aggregate size was larger than the target 150-250 nm diameter from previous experiments. Since the dispersion exhibited colloidal stability and the objective was to find if a change in RI as a function of concentration could be observed, this was considered adequate. Dispersions were mixed with concentrations of 0.5, 1.5, 2.5 and 3.5 wt%. The RI of the DI water in which the nanoparticles was dispersed was measured at 1.3324 at a wavelength of 589 nm and temperature of 68 °F. The number was considered close enough to the 1.33335 reported in literature at the same conditions (Wohlfarth, 2008)

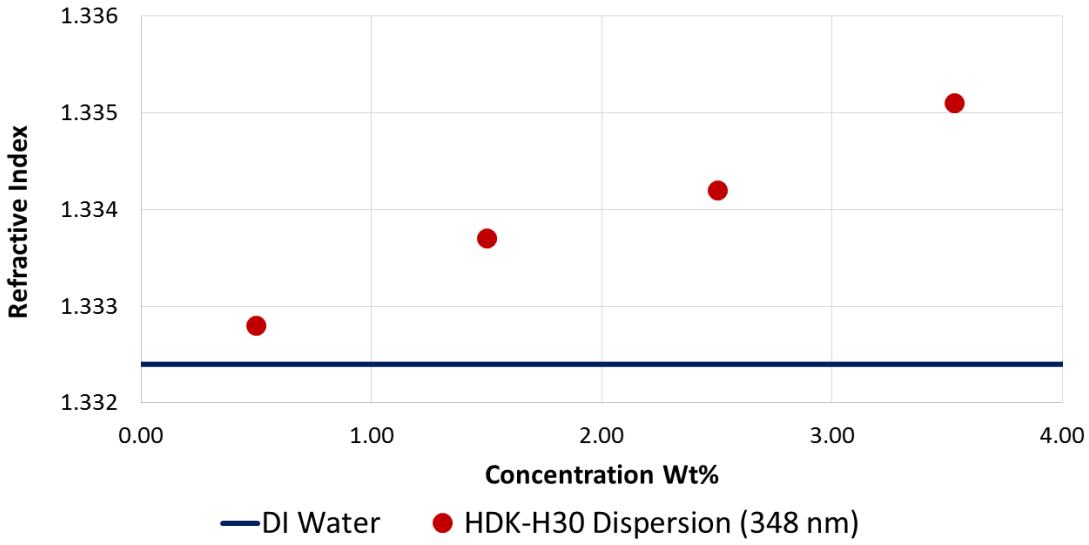

Figure 5.41 RI as a function of HDK-H30 aqueous dispersion concentration. Average aggregate diameter was measured at 384 nm. RI displayed a linear dependence to concentration. $R^2 = 0.989$.

5.3.6.2 RI Experiment #1

After generating the foam, it was compressed and sampled at ~400 psi intervals. The foam drained liquid was sampled 15 minutes after each pressure increment to allow foam excess liquid to drain to the bottom.

DI water flow rate (mL/min)	Pressure drop (psi)
5	4.3
10	8.8
15	13.06
20	17.38
25	21.8

Table 5.18 Reference beadpack flow data for RI experiment #1. Outlet pressure was set at 200 psi. Calculated permeability was 28.2 Darcy. R^2 value of data fit was 0.9999.

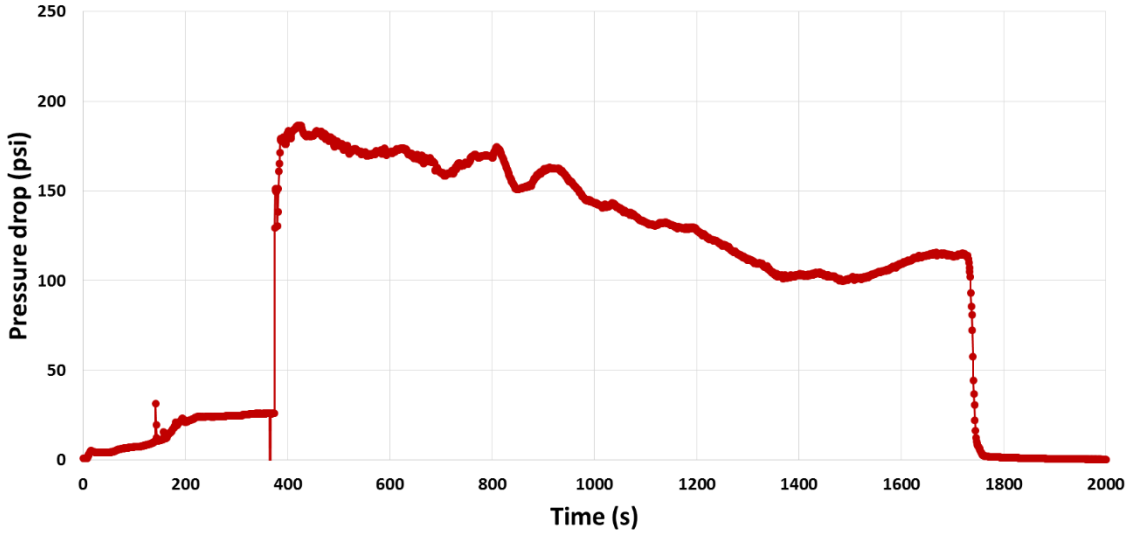

Figure 5.42 Beadpack pressure drop of RI experiment #1. Foam generated with compressed N_2+1.91 wt% HDK-H30 aqueous dispersion. Batch average particle aggregate diameter was 244 nm. NaCl concentration was 4 wt%. Outlet pressure was initially set at 200 psi, but had to be gradually adjusted to 250 psi over the course of the experiment. From t=0 to ~380 s, system was being pressurized with a 5mL/min aqueous dispersion flow rate. At t~380 s flow rates were 5mL/min aqueous dispersion and 15 mL/min compressed N_2. Steady state assumed at around t~700s, time at which compression vessel loading began.

During this experiment the extra pressure given to the compressed nitrogen was higher than needed. When nitrogen flow was initiated at t~380 s, foam was almost immediately witnessed, but it seemed to flow at a faster rate than previously observed. Beadpack pressure drop started to gradually decrease. This was attributed to the fact that

the pressure in the nitrogen accumulator was greater than the pressure drop foam generated at steady state and at these flow rates would produce. The excessive nitrogen pressure allowed it to expand and flow at a higher flow rate than the 15 mL/min set point. This flow behavior started to be more closely to that or pure gas as explained in section 5.3.2.4.

To correct for the detected flow behavior backpressure was increased. It appeared that the adjustment had worked, and steady state was assumed at *t*~700s. At this time the loading of the compression began. Pressure drop increased for a short period of time after peaking at *t*~810s, but then continued to decrease until through adjustments finally stabilized at *t*~1350s. Due to the described events, a qualitatively noticeable larger bubble size and larger measured quality were observed in this experiment in comparison to those in section 5.3.2 and 5.3.4where foams were generated under pressure with the same nanoparticles.

It is possible the beadpack foam generation pressure drop might have been underestimated due to the larger permeability measured after the beadpack was repacked. The values in Table 5.18 give the impression they are larger by ~2 Darcy than those found in Tables 5.14, 5.15, 5.16 and 5.17. Since the beadpack had to be repacked for the next experiment, this notion was not explored with more detail.

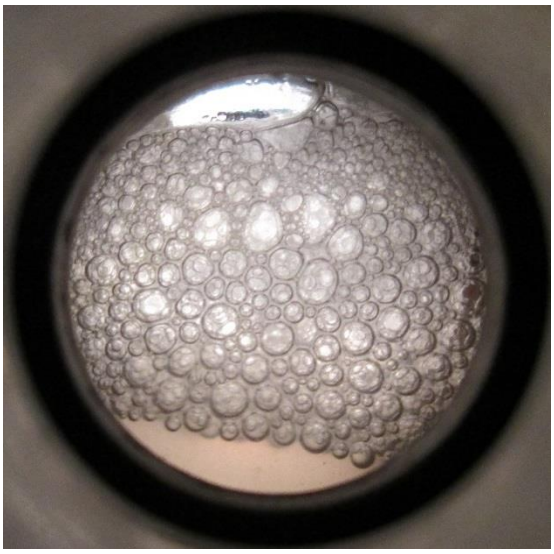

Figure 5.43 Foam generation observed during RI experiment #1.

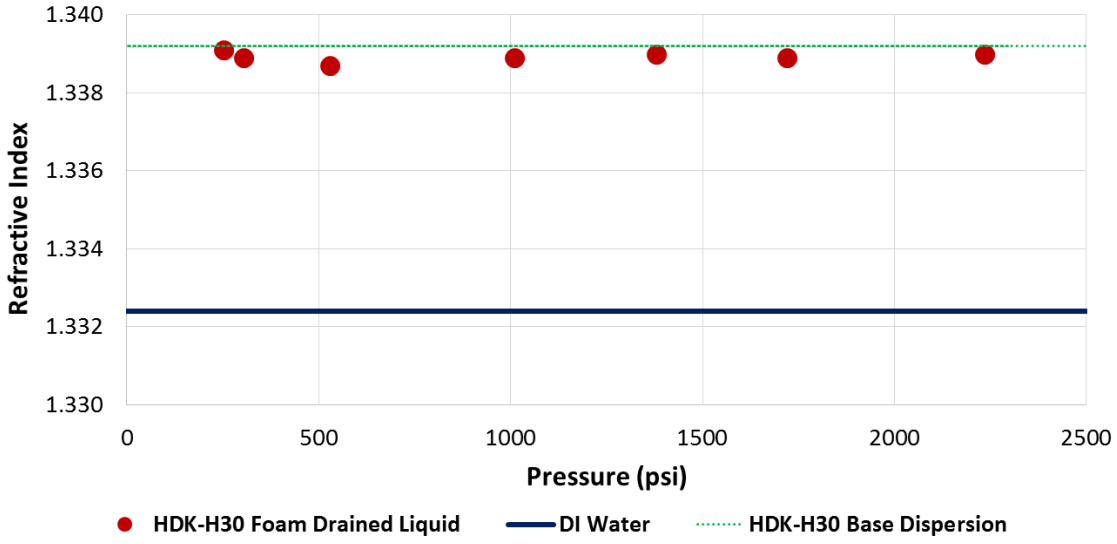

Figure 5.44 RI experiment #1. RI of sampled foam drained liquid at different pressures. Measured P_o=252 psi. Measured initial foam quality 78%. Measured RI of base HDK-H30 dispersion 1.3392. Samples were taken 15 min after each pressure increment to let liquid drain to bottom.

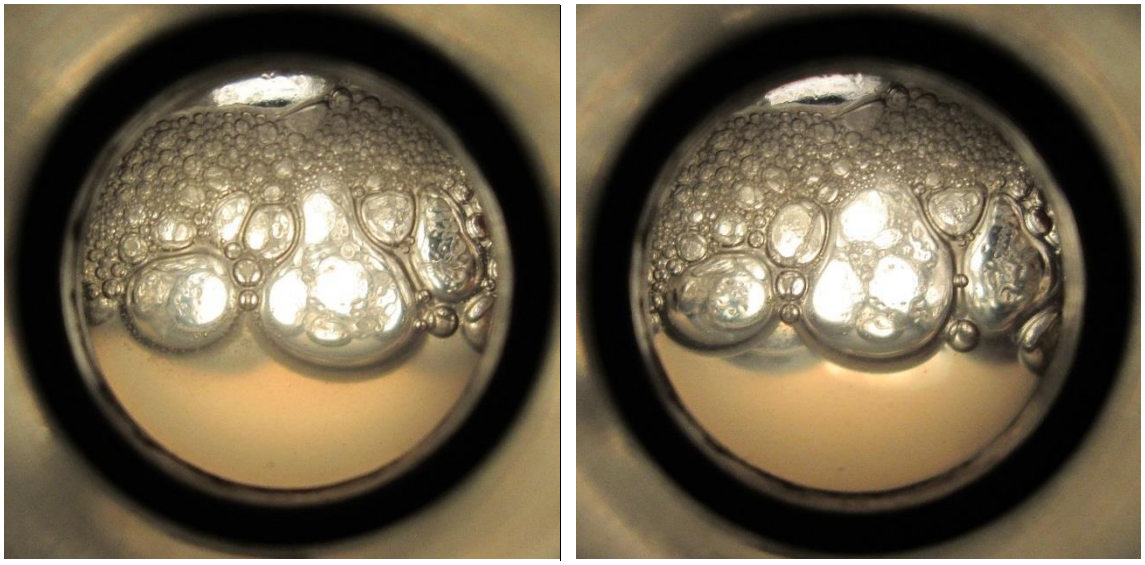

Figure 5.45 RI experiment #1 foam long term stability test. Photograph on the right was taken 164 minutes after photograph on the left.

The RI of the samples taken was consistently around ~1.3392 which was the RI of the stock dispersion. It is possible this indicates a constant nanoparticle concentration in the foam liquid phase, however this is believed to be unlikely.

5.3.6.3 RI Experiment #2

Due to the unexpected beadpack pressure drop behavior in RI experiment #1, a second experiment was performed to confirm the results from experiment #1. Foam target quality was lowered to 60% for the second experiment vs. the 75% used in all previous pressurized foam generation experiments. Since measuring compressibility was not the objective, it was thought increasing the liquid proportion would make it easier for excess liquid to drain to the bottom during compression. Foam generation flow rates were set at 8

mL/min aqueous phase and 12 mL/min gas phase for a target quality of 60%. After generating the foam, it was compressed and sampled at ~500 psi intervals. The foam drained liquid was sampled 30 minutes after each pressure increment to allow foam excess liquid to drain to the bottom. The time was increased from 15 to 30 minutes compared to the previous experiment.

DI water flow rate (mL/min)	Pressure drop (psi)
5	6.1
10	12
15	18.05
20	24.3
25	30.65

Table 5.19 Reference beadpack flow data for RI experiment #2. Outlet pressure was set at 200 psi. Calculated permeability was 22.2 Darcy. R^2 value of data fit was 0.9998.

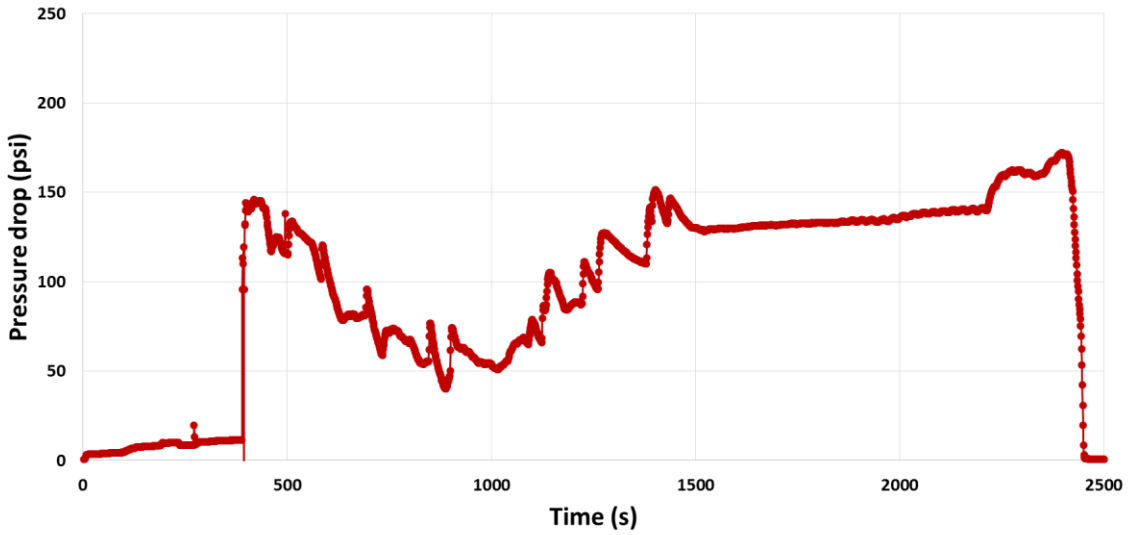

Figure 5.46 Beadpack pressure drop of RI experiment #2. Foam generated with compressed N_2+1.9 wt% HDK-H30 aqueous dispersion. Batch average particle aggregate diameter was 215 nm. NaCl concentration was 4 wt%. Outlet pressure was set at 200 psi. From t=0 to ~400 s, system was being pressurized with an 8 mL/min aqueous dispersion flow rate. At t~400 s flow rates were 8mL/min aqueous dispersion and 12 mL/min compressed N_2. Steady state assumed at around t~1200s, time at which compression vessel loading began.

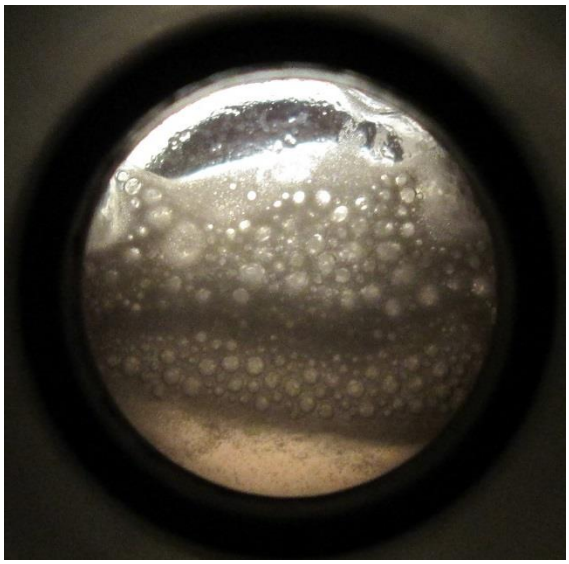

Figure 5.47 Foam generation observed during RI experiment #1.

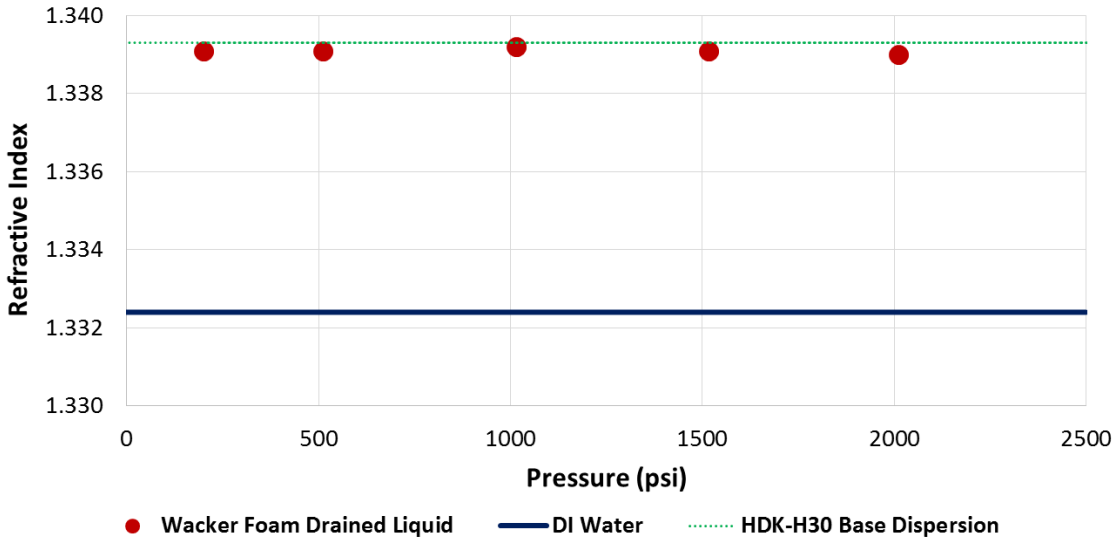

Figure 5.48 RI experiment #2. RI of sampled foam drained liquid at different pressures. Measured P_o=201 psi. Measured initial foam quality 52.3%. Measured RI of base HDK-H30 dispersion 1.3393. Samples were taken 30 min after each pressure increment to let liquid drain to bottom.

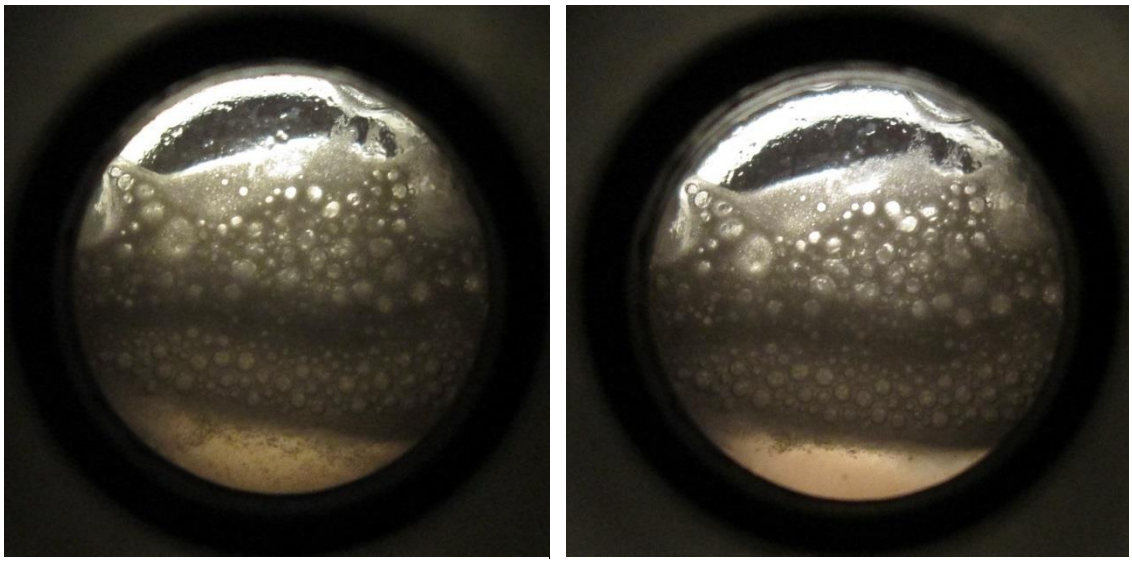

Figure 5.49 RI experiment #2 foam long term stability test. Photograph on the right was taken 174 minutes after photograph on the left.

The RI of the samples taken was consistently around ~1.3393 which was the RI of the stock dispersion. The results from RI experiment #2 appear to be practically the same than those in RI experiment #1, which show that the RI of the sampled foam liquid at various pressures was the same as the base dispersion. It was concluded that RI was not a good method to detect HDK-H30 nanoparticles concentration changes in the foam's liquid phase once foam had been generated. It might appear that the nanoparticle concentration in the foam's liquid phase remained constant during compression, but the fact that RI was virtually the same as the stock solution indicates this is unlikely. It is thought that at least some nanoparticle aggregates should have migrated to the G/W interface to generate the stable foams and this was not successfully identified.

5.3.7 Wrinkled Bubble

This section describes the presence of "wrinkled" or "crumpled" bubbles in solid particle stabilized bubbles or foams. The purpose it to describe a potential explanation on why the armored bubble effect was not detected in this research.

The work by Maestro et al (2014), where the CTAB + Ludox TMA recipe was obtained, showed that the nanoparticle layer surrounding a single bubble does have some rigidity over a certain compression range. The authors determined this by calculating elastic modulus of a single bubble as it was compressed. The mechanism described that as compression occurs, the nanoparticle layer reaches a jammed state which resists compression but once it reaches the limit of its elastic modulus it buckles. This process likely leads to the creation of wrinkled bubbles throughout the foam coarsening process of solid particle stabilized foams.

During foam coarsening an analogous process occurs in some of the bubbles due to pressure differentials in a foam system. The pressure differentials will result in compression and subsequent buckling of these same bubbles. Having buckled the bubbles converge to a zero mean curvature, at which point there is a zero pressure differential and coarsening is arrested. The authors did not characterize what occurred after the layer buckled. It was also stated that this work cannot be related directly to foams since the pressure differentials and surface tension of bubbles in a foam system depends on bubble geometry. Also, it was noted this process only qualitatively explains the process of shrinking bubbles in a foam, but does not explain why coarsening can also be arrested in larger bubbles.

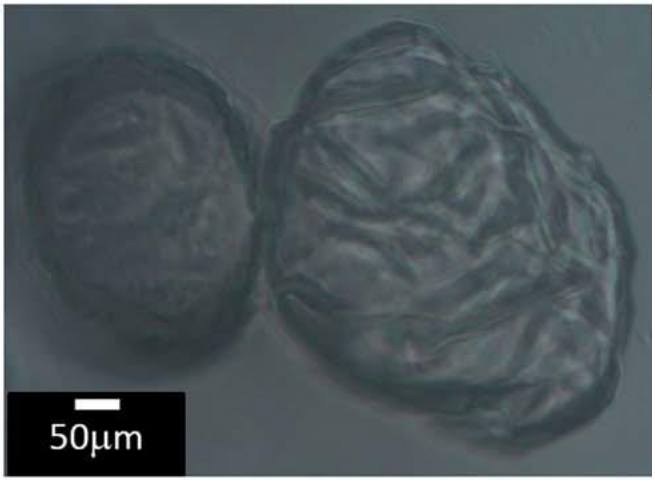

Figure 5.50 Wrinkled bubble observed by Maestro et al (2014). The observed bubbles remained stable over a 10 day period between 30 and 40 days after generation. $2*10^{\wedge-4}$ M CTAB+1wt % Ludox TMA dispersion used. Foams generated and coarsened at atmospheric pressures.

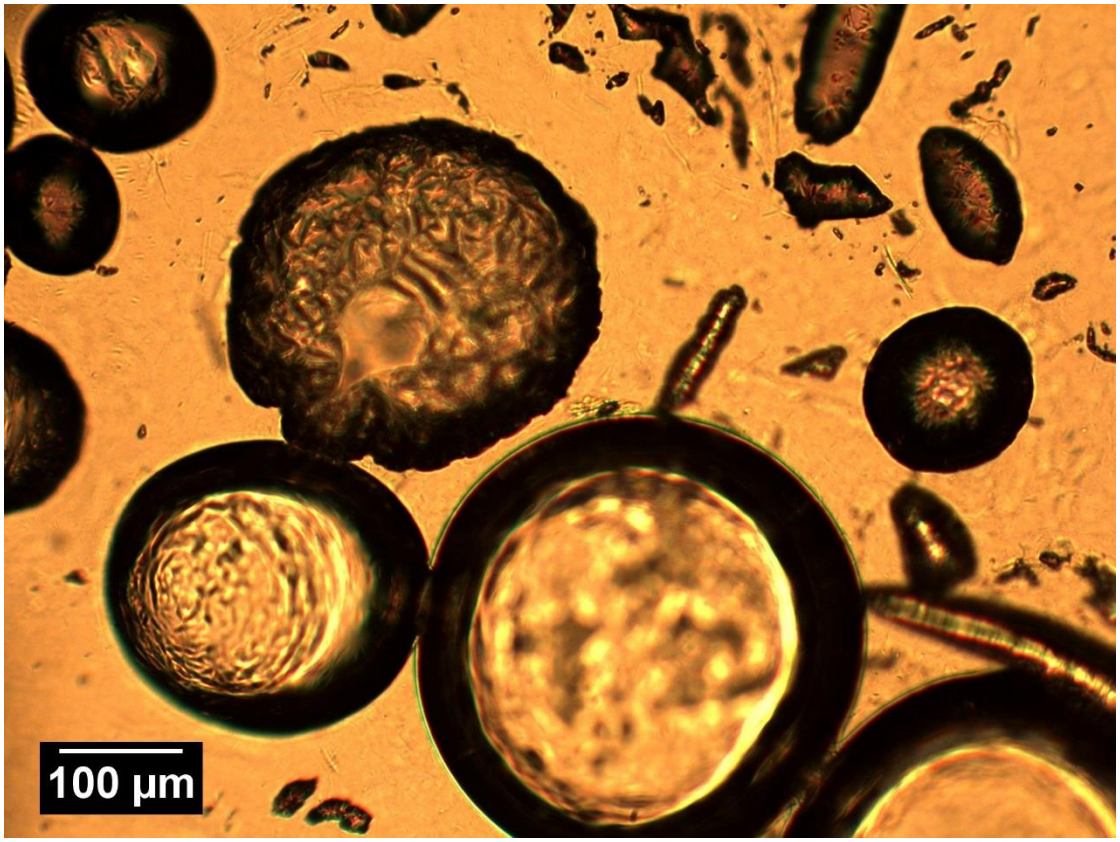

Figure 5.51 Captured image of 2*10^-4 M CTAB+1.5wt % Ludox TMA wrinkled bubble. Image was captured with a 10x magnification. Captured after 10 days of generating foam.

Figure 5.51 shows that the wrinkled bubbles were also observed when the foams were made with the leveraged recipe. The only difference in the recipe was the slightly larger nanoparticle concentration of 1.5 wt%. A Nikon Labophot-Pol microscope with digital output was used to capture CTAB + Ludox TMA foam/bubble images. The foams were generated at atmospheric pressure by shaking the vial containing the nanoparticle and surfactant solution.

A nonconductive force distribution geometry or collective buckling of the nanoparticle layers of bubbles is presentenced as a possible explanation for the inability to observe the armored bubble effect in this research. Even if the solid particle layers studied do have some rigidity, it is possible that the geometry of bubbles in a foam is not conductive to the even distribution of forces. In which case the bubbles in a foam easily deform or buckle when compressive forces are exerted. If the case is that foam geometry can evenly distribute forces, the magnitude of the rigidity of the nanoparticles surfaces is likely not sufficient for the apparatus in this research to detect. Additionally if the layers have limited rigidity, this would imply that nanoparticle stabilized foam compressibility would be the same as that of a surfactant stabilized foam after the onset of buckling.

If the nanoparticles in the G/W interfaces in foam system are permanently adsorbed and remain in the G/W interface as it buckles due to compression, this would indicate that nanoparticle concentration change in the liquid phase would be zero since no additional particles are migrating to the liquid phase. The purpose of the RI experiments was to demonstrate this, although the results were not conclusive.

5.4 Overall Chapter Discussions

The purpose of the first titration experiments, section 5.3.1, was to determine which nanoparticles or surfactant nanoparticles combination could be used to generate long term stable foams under cement pH and ionic conditions. In the case of surfactant titrations, if the surfactant would destabilize the particles prior to foam generation, then it would be concluded that only surfactant would stabilize the foam and not the combination of nanoparticles and surfactant. The first surfactant titration experiment was to observe if the Cembinder W50 Nanoparticles were stable with the amine Oxide surfactant. This

experiment was done to support the conclusion from Chapter 4 claiming that the high amine oxide surfactant concentration used to generate the foam and foamed cement likely destabilized the particles.

A range of foam generation pressures was tested, ideally if no mass transfer into the aqueous phase took place, a low starting pressure would have higher compressibility and would yield the largest nanoparticle surface density increment at a final compression pressure. Nonetheless, recall the main purpose of generating foams under pressure was to mitigate solubility effects. It was decided that to make solubility effects negligible a foam generation pressure of 200 would be sufficient as described in section 5.2.1. This was the reason most foams were generated in a 150-250 psi pressure range. This initial pressure would also allow for a 4.6x hypothetical nanoparticle surface density increment at a final pressure of 2000 psi (following the methods from section 5.2.7).

Basic foam generation/flow properties through porous media were researched in order to have some understanding of the process and be able to generate uniform foams with confidence. Radically increased pressure drop was a consistent indication of the presence of foam. One thorough and comprehensive explanation has been presented by Hirasaki & Lawson (1985). Hirasaki & Lawson proposed that Darcy's law in combination with Hagen-Poiseuille law can be used to describe foam flow if the following three factors are considered in the Hagen-Poiseuille law:

- The Newtonian viscosity of any liquid slugs between gas bubbles
- A resistance that manifests itself as an interface deformation
- A surface traction that results from a surface tension gradient

In this research, the increased pressure drop factor was found to be important not only to foresee/verify the generation and subsequent flow of foam through the view cell, but also to address some equipment limitations of the apparatus after having being adapted it for this research. The restrictions of the apparatus appeared to be evident after running a few experiments. The apparatus was originally designed to be used to generate emulsions/foams with liquid CO2 or supercritical CO2 at relatively high pressures (2000+ psia). These fluids have a much smaller compressibility relative to the lower pressurized nitrogen gas or air used in this research (14.7-800 psia). When foam was being generated, the increased friction force/pressure needed to be overcome would almost completely halt flow until both the gas and aqueous dispersion sources were pressurized enough to reinitiate flow. At this point more foam would be generated, further increasing the pressure required for continuous flow. This process would continue generating slugs of foam until the whole system was full of foam and would eventually reach a steady state. With low compressibility liquid or gas source phases, this phenomenon does not present a problem for this apparatus. Pressurization occurs relatively fast, as the ISCO syringe pump's piston compresses/displaces the fluids. With a relatively large compressibility source fluid, such as the gas phase at the pressures used in this research, the increased compressibility represented a challenge. The size of the reservoirs in the ISCO pumps as well as the waste accumulator meant that it was likely to run out of source gas before steady state was reached. This is the reasoning behind setting the initial pressure of the source gas phase between 50-100 psi higher than the foam final outlet pressure (pressure regulator set point).

The purpose of the RI experiments was an attempt to detect nanoparticle concentration changes in the liquid, this could be a potential indication of permanent nanoparticle adsorption into to G/W interface over the studied compression ranges. Although not implemented in this research, two alternate methods are proposed. Surfactant could potentially be used a tracer and its concentrations in the foam liquid phase measured during compression. Additionally, luminescent tracer nanoparticles could also possibly be used for this purpose.

5.5 CHAPTER CONCLUSIONS

During the nanoparticle stability tests, cement ionic and pH conditions and high surfactant concentrations showed to be a harsh environment for many of the nanoparticles. At this point, a proof of concept approach in a pure gas + water system was considered to be advantageous to potentially notice any compressibility alteration effects by the presence of an armored bubble. Thus the presence of cement was eliminated from the compressibility measurement experiments. In addition, if foamed cement was to be stabilized by a combination of surfactant and nanoparticles, it would have to be proved the nanoparticles are supporting stabilization and are not a mere spectator component. A type of nanoparticles (HDK-H30) where found to generate stable foams in air + water systems. The HDK-H30 hydrophobic silica nanoparticles were able to generate stable foams without the need for surfactant, eliminating an additional variable. These foams also displayed some resistance to alkaline environments.

An apparatus that had been previously validated to generate CO2/water foams under pressurized conditions by Hariz (2012) and Worthen et al (2013b) was adapted to generate air + water or nitrogen + water foams and load them into the compression vessel.

Using this apparatus nanoparticle stabilized foams were successfully generated at pressurized conditions. Tests were performed with three different kinds of nanoparticles (3M PEG coated, EOR-50 and HDK-H30) to generate compressed air + water or nitrogen + water foams. The three types of nanoparticles successfully generated foams, but only the HDK-H30 foams exhibited the required long term stability needed to measure compressibility (1+ hours).

Specific to the beadpack in this apparatus, optimal foam generation flow rates were determined to be 5 mL/min aqueous phase and 15 mL/min gas phase. Even though these flow rates would ideally generate a 75% quality foam, measurements showed that foam quality was usually ~70%. The lower foam quality was likely as a result of gas phase compression and gas dissolution during generation. Various foam generation pressures were utilized ranging from ~100 to ~500 psia. The compressibility of these foams was successfully measured. All of the tested foams displayed long term stability during the time interval over which the compressibility measurement experiments took place, usually between one and two hours.

An additional recipe know to generate nanoparticle stabilized foams was tested. The recipe used a combination of CTAB surfactant and Ludox TMA uncoated silica nanoparticles. The recipe was found in literature on a research publication by Maestro et al (2014). The compressibility of foam generated with this recipe was also tested. The foam generated with this recipe too exhibited long term stability. Foams using this recipe were also generated at atmospheric pressures and left to coarsen over a period of 10 days. A microscopic image of a bubble from this foam was captured to observe wrinkled bubbles as the research by Maestro et al (2014) had shown.

Compressibility did not appear to be altered in foams stabilized purely by hydrophobic silica nanoparticles (HDK-H30) or a combination of surfactant and hydrophilic silica nanoparticles (CTAB + Ludox TMA). The measured compressibility of these foams showed compressibility behavior that was very similar to an analogous ideal gas + water mixture.

Various cases were considered to explain the inability to observe the armored bubble effect. The first is that the concentration of utilized nanoparticles in G/W interface was never sufficient to form a closed packed layer even after compression. A direct measurement of nanoparticle surface concentration is not available and it is difficult to infer such measurement. As a result, estimating the likelihood that enough nanoparticles are present at the G/W bubble interface that hypothetically result in rigid bubbles during compression is challenging.

Even if the nanoparticle surface density was sufficient to form closed packed layers, it is possible the magnitude of the resistance to compression is relatively small and the apparatus is not sensitive enough to detect it. Other phenomena might take place which prevent the packed layer from having resistance to compression. As pressure is applied the nanoparticles might be ejected at the same rate the bubble's surface is compressed. Another possibility is that even if the particles remain in the G/W interface, they begin piling on top of each other forming stacked layers.

Two potential explanations were deduced by the work by Maestro et al (2014) described in section 5.3.7. The layers might be rigid, but geometry of bubbles in a foam does not conduct to the distribution of forces and the bubbles easily deform. Alternatively,

the layers might have limited rigidity and can evenly distribute forces, but after reaching the rigidity limit the layers buckle and no longer resists compression.

Chapter 6

Conclusions

6.1 Influence of Nanoparticles on Cement Strength

- Cembinder W50 uncoated silica nanoparticles did not show significant improvements on class H cement average compressive strength using the chosen experimental parameters. In fact in some concentrations it appeared to have an adverse effect. At the 0.15% bwoc and 0.5% bwoc concentrations tested, average compressive strength was correspondingly 8.85% and 16.4% lower than its pure H cement counterpart. At the 1% bwoc cement concentration, average compressive strength was 7.28% greater than its pure H counterpart. Compressive strength standard deviation from their mean for all recipes was between ± 11.8% and 13.1 %.
- Cembinder W50 uncoated silica nanoparticles appeared to have an overall adverse effect on class H cement splitting tensile strength using the chosen experimental parameters. The average splitting tensile strengths of the 0.15%, 0.5% bwoc and 1% bwoc recipes were lower than their pure class H counterpart by 22.8% 17.1% and 3.75% respectively. It is important to remark that the pure class H cement and 0.15 % bwoc recipes showed the largest splitting tensile strength standard deviation being 25% from their mean. The 0.5% bwoc and 1% bwoc recipes had corresponding standard deviations of 15% and 13% from the their mean.
- Higher Cembinder W50 nanoparticle concentrations were not tested due to blending limitations arising from the slurry thickening upon addition. Thickening at concentrations greater than 1% bwoc nanoparticles made it extremely difficult to obtain uniform mixing.

6.2 COMPRESSIBILITY OF FOAM AND FOAMED CEMENT

- The compressibility measurement apparatus used in this research was validated for various single phase fluids including air, water and CO_2. The validation experiments allowed the estimation of the compressibility of the apparatus itself. Using this information a method was developed to separate the compressibility contribution from the apparatus from the compressibility of the test fluid.
- A compressibility benchmark was established by calculating the compressibility of an ideal gas + water mixture with the same initial quality. The effects of gas dissolution at equilibrium in compressibility were also calculated. The equilibrium gas dissolution adjusted compressibility served as a limiting case boundary to explain potential deviations from the ideal gas + water mixture compressibility.
- The foam generated with the Amine Oxide 9% bwow + 0.5% Cembinder W50 recipe displayed increased viscous properties vs. its counterpart which did not have nanoparticles. This was investigated as a potential enhancement of stability by the presence of nanoparticles, although the nanoparticle stability tests performed in Chapter 5 showed this was unlikely. The most reasonable explanation was the gelling effect caused by nanoparticles becoming unstable due to large surfactant concentration.
- Mass transport of gas molecules (dissolution into aqueous phase) affected the compressibility measurements of foams or foamed cement that were generated at atmospheric conditions. The effects appeared to be more noticeable in foams/foamed cement that had long term stability. The most likely explanation is that the large surface area between the air and water phases in foams increased the

mass transport rate throughout the compression of the fluids. Compressing an air + water mixture made with pressurized air showed very minor effects of gas dissolution upon gas/water compressibility. It was concluded that generating foams under pressurized conditions and with pure nitrogen would minimize gas dissolution effects in compressibility measurements.

6.3 COMPRESSIBILITY OF NANOPARTICLE STABILIZED FOAMS

- Cement ionic and pH conditions showed to be a harsh environment for many of the nanoparticles whose stability was tested. A proof of concept approach in a pure gas + water system was considered to be advantageous to potentially notice any compressibility alteration effects by the presence of an armored bubble. A type of nanoparticles (HDK-H30) where found to generate stable foams in air + water systems. The HDK-H30 hydrophobic silica nanoparticles were able to generate stable foams without the need for surfactant, eliminating an additional variable.

- Nanoparticle stabilized foams were successfully generated at pressurized conditions. Various generation pressures were utilized ranging from ~100 to ~500 psia. The compressibility of these foams was successfully measured. The foams displayed long term stability. Foam stability was at least the duration over which the compressibility measurement experiments took place, usually between one and two hours.

- An additional recipe, CTAB + Ludox TMA nanoparticles, previously researched by Maestro et al (2014) was found to generate long term nanoparticle stabilized

foams with the aid of surfactant. The compressibility of foam generated with this recipe was also tested

- Compressibility did not appear to be altered in foams stabilized purely by hydrophobic silica nanoparticles (HDK-H30) or a combination of surfactant and hydrophilic silica nanoparticles (CTAB + Ludox TMA). The measured compressibility of these foams showed compressibility behavior that was very similar to an analogous ideal gas + water mixture.
- Various explanations are presented to explain the lack of the presence of the armored bubble effect
    - Concentration of utilized nanoparticles in G/W interface is not sufficient to form closed packed layer even after compression in the studied G/W surface compression ranges
    - A nanoparticle closed pack layer is forming, but as pressure is applied particles pop of G/W interface
    - If closed pack layer is forming and nanoparticles stay at G/W interface as pressure is applied, the magnitude of the reduction in compressibility is relatively small and the apparatus used in this research does not have the capability to detect it.
    - If closed pack layer is forming and nanoparticles stay at G/W interface as pressure is applied, it might have limited rigidity at which point the

nanoparticle layer buckles and the apparatus was not able to detect this development

- If closed pack layer is forming and nanoparticles stay at G/W interface as pressure is applied, nanoparticle layers might have some rigidity, but foam geometry might not favor the distribution of forces
- If closed pack layer is forming and nanoparticles stay at G/W interface as pressure is applied, it might have limited rigidity at which point the nanoparticles start stacking on top of each other forming stacked layers
- The nano-particles may simply not create an armored surface that can withstand additional compression.

- If the studied nanoparticle stabilized foams do have some resistance to compression and it was too small to detect, the reduction in compressibility would not be of practical use in foamed cement applications.
- A direct measurement of nanoparticle surface concentration is not available and it is difficult to infer such measurement. Thus it is difficult to independently assess the possibility that insufficient nanoparticles are present on the bubble surfaces to result in rigid bubbles during compression.

Appendices

A1 Nanoparticle Stability Titration Experiments

Sample volume (mL)	Added titrant volume (mL)	pH	Conductivity (milliSiemens/cm)	Observations
30	0	10.7	3.3	No changes
33	3	10.6	4.46	No changes
36	6	10.7	5.68	No changes
39	9	10.7	6.85	No changes
42	12	10.8	7.61	No changes
45	15	10.9	8.45	No changes
55	25	11	10.61	No changes
60	30	11.1	11.35	Cloudy
65	35	11.2	11.95	Cloudy
70	40	11.4	12.17	Gel

Table A.1 Results from titration of pH 12.73 and 36.2 milliSiemens/cm cement filtrate into Nexsil 5000 nanoparticle stock solution.

Sample volume (mL)	Added titrant volume (mL)	pH	Conductivity (milliSiemens/cm)	Observations
20	0	10.8	3.26	No changes
21	1	11.1	3.82	No changes
22	2	11.4	4.333	No changes
23	3	11.6	5.05	No changes
24	4	11.8	5.65	No changes
25	5	12	6.66	No changes
26	6	12.1	7.63	No changes
27	7	12.1	8.6	No changes
28	8	12.2	10	No changes
29	9	12.3	11.74	No changes
30	10	12.3	12.45	Cloudy
32	12	12.4	14.12	Gel

Table A.2 Results from titration of 0.5M NaOH into Nexsil 5000 nanoparticle stock solution. 0.5M NaOH solution had a measured pH of 13.72 and a conductivity of 82.8 milliSiemens/cm.

Sample volume (mL)	Added titrant volume (mL)	pH	Conductivity (milliSiemens/cm)	Observations
20	0	10.8	3.25	
22	2	10.5	10	No changes
24	4	10.2	17.42	No changes
26	6	10.1	22.1	No changes
28	8	10.1	25	No changes
30	10	9.9	29.36	No changes
35	15	9.9	35	Cloudy
40	20	9.9	36.2	Gel

Table A.3 Results from titration of 1M NaCl into Nexsil 5000 nanoparticle stock solution. 1M NaCl solution had a measured pH of 7.5 and a conductivity of 80 milliSiemens/cm.

Sample volume (mL)	Added titrant volume (mL)	pH	Conductivity (milliSiemens/cm)	Observations
20	0	8.9	7.41	
30	10	9.6	10.06	No changes
40	20	10.3	11.69	No changes
50	30	10.7	12.88	No changes
60	40	11.4	14.05	No changes
65	45	12	15.02	No changes

Table A.4 Results from titration of pH 12.73 and 36.2 milliSiemens/cm cement filtrate into 3M PEG coated nanoparticle stock solution.

Sample volume (mL)	Added titrant volume (mL)	pH	Conductivity (milliSiemens/cm)	Observations
20	0	8.9	7.51	
30	10	13.3	36	No changes
40	20	13.5	67.4	No changes
50	30	13.75	88	No changes
60	40	14	105	No changes

Table A.5 Results from titration of 1M NaOH into 3M PEG coated nanoparticle stock solution. 1M NaOH solution had a measured pH of 14 and the conductivity reading was above the 112 milliSiemens/cm limit of the used conductivity meter.

Sample volume (mL)	Added titrant volume (mL)	pH	Conductivity (milliSiemens/cm)	Observations
10	0	9	6.94	
20	10	8.9	38.9	No changes
30	20	8.9	50.6	No changes
40	30	8.9	58.5	No changes

Table A.6 Results from titration of 1M NaCl into 3M PEG coated nanoparticle stock solution. 1M NaCl solution had a measured pH of 7.5 and a conductivity of 80 milliSiemens/cm.

Sample volume (mL)	Added titrant volume (mL)	pH	Conductivity (milliSiemens/cm)	Observations
20	0	10.3	2.25	
30	10	11	6.55	No changes
40	20	11.5	9.69	No changes
50	30	11.8	11.71	No changes
60	40	11.9	13.62	No changes

Table A.7 Results from titration of pH 12.73 and 36.2 milliSiemens/cm cement filtrate into EOR 5XS nanoparticle stock solution.

Sample volume (mL)	Added titrant volume (mL)	pH	Conductivity (milliSiemens/cm)	Observations
20	0	10.3	2.14	
30	10	13.25	26.3	No changes
40	20	13.5	50.5	No changes
50	30	13.75	66.6	No changes
60	40	14	80.5	No changes

Table A.8 Results from titration of 1M NaOH into EOR 5XS nanoparticle stock solution. 1M NaOH solution had a measured pH of 14 and the conductivity reading was above the 112 milliSiemens/cm limit of the used conductivity meter.

Sample volume (mL)	Added titrant volume (mL)	pH	Conductivity (milliSiemens/cm)	Observations
20	0	10.3	2.274	
30	10	9.5	53.5	No changes
40	20	9.3	80.6	No changes
50	30	9.3	96.6	No changes
60	40	9.2	108.9	No changes

Table A.9 Results from titration of 3M NaCl into EOR 5XS nanoparticle stock solution. 3M NaCl solution had a measured pH of 6.7 and the conductivity reading was above the 112 milliSiemens/cm limit of the used conductivity meter.

A2 BUBBLE SIZE MEASUREMENTS

Bubble #	Diameter (micron)
1	285
2	214
3	469
4	303
5	245
6	412
7	228
8	228
9	285
10	182
11	353
12	205
13	299
14	167
15	205
16	205
17	299
18	292
19	214
20	160
21	178
22	292
23	220
24	255
25	185
26	205
27	178
28	199
29	185
30	315

Bubble #	Diameter (micron)
31	205
32	178
33	167
34	303
35	171
36	214
37	138
38	199
39	205
40	189
41	151
42	220
43	228
44	189
45	245
46	205
47	214
48	208
49	228
50	195
51	214
52	151
53	247
54	182
55	205
56	228
57	189
58	147
59	167
60	205

Bubble #	Diameter (micron)
61	214
62	178
63	178
64	228
65	214
66	167
67	267
68	245
69	205
70	252
71	178
72	205
73	178
74	279
75	178
76	245
77	245
78	205
79	228
80	267
81	214
82	178
83	138
84	245
85	189
86	228
87	214
Average	221

Table A.10 Diameter in microns (μm) of bubbles selected for average bubble diameter approximation corresponding to Figure 5.22 in section 5.3.3.

Bubble #	Diameter (micron)
1	234
2	252
3	315
4	351
5	285
6	220
7	208
8	769
9	269
10	610
11	484
12	257
13	660
14	635
15	427
16	160
17	269
18	600
19	677
20	175
21	694
22	220
23	192
24	419
25	584
26	185
27	427
28	311
29	735
30	234

Bubble #	Diameter (micron)
31	269
32	317
33	484
34	635
35	460
36	301
37	635
38	535
39	376
40	360
41	408
42	510
43	376
44	618
45	600
46	518
47	351
48	327
49	376
50	335
51	285
52	743
53	408
54	185
55	434
56	311
57	252
58	285
59	501
60	427

Bubble #	Diameter (micron)
61	393
62	315
63	376
64	199
65	360
66	367
67	311
68	340
69	451
70	234
71	360
72	401
73	451
74	315
75	376
76	234
77	234
78	376
79	315
80	384
81	257
82	393
83	443
84	340
85	220
86	252
87	269
88	234
89	351
90	443
Average	221

Table A.11 Diameter in microns (μm) of bubbles selected for average bubble diameter approximation corresponding to Figure 5.23 in section 5.3.3

References

ASTM standards C496/C496M-11, C470/470M-09 and C109/C109M – 11b

Benge, O. G., Spangle, L. B., & Sauer Jr, C. W. (1982, January). Foamed Cement-Solving Old Problems with a New Technique. In SPE Annual Technical Conference and Exhibition. Society of Petroleum Engineers.

Berra, M., Carassiti, F., Mangialardi, T., Paolini, A. E., & Sebastiani, M. (2012). Effects of nanosilica addition on workability and compressive strength of Portland cement pastes. Construction and Building Materials, 35, 666-675.

Binks, B. P. (2002). Particles as surfactants—similarities and differences.Current Opinion in Colloid & Interface Science, 7(1), 21-41.

Binks, B. P., & Clint, J. H. (2002). Solid wettability from surface energy components: relevance to Pickering emulsions. Langmuir, 18(4), 1270-1273.

Binks, B. P., & Horozov, T. S. (2005). Aqueous foams stabilized solely by silica nanoparticles. Angewandte Chemie, 117(24), 3788-3791.

Binks, B. P., & Lumsdon, S. O. (2000). Influence of particle wettability on the type and stability of surfactant-free emulsions. Langmuir, 16(23), 8622-8631.

Björnström, J., Martinelli, A., Matic, A., Börjesson, L., & Panas, I. (2004). Accelerating effects of colloidal nano-silica for beneficial calcium–silicate–hydrate formation in cement. Chemical Physics Letters, 392(1), 242-248.

Chatterji, J., Cromwell, R. S., Brenneis, C. R., King, B. J., Gray, D. W., & Zamora, F. (2003). U.S. Patent No. 6,547,871. Washington, DC: U.S. Patent and Trademark Office.

Davies, D. R., Hartog, J. J., & Cobbett, J. S. (1981, January). Foamed Cement-A Cement with Many Applications. In Middle East Technical Conference and Exhibition. Society of Petroleum Engineers.

De la Roij, R., Egyed, C., & Lips, J. P. (2012, January). Nano-engineered oil well cement improves flexibility and increases compressive strength: A laboratory study. In SPE International Oilfield Nanotechnology Conference and Exhibition. Society of Petroleum Engineers.

Green, Don W., Perry, Robert H. Perry's Chemical Engineers' Handbook, Eighth Edition. Densities of Aqueous Inorganic Solutions at 1 ATM, Chapter 2 (McGraw-Hill Professional, 2008 1997 1984 1973 1963 1950 1941 1934), AccessEngineering

Halliburton Red Book Engineering Tables, Halliburton Services (1994).

Harlan, T. D., Foreman, J. M., Reed, S. D., & Griffith, J. E. (2001, January). Foamed Cement Selection for Horizontal Liners Proves Effective for Zonal Isolation—Case History. In SPE Rocky Mountain Petroleum Technology Conference. Society of Petroleum Engineers.

Hariz, T.R. Nanoparticle-Stabilized CO2 Foams for Potential Mobility Control Applications, M.S.E. Thesis, The University of Texas at Austin (2012).

Hilgenfeldt, S., Koehler, S. A., & Stone, H. A. (2001). Dynamics of coarsening foams: accelerated and self-limiting drainage. Physical review letters, 86(20), 4704.

Hirasaki, G. J., & Lawson, J. B. (1985). Mechanisms of foam flow in porous media: apparent viscosity in smooth capillaries. Society of Petroleum Engineers Journal, 25(2), 176-190.

Horozov, T. S. (2008). Foams and foam films stabilised by solid particles. Current Opinion in Colloid & Interface Science, 13(3), 134-140.

Jalal, M., Mansouri, E., Sharifipour, M., & Pouladkhan, A. R. (2012). Mechanical, rheological, durability and microstructural properties of high performance self-compacting concrete containing SiO< sub> 2</sub> micro and nanoparticles. Materials & Design, 34, 389-400.

Khaloo, A. R., Vayghan, A. G., & Bolhasani, M. (2011). Mechanical and Microstructural Properties of Cement Paste Incorporating Nano Silica Particles with Various Specific Surface Areas. Key Engineering Materials, 478, 19-24.

Kopp, K., Reed, S., Foreman, J., Carty, B., & Griffith, J. (2000, January). Foamed cement vs. conventional cement for zonal isolation-case histories. In SPE Annual Technical Conference and Exhibition. Society of Petroleum Engineers.

Korson, L., Drost-Hansen, W., & Millero, F. J. (1969). Viscosity of water at various temperatures. The Journal of Physical Chemistry, 73(1), 34-39.

Land, G., & Stephan, D. (2012). The influence of nano-silica on the hydration of ordinary Portland cement. Journal of Materials Science, 47(2), 1011-1017.

Nazari, A., & Riahi, S. (2011). Splitting tensile strength of concrete using ground granulated blast furnace slag and SiO_2 nanoparticles as binder. Energy and Buildings, 43(4), 864-872.

Maestro, A., Rio, E., Drenckhan, W., Langevin, D., & Salonen, A. (2014). Foams stabilised by mixtures of nanoparticles and oppositely charged surfactants: relationship between bubble shrinkage and foam coarsening. Soft matter.

MacArthur, C. G. (1916). Solubility of oxygen in salt solutions and the hydrates of these salts. The Journal of Physical Chemistry, 20(6), 495-502.

Martin, J. E., Wilcoxon, J. P., Schaefer, D., & Odinek, J. (1990). Fast aggregation of colloidal silica. Physical Review A, 41(8), 4379.

Martinez, A. C., Rio, E., Delon, G., Saint-Jalmes, A., Langevin, D., & Binks, B. P. (2008). On the origin of the remarkable stability of aqueous foams stabilised by nanoparticles: link with microscopic surface properties. Soft Matter, 4(7), 1531-1535.

McElfresh, P. M., & Go Boncan, V. C. (1982, January). Applications of Foam Cement. In SPE Annual Technical Conference and Exhibition. Society of Petroleum Engineers.

Moore, S., Miller, M., Faul, R., & D'Agostino, J. (2000, January). Foam cementing applications on a deepwater subsalt well-case history. In IADC/SPE Drilling Conference. Society of Petroleum Engineers.

Nelson, E. & Guillot, D. (2006). *Well cementing*. Sugar Land, Tex: Schlumberger.

Nordström, J., Matic, A., Sun, J., Forsyth, M., & MacFarlane, D. R. (2010). Aggregation, ageing and transport properties of surface modified fumed silica dispersions. Soft matter, 6(10), 2293-2299.

NIST (National Institute of Standards and Technology). Thermophysical Properties of Fluid Systems. http://webbook.nist.gov/chemistry/fluid/

Paunov, V. N., Binks, B. P., & Ashby, N. P. (2002). Adsorption of charged colloid particles to charged liquid surfaces. Langmuir, 18(18), 6946-6955.

Potapov, V. V., Shitikov, E. S., Trutnev, N. S., Gorbach, V. A., & Portnyagin, N. N. (2011). Influence of silica nanoparticles on the strength characteristics of cement samples. Glass Physics and Chemistry, 37(1), 98-105.

Qing, Y. E., Zenan, Z., Li, S., & Rongshen, C. (2006). A comparative study on the pozzolanic activity between nano-SiO2 and silica fume. Journal of Wuhan University of Technology-Mater. Sci. Ed., 21(3), 153-157.

Ravi, K., Bosma, M., & Gastebled, O. (2002, January). Safe and economic gas wells through cement design for life of the well. In SPE Gas Technology Symposium. Society of Petroleum Engineers.

Sander, R. (1999). Compilation of Henry's law constants for inorganic and organic species of potential importance in environmental chemistry.

Santra, A. K., Boul, P., & Pang, X. (2012, January). Influence of Nanomaterials in Oilwell Cement Hydration and Mechanical Properties. In SPE International Oilfield Nanotechnology Conference and Exhibition. Society of Petroleum Engineers.

Shih, J. Y., Chang, T. P., & Hsiao, T. C. (2006). Effect of nanosilica on characterization of Portland cement composite. Materials Science and Engineering: A, 424(1), 266-274.

Smith, N. O., Kelemen, S., & Nagy, B. (1962). Solubility of natural gases in aqueous salt solutions—II: Nitrogen in aqueous NaCl, CaCl2, Na2SO4 and MgSO4 at room temperatures and at pressures below 1000 psia. Geochimica et Cosmochimica Acta, 26(9), 921-926.

Stocco, A., Rio, E., Binks, B. P., & Langevin, D. (2011). Aqueous foams stabilized solely by particles. Soft Matter, 7(4), 1260-1267.

Tinsley, J. M., Miller, E. C., Sabins, F. L., & Sutton, D. L. (1980). Study of factors causing annular gas flow following primary cementing. Journal of Petroleum Technology, 32(08), 1-427.

Tsivilis, S., & Parissakis, G. (1995). A mathematical model for the prediction of cement strength. Cement and concrete research, 25(1), 9-14.

Wiebe, R., Gaddy, V. L., & Heins Jr, C. (1933). The solubility of nitrogen in water at 50, 75 and 100 from 25 to 1000 atmospheres. Journal of the American Chemical Society, 55(3), 947-953.

Worthen, A. J., Bagaria, H. G., Chen, Y., Bryant, S. L., Huh, C., & Johnston, K. P. (2013a). Nanoparticle-stabilized carbon dioxide-in-water foams with fine texture. Journal of colloid and interface science, 391, 142-151.

Worthen, A. J., Hariz, T., Huh, C., Aroonsri, A., Johnston, K. P., & Bryant, S. L. (2013b, September). Conditions for Generating Nanoparticle-Stabilized CO Foams in Fracture and Matrix Flow. In SPE Annual Technical Conference and Exhibition. Society of Petroleum Engineers.

Wohlfarth, C. (2008). Refractive index of water. In Refractive Indices of Pure Liquids and Binary Liquid Mixtures (Supplement to III/38) (pp. 37-41). Springer Berlin Heidelberg.

Zang, D. Y., Rio, E., Langevin, D., Wei, B., & Binks, B. P. (2010). Viscoelastic properties of silica nanoparticle monolayers at the air-water interface. The European Physical Journal E: Soft Matter and Biological Physics, 31(2), 125-134.

Zhang, W., Thompson, K. E., Reed, A. H., & Beenken, L. (2006). Relationship between packing structure and porosity in fixed beds of equilateral cylindrical particles. Chemical Engineering Science, 61(24), 8060-8074.